



NAVAL POSTGRADUATE SCHOOL

MONTEREY, CALIFORNIA

THESIS

**INTER-ANNUAL VARIABILITY OF THE ACOUSTIC
PROPAGATION IN THE YELLOW SEA IDENTIFIED
FROM A SYNOPTIC MONTHLY GRIDDED DATABASE
AS COMPARED WITH GDEM**

by

Colleen M. McDonald

September 2016

Thesis Advisor:

Co-Advisor:

Peter C. Chu

Tetyana Margolina

Approved for public release. Distribution is unlimited.

THIS PAGE INTENTIONALLY LEFT BLANK

REPORT DOCUMENTATION PAGE			<i>Form Approved OMB No. 0704-0188</i>	
Public reporting burden for this collection of information is estimated to average 1 hour per response, including the time for reviewing instruction, searching existing data sources, gathering and maintaining the data needed, and completing and reviewing the collection of information. Send comments regarding this burden estimate or any other aspect of this collection of information, including suggestions for reducing this burden, to Washington headquarters Services, Directorate for Information Operations and Reports, 1215 Jefferson Davis Highway, Suite 1204, Arlington, VA 22202-4302, and to the Office of Management and Budget, Paperwork Reduction Project (0704-0188) Washington, DC 20503.				
1. AGENCY USE ONLY (Leave blank)		2. REPORT DATE September 2016		3. REPORT TYPE AND DATES COVERED Master's thesis
4. TITLE AND SUBTITLE INTER-ANNUAL VARIABILITY OF THE ACOUSTIC PROPAGATION IN THE YELLOW SEA IDENTIFIED FROM A SYNOPTIC MONTHLY GRIDDED DATABASE AS COMPARED WITH GDEM			5. FUNDING NUMBERS	
6. AUTHOR(S) Colleen M. McDonald				
7. PERFORMING ORGANIZATION NAME(S) AND ADDRESS(ES) Naval Postgraduate School Monterey, CA 93943-5000			8. PERFORMING ORGANIZATION REPORT NUMBER	
9. SPONSORING /MONITORING AGENCY NAME(S) AND ADDRESS(ES) N/A			10. SPONSORING / MONITORING AGENCY REPORT NUMBER	
11. SUPPLEMENTARY NOTES The views expressed in this thesis are those of the author and do not reflect the official policy or position of the Department of Defense or the U.S. Government. IRB number ____N/A____.				
12a. DISTRIBUTION / AVAILABILITY STATEMENT Approved for public release. Distribution is unlimited.			12b. DISTRIBUTION CODE	
13. ABSTRACT (maximum 200 words) This research investigates the inter-annual acoustic variability in the Yellow Sea identified from the Synoptic Monthly Gridded-World Ocean Database (SMG-WOD) as compared with the Navy's Global Digital Environmental Model (GDEM). The SMG-WOD has a horizontal resolution of 1°, 28 vertical levels from the surface to 3000 m depth and one-month temporal increments allowing individual years of acoustic data to be analyzed, whereas GDEM is a climatological database with a horizontal resolution of 1/4° and 78 vertical levels. The Yellow Sea is a semi-enclosed basin located between China and Korea with a mean depth of 40m; acoustics are driven by shallow water dynamics and interaction with the bottom. Seven distinct locations were selected for acoustic comparison based on various depths and bottom types. Composite analysis of the sound speed profiles reveals evident inter-annual variability at all locations, superimposed into a strong seasonal variability. Overall, SMG-WOD produces longer propagation ranges than GDEM in the winter, while ranges in the summer are similar within the two datasets, as modeled in BELLHOP. The most reflective bottom sediment (gravel) produced the longest ranges in both summer and winter, in contrast to other locations, which presented higher attenuation values and produced extremely limited ranges in the summer. Inter-annual variability, as expressed by extended acoustic ranges in SMG-WOD, indicates the need for a dataset with temporal resolution but optimally with higher vertical and horizontal resolution.				
14. SUBJECT TERMS Yellow Sea, inter-annual variability, shallow water acoustics, GDEM, Synoptic Monthly Gridded (SMG)-WOD, BELLHOP			15. NUMBER OF PAGES 161	
			16. PRICE CODE	
17. SECURITY CLASSIFICATION OF REPORT Unclassified	18. SECURITY CLASSIFICATION OF THIS PAGE Unclassified	19. SECURITY CLASSIFICATION OF ABSTRACT Unclassified	20. LIMITATION OF ABSTRACT UU	

THIS PAGE INTENTIONALLY LEFT BLANK

Approved for public release. Distribution is unlimited.

**INTER-ANNUAL VARIABILITY OF THE ACOUSTIC PROPAGATION IN THE
YELLOW SEA IDENTIFIED FROM A SYNOPTIC MONTHLY GRIDDED
DATABASE AS COMPARED WITH GDEM**

Colleen M. McDonald
Lieutenant Commander, United States Navy
B.A., Villanova University, 2005

Submitted in partial fulfillment of the
requirements for the degree of

**MASTER OF SCIENCE IN METEOROLOGY AND PHYSICAL
OCEANOGRAPHY**

from the

**NAVAL POSTGRADUATE SCHOOL
September 2016**

Approved by: Peter C. Chu, Ph.D.
Thesis Advisor

Tetyana Margolina, Ph.D.
Co-Advisor

Peter C. Chu, Ph.D.
Chair, Department of Oceanography

THIS PAGE INTENTIONALLY LEFT BLANK

ABSTRACT

This research investigates the inter-annual acoustic variability in the Yellow Sea identified from the Synoptic Monthly Gridded-World Ocean Database (SMG-WOD) as compared with the Navy's Global Digital Environmental Model (GDEM). The SMG-WOD has a horizontal resolution of 1° , 28 vertical levels from the surface to 3000 m depth and one-month temporal increments allowing individual years of acoustic data to be analyzed, whereas GDEM is a climatological database with a horizontal resolution of $1/4^\circ$ and 78 vertical levels. The Yellow Sea is a semi-enclosed basin located between China and Korea with a mean depth of 40m; acoustics are driven by shallow water dynamics and interaction with the bottom. Seven distinct locations were selected for acoustic comparison based on various depths and bottom types. Composite analysis of the sound speed profiles reveals evident inter-annual variability at all locations, superimposed into a strong seasonal variability. Overall, SMG-WOD produces longer propagation ranges than GDEM in the winter, while ranges in the summer are similar within the two datasets, as modeled in BELLHOP. The most reflective bottom sediment (gravel) produced the longest ranges in both summer and winter, in contrast to other locations, which presented higher attenuation values and produced extremely limited ranges in the summer. Inter-annual variability, as expressed by extended acoustic ranges in SMG-WOD, indicates the need for a dataset with temporal resolution but optimally with higher vertical and horizontal resolution.

THIS PAGE INTENTIONALLY LEFT BLANK

TABLE OF CONTENTS

I.	INTRODUCTION.....	1
II.	OCEANOGRAPHY OF THE YELLOW SEA.....	7
	A. GEOGRAPHY	7
	B. EXTERNAL FORCING	7
	C. THERMOHALINE STRUCTURE.....	8
	D. CIRCULATION.....	10
	E. TIDES, EDDIES, INTERNAL WAVES.....	11
	F. INTERANNUAL VARIABILITY.....	14
III.	THEORY OF ACOUSTIC PROPAGATION IN THE SHALLOW WATER ENVIRONMENT	15
IV.	DATA	21
	A. BATHYMETRY DATABASE.....	21
	B. SEDIMENTS DATABASE	21
	C. GEOACOUSTIC PARAMETERS	23
	D. SMG-WOD	24
	E. GDEM	27
V.	METHODS.....	31
	A. EOF ANALYSIS	31
	B. BELLHOP	32
	C. QUANTIFYING UNCERTAINTY.....	36
	D. MATLAB.....	36
VI.	RESULTS AND DISCUSSION	37
	A. LOCATIONS: BOTTOM SEDIMENTS AND BATHYMETRY	37
	B. TEMPERATURE AND SALINITY DATA FOR GDEM AND SMG-WOD	39
	1. Temperature.....	39
	2. Salinity	42
	C. SOUND SPEED PROFILES.....	45
	1. Mean SSPs	45
	2. SSP Structural Variation	48
	3. SSP Anomaly at Depth	51
	D. EOF ANALYSIS	56

E. TRANSMISSION LOSS ANALYSIS	60
VII. CONCLUSION	69
APPENDIX A. COMPLETE SEDIMENT LIST.....	73
APPENDIX B. ADDITIONAL SMG-WOD TEMPERATURE AND SALINITY FIGURES	83
APPENDIX C. SSP MEANS.....	85
APPENDIX D. EOF.....	93
APPENDIX E. SSP VARIABILITY.....	101
APPENDIX F. TRANSMISSION LOSS	115
APPENDIX G. PROPAGATION POLAR PLOTS.....	123
APPENDIX H. TRANSMISSION LOSS STANDARD DEVIATION YEARS.....	131
LIST OF REFERENCES.....	137
INITIAL DISTRIBUTION LIST	143

LIST OF FIGURES

Figure 1.	Chinese Naval Bases in the Yellow Sea. Source: OSD (2012).	2
Figure 2.	Observed Indicators of a Changing Global Climate. Adapted from IPCC (2013).	5
Figure 3.	Thermocline Seasonal Variability in the China Seas. Source: Hao et al. (2012).	9
Figure 4.	Yellow Sea Current System. Source: Zang et al. (2003).	11
Figure 5.	Yellow Sea Tidal Currents. Source: Chough et al. (2002).	13
Figure 6.	SPP and Propagation Paths. Source: Allen (1980).	16
Figure 7.	Attenuation versus Frequency. Source: Hamilton (1972).	18
Figure 8.	Global XBT Coverage in WOD13.	27
Figure 9.	GDEM Database Shown as a Subset of MOODS. Source: Carnes (2009).	29
Figure 10.	Bellhop Structure. Source: Porter (2011).	35
Figure 11.	HFEVA Sediments with Bathymetry Overlay in the Yellow Sea.	38
Figure 12.	Seasonal Variability of GDEM SST in the Yellow Sea.	40
Figure 13.	SMG-WOD (1945) Seasonal Variability of SST in the Yellow Sea.	40
Figure 14.	GDEM and SMG-WOD (1945) Temperature Variation with Depth.	41
Figure 15.	GDEM Seasonal Salinity.	42
Figure 16.	SMG-WOD (2014) Seasonal Salinity.	44
Figure 17.	GDEM and SMG-WOD (2014) Salinity Variation with Depth.	45
Figure 18.	Location A: SMG-WOD and GDEM Mean SSPs.	47
Figure 19.	Location C: SMG-WOD and GDEM Mean SSPs.	48
Figure 20.	Location A: SSP Structural Variation.	49
Figure 21.	Location F: SSP Structural Variation.	50

Figure 22.	Location A: Standard Deviation of SMG-WOD ΔC .	51
Figure 23.	Location F: SSP Anomalies.	52
Figure 24.	Location F: Cumulative Ncr for SSP Anomalies.	53
Figure 25.	Various Binning SMG-WOD Data to Compare ΔC .	55
Figure 26.	Compare ΔC by Month.	56
Figure 27.	Location A: Eigenvalues and Mode Variance.	57
Figure 28.	Location C: Eigenvalues and Mode Variance.	58
Figure 29.	Location O: Eigenvalues and Mode Variance.	59
Figure 30.	Figure 30. TL Location A.	61
Figure 31.	TL Location E.	62
Figure 32.	Location A: Polar Plots of Propagation Range.	64
Figure 33.	Location E: Polar Plots of Propagation Range.	65
Figure 34.	Total TL GDEM and SMG-WOD.	66

LIST OF TABLES

Table 1.	Comparison of Naval and Oceanographic Depth Zones. Source: NAS (2000).....	4
Table 2.	Inputs to Universal Shallow Water Propagation Model. Adapted from Rogers (1981).....	20
Table 3.	HFEVA Sediment Categories. Source: NAVO (2006).....	23
Table 4.	Geoacoustic Parameters Index. Source: Cintron (2001).....	24
Table 5.	WOD13 Datasets and the Instruments Sources that Contribute Data. Source: Boyer et al. (2013).	25
Table 6.	SMG-WOD Depth Layers. Source: Rodriguez (2016).....	26
Table 7.	Bellhop TL Runs.....	35
Table 8.	Locations A through O by Depth and Bottom Type.....	39
Table 9.	Variances of the Leading EOF modes of Synoptic Monthly Anomaly at All Locations.....	59
Table 10.	Transmission Loss Values SMG-WOD January.	67
Table 11.	Transmission Loss Values GDEM January.	67
Table 12.	Transmission Loss Values SMG-WOD August.	68
Table 13.	Transmission Loss Values GDEM August.	68
Table 14.	Sediment Type Definitions from the Enhanced database. Source: NAVO (2006).	73

THIS PAGE INTENTIONALLY LEFT BLANK

LIST OF ACRONYMS AND ABBREVIATIONS

ADCP	Acoustic Doppler Current Profiler
AIP	air independent propulsion
ASW	anti-submarine warfare
CTD	conductivity, temperature, and density
EAM	East Asian monsoon
EAMI	East Asian monsoon index
EASM	East Asian summer monsoon
EAWM	East Asian winter monsoon
ECSCE	East China Sea cold eddy
EOF	empirical orthogonal function
GUI	graphical user interface
MCM	mine countermeasures
METOC	meteorology and oceanography
MODAS	Modular Ocean Data Assimilation System
MOODS	Master Oceanographic Observational Data Set
NOAA	National Oceanic and Atmospheric Administration
NAVO	NAVOCEANO, Naval Oceanographic Office
NRL	Naval Research Laboratory
OSD	optimal spectral decomposition
PC	principal component
PCA	principal component analysis
PPT	parts per thousand
S	salinity
SD	standard deviation
SMG	synoptic monthly gridded
SONAR	sound, navigation, and ranging
SSP	sound speed profile
SST	sea surface temperature
Sv	Sverdrup (unit of water mass transport)
T	temperature

TSWC	Tsushima Warm Current
TL	transmission loss
USW	undersea warfare
WOA	World Ocean Atlas
WOD	World Ocean Database
XBT	expendable bathymetric thermograph
YSCWM	Yellow Sea cold water mass
YSWC	Yellow Sea Warm Current

ACKNOWLEDGMENTS

First and foremost, I would like to thank Professor Peter Chu for the time and effort he put forth as my thesis advisor. Despite a demanding schedule as a professor and department chair, he always made time for me and handled my questions with grace. I am grateful for his guidance, support, and ability to foster a friendly working environment.

In addition, I want to give a heartfelt thanks to my co-advisor, Dr. Tetyana Margolina. She always addressed my questions with guidance and reassurance. Her expertise with MATLAB is truly impressive and allowed me to present my results more effectively. I appreciate that she made this a professionally rewarding experience, and I will never forget the time she dedicated toward my success.

Finally, I want to thank my program officer, CDR Paula Travis, for her role as a sounding board and mentor throughout the challenges during this process. I am grateful for the personal time and energy she invested in the process to ensure a smooth journey with a positive outcome.

THIS PAGE INTENTIONALLY LEFT BLANK

I. INTRODUCTION

The U.S. Navy has long sought the tactical advantage in the realm of Undersea Warfare (USW)—including Anti-Submarine Warfare (ASW) and Mine Countermeasures (MCM)—by understanding the operational environment and employing sensors efficiently and effectively, in accordance with the environmental conditions. The navy with the strongest understanding of ocean acoustics holds a tactical advantage in operations such as USW, ASW and MCM.

The Yellow Sea is selected for this research due to its strategic political relevance and the scientific opportunity it presents to further research in shallow water acoustics. In recent years, the United States has shifted focus from long-standing engagement in the Middle East to an emphasis on the Asia-Pacific region, creating a colloquial phrase in the defense arena known as the “Pivot to the Pacific.”

In the fall of 2011, the Obama Administration issued a series of announcements indicating that the United States would be expanding and intensifying its already significant role in the Asia-Pacific....Much of the “pivot” to the Asia-Pacific is a continuation and expansion of policies already undertaken by previous administrations....That said, there are a number of new aspects of the shift. The most dramatic lie in the military sphere. (Manyin et al. 2012)

The Pacific is vast and expansive, and the Yellow Sea nested within it is of significance due to its position between China and South Korea. As one of the most flexible and forward forces, the U.S. Navy has increased operations and presence in the various Pacific seas, including the Yellow Sea. Throughout this paper, the term Navy refers to the U.S. Navy unless otherwise stated.

The Navy has a particular interest in this region due to the location of the China’s Northern Fleet at Qingdao. As of 2012, the Chinese naval base at Qingdao was home to more than 20 Chinese submarines and over 40 surface ships (Figure 1) (OSD 2012). The location of this base provides the Chinese naval forces unimpeded access to the Yellow Sea and by extension, access to the South China Sea, the Philippine Sea, and the Sea of Japan.



Figure 1. Chinese Naval Bases in the Yellow Sea. Source: OSD (2012).

The Navy also operates within these waters to ensure freedom of access and navigation to all U.S. forces and commercial traffic in international waters (McDevitt et al. 2012). Therefore, the Navy relies upon the most current and accurate environmental data, particularly acoustic expertise, to communicate safely with submarine assets but also to locate MCM operations in such shallow waters.

Historically, deep-water acoustics has been the focus of sound propagation research in the ocean, but this shifted in the early 1990s, as scientists realized the increased dynamics and dimensionality presented by shallow water acoustics. Today, propagation of sound in shallow water has become the main focus of underwater

acoustics research, as it has applications to the military, engineers, and scientists (Oh, 2013). As the understanding of shallow water acoustics has grown, so has the realization of the number of parameters affecting sound speed, and the complexity of models for shallow water acoustics also has increased. This thesis supports continuing the work of the Naval Research Program topic “synoptic monthly gridded and ocean modeled data to assess submarine vulnerability” (Chu 2016).

The desire to reduce submarine vulnerability resides in being able to detect submarines, particularly those that are ultra-quiet due to air independent propulsion (AIP). Diesel submarines run on AIP, and there are 18 of them just in Qingdao (Figure1). The Navy predominantly used mid-frequency sonar for prosecuting AIP diesel submarines; the mid-frequency range for this paper is considered to be 1kHz to 10kHz (DOJ 2016). The full extent of naval sonar capability extends beyond this mid-range, and the Navy will sometimes use specific systems that are of lower frequency for long-range detection, or higher frequencies as the tactical situation requires.

While temperature and salinity are the primary contributors to determining how sound will propagate in the water column, the transmission of sound in shallow water is also dependent on the bottom type. For naval operations, MCM in particular, the depth of the water and the bottom type are crucial factors in modeling and predicting acoustic propagation. As this research is on the Yellow Sea, with relatively shallow water depths in comparison to the rest of the world’s ocean, defining the use of the terms shallow water, very shallow water, or deep water is required. Terms used to define water depths differ between the Navy and the oceanography community (Table 1). In scientific and academic arenas, shallow water is alternately defined as a condition where the ratio of water depth to wavelength of the sound is very small, which can be vague and requires definition per every application.

Table 1. Comparison of Naval and Oceanographic Depth Zones.
Source: NAS (2000).

	Definition* (ft.)		Definition (m)
Surf zone	0-10	Surf zone	Zone of wave energy dissipation
Very shallow water	10-40	Inner shelf	0-30
Shallow water	40-200	Middle shelf	30-100
Deep water	>200	Outer shelf	100-130
		Slope	>130

*Note change of units between the naval and oceanographic depth zone columns.

Observations suggest that the sea surface is warming due to climate change, particularly in the past few decades (IPCC, 2013; also see Figure 1). Shallow bodies of water are especially vulnerable to this effect, as there is more warming per depth of water in which to operate. An increased sea surface temperature may alter the water density, and dependent on the air-sea interactions, the pycnocline also may be impacted.

The Intergovernmental Panel on Climate Change (IPCC) consists of thousands of interdisciplinary scientists who come together annually to review research completed on climate change, its impact and solutions, and how to frame the problem for the average citizen and policy maker. IPCC first met in 1988, and it has since grown to include over 190 participating countries. It is valuable to note that IPCC does not perform any experimentation of its own or, nor does it seek political gain. The panel serves as a sounding board and equalizer of information to show that the world climate is in fact warming due to anthropogenic causes (Anderegg et al. 2010; Solomon et al. 2009). To put this in terms for this research, if oceans are warming more rapidly now than ever before, then perhaps the climatologic databases dating back to 1945 or earlier are no longer accurate enough for acoustic modeling to meet the needs of the Navy.

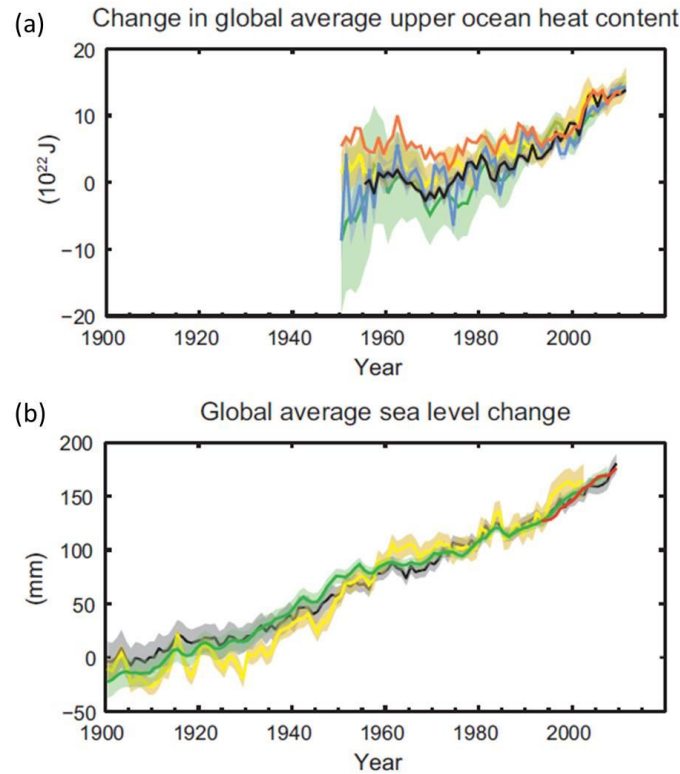


Figure from Working Group I to the Fifth Assessment report on the IPCC Report for 2013. “(a) change in global mean upper ocean heat content aligned to 2001–2010, and relative to the mean of all datasets for 1970. ... (b) global mean sea level relative to the 1900–1905 mean of the longest running dataset, and with all datasets aligned to have the same value in 1993. Time series show annual values, and where assessed, uncertainties are indicated by colored shading” (IPCC 2013).

Figure 2. Observed Indicators of a Changing Global Climate.
Adapted from IPCC (2013).

Uncertainty in the environmental input data, uncertainty due to sensitivity or settings of the model, and uncertainty due to sensitivity of the receiver cause the uncertainty in acoustic propagation. As the term “uncertainty” can be vague and alternately defined, this work will defer to the definition provided by Emerson et al. (2015) that uncertainty is the variability in both environmental and system-related inputs. Acoustic uncertainty is inferred from the measured variability of transmission loss, and it should be noted that uncertainty and variability are generally different, although sometimes used interchangeably.

Addressing acoustic propagation uncertainty, particularly transmission loss, is a growing area of study, as the amount of uncertainty in an acoustic prediction provides valuable information for the military or civilian operator of sonar equipment. Error localization and the source of the sound contribute to the acoustic uncertainty. Research has shown that uncertainty in acoustic modeling is also seasonally dependent, where summer sound speed profiles (SSPs) revealed a Gaussian-type distribution, and winter SSPs displayed non-Gaussian type (Chu et al. 2002).

This thesis is organized as follows: Chapter II describes the Yellow Sea oceanography, and Chapter III discusses theoretical aspects of acoustic propagation in the shallow water environment. Chapters IV and V contain descriptions of data and methods, respectively. Results are described and discussed in Chapter VI. Conclusions and recommendations are presented in Chapter VII.

II. OCEANOGRAPHY OF THE YELLOW SEA

A. GEOGRAPHY

The Yellow Sea is a shallow basin enclosed by China to the west and Korea to the east; it interacts with the northern edge of the East China Sea at 32° N. The entire basin is mostly shallow with a mean depth of 50 m or less and a maximum depth of 140 m. The only location of water deeper than 70m is within a center line trench in the Yellow Sea. Chu et al (2005) explain the orientation of this trench and depth as “the deepest water is confined to a north-south-oriented trench which runs from the northern boundary south to the 100m isobaths where it fans out onto the continental shelf break.” With such shallow average depth, we can classify most of the region of interest as shallow water.

Seasonal impacts on the thermohaline structure of the Yellow Sea are well researched and documented. The bathymetry of the Yellow Sea, having “such a broad and shallow continental shelf sea suggest that the water column will be readily affected by seasonally varying atmospheric conditions such as heating, cooling and wind stress” (Chu et al. 2005). Changes in the atmospheric conditions would contribute to an overall understanding of the interannual variability have also been researched, such as fresh water river outflow and sea surface temperature (SST), but none of the previous research directly researches the interannual variability of the SSP and thus the interannual variability of acoustic transmission loss throughout the Yellow Sea. The sensitivity of this body of water to seasonal forcing is expected to be important too due to strong monsoon.

B. EXTERNAL FORCING

Atmospheric forcing plays significant role in the thermal structure throughout the Yellow Sea. As weather patterns shift due to seasonal and interannual variability, the effective air-sea interaction can alter the acoustic properties of the water. Storms increase the wind stress contributing to mixing and deepening of the thermocline, and increased precipitation will alter the local salinity.

The Yangtze River, also referred to as the Changjiang River, supplies nearly 80% of the fresh water that enters the Yellow Sea and subsequently, the adjoining seas. The discharge of this river provides the key source of fresh water in the region. Data revealing the variation in output volume transport may be useful in understanding the fresh water intrusion in the Yellow Sea and allow for prediction.

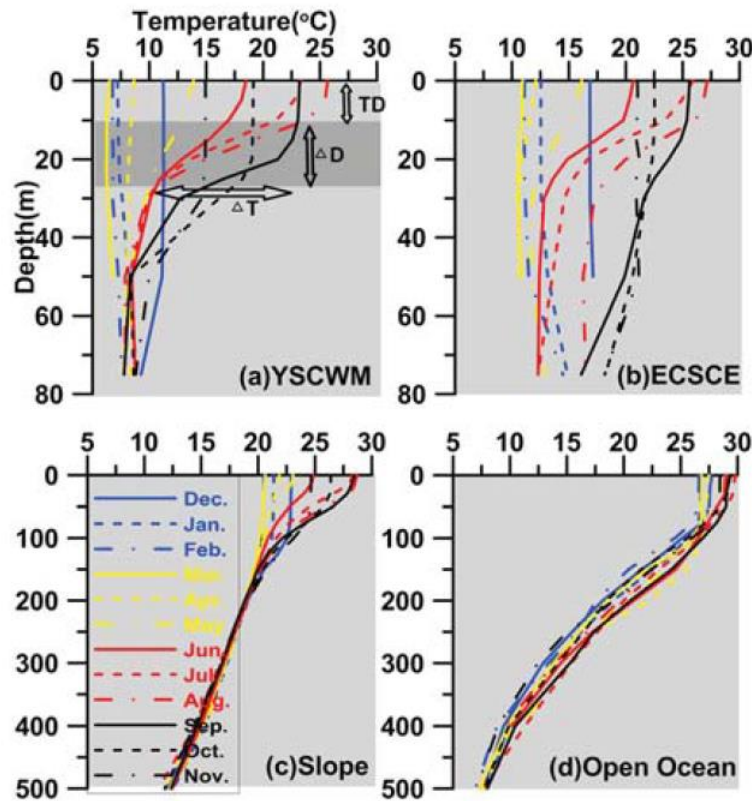
Its monthly mean transport has a large seasonal variation from 0.010 Sv ($1\text{Sv}=10^6\text{m}^3/\text{s}$) in January to 0.048Sv in July around an annual mean of 0.030 Sv, and large interannual variations in the annual mean from 0.022 to 0.035 Sv during the 19-year period from 1970 to 1988. (Ichikawa and Beardsley 2002)

Large interannual variation of the volume of fresh water entering the Yellow Sea suggests that there may be a large interannual variability in the SSP as the cooler, fresher water of the Yangtze River flows into the Yellow Sea.

C. THERMOHALINE STRUCTURE

Previous research on the Yellow Sea thermal structure by Fralick in 2001 shows a strong correlation between the SST and the thermocline gradient. However, his research did not address interannual variability. Researchers have further explored spatial and temporal variability of SST and many of them are able to draw conclusions of warming SSTs in the marginal seas of China from the 1980s and onward (Bao and Ren 2014; Park et al. 2015).

Previous studies have shown that the Yellow Sea, as a shallow body of water, displays high seasonal variability in the thermocline and halocline as compared to the deeper open ocean. Hao et al. (2012) confirms the absence of a thermocline during winter months in the Yellow Sea Cold Water Mass (YSCWM) and the adjacent East China Sea cold eddy (ECSCE) (Figure 3).



Climatological monthly mean temperature profiles in the (a) Yellow Sea cold water mass (YSCWM), (b) East China Sea cold eddy (ECSCE), (c) slope, and (d) open ocean. The locations are specifically chosen to reveal how water depth affects the sensitivity to atmospheric forcing.

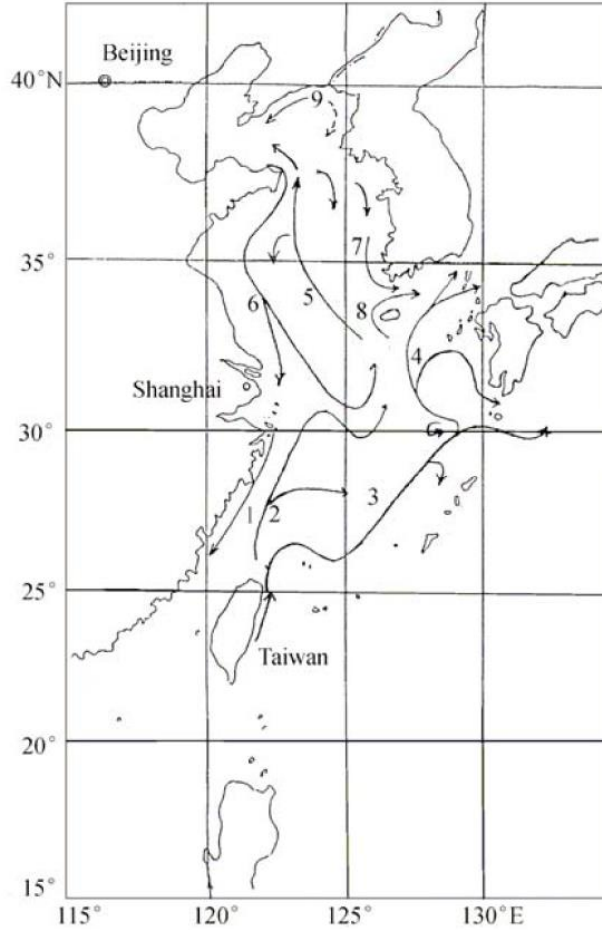
Figure 3. Thermocline Seasonal Variability in the China Seas.
Source: Hao et al. (2012).

These seasonal thermocline patterns showed similar results when studied by Chu et al. (2003). As an introduction, “the seasonal variability of the atmospheric forcing is evident in the strong winter monsoon (north to northeast) and weak summer monsoon (southeast)” (Chu et al. 2003). As strong seasonal thermohaline variability is typical for shallow bodies of water, one can readily apply the results of experimentation in Yellow Sea to other shallow bodies that are of interest to the Navy such as the Arabian Gulf.

D. CIRCULATION

The Yellow Sea circulation has been studied for nearly a century with some initial characterization of the Yellow Sea Warm Current (YSWC) dating back to 1930. However, some of the earlier published research on the source of the YSWC water has been updated over the past two decades. Research by Zang et al. (2003) clarifies that the origin of the YSWC is a mixture of water from the Tsushima Warm Current (TSWC) and the continental shelf of the East China Sea (ECS), as opposed to the older hypothesis that it was a branch from the Kuroshio. This discovery was verified through the extensive employment of CTDs, drifter buoys, ADCPs, and satellite data, which traced the source and paths of the currents.

While the river discharge accounts for the fresh water intrusion into the Yellow Sea, the “YSWC is the main component of the YS circulation and also a flow transporting the external water with high T and high S into the YS” (Zang et al. 2003). The general flow pattern is the YSWC running northward in the center of the Yellow Sea bringing salty warm water, with coastal currents bringing fresher and cooler water southward along the outer edges of the Yellow Sea. As seen in Figure 4, the interacting currents that impact water transport in the Yellow sea are labeled.



Schematic pattern of circulation in the YS and ECS in the cold season. 1, Minzhe coastal current; 2, Taiwan warm current; 3, Kuroshio; 4, Tsushima warm current; 5, Yellow Sea warm current; 6, Yellow Sea coastal current; 7, Korea coastal current; 8, Cheju warm current; 9, Liaonan coastal current.

Figure 4. Yellow Sea Current System. Source: Zang et al. (2003).

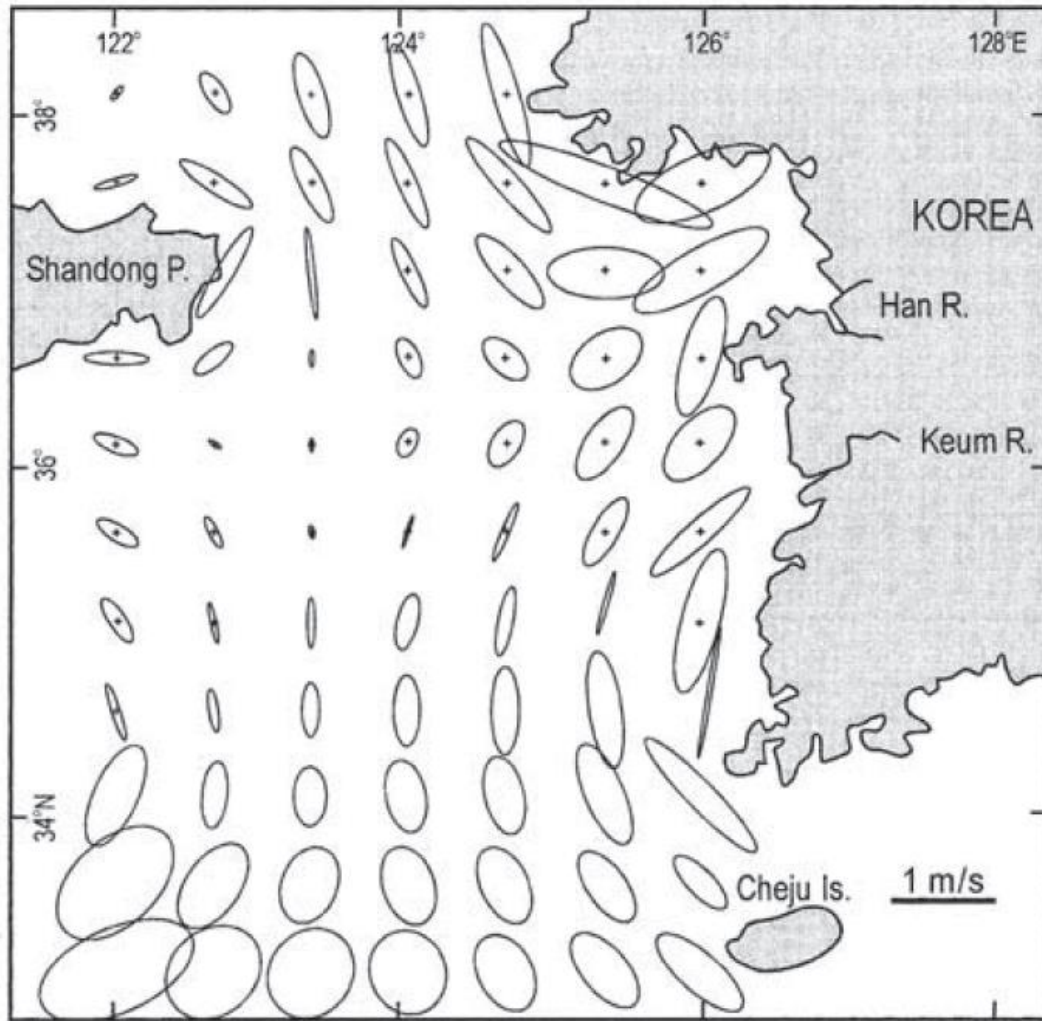
E. TIDES, EDDIES, INTERNAL WAVES

Tides and induced tidal currents in the Yellow Sea play an important role in the acoustic variation in the region. Oh et al. (2013) showed the dependence of acoustic variation on tides by modeling environmental data collected from a system of six CTDs deployed from buoys at a fixed ocean observation station in the Yellow Sea. The tide system and patterns in the Yellow Sea not only induce mixing of water properties, but the tides also contribute to sediment transport that is a complex process occurring through the Yellow Sea. Rivers along the coast of Korea are continually depositing fine grain

sediments eastward into the Yellow sea and then southward, developing a “mud belt” 60 m thick along the Korean peninsula (Chough et al. 2002). The dispersion of sediments and the bottom type plays a significant role in shallow water acoustics as will be addressed later in this thesis.

The tidal currents are strongest in the northeastern Yellow Sea (Figure 5); the stronger the current, the larger the tidal ellipse. The strength of the tides in the Yellow Sea is significant as “tidal currents are over 1 m/s in Kyonggi Bay and near the southeastern tip of the Korean peninsula and diminish in speed offshore, trending nearly N-S in the central Yellow Sea” (Chough et al. 2002). The coastal regions throughout the Yellow Sea often experience diurnal tidal patterns beyond 4m. The monsoonal winds also affect the surface currents, changing the overall northward surface flow in the summer to a southward flow in the winter (Chough et al. 2002).

Internal waves contribute to the overall mixing and turbulence within the water masses of the Yellow Sea and impact sound speed profiles. The strongest signature of solitary internal waves, were initiated at the continental shelf break with waters moving from the ECS to the Yellow Sea (Hsu et al. 2000). The primary source for observing the internal waves in the region was by use of synthetic aperture radar (SAR) via satellites. This resulted in imagery output where heights and directions of the internal waves were calculated from known settings. The internal waves were present year round, but most notably, it sharpened the pycnocline across the shelf by the end of the summer (Liu et al. 2008).



The M2 tidal model of the Yellow Sea shows the anti-clockwise rotation of tidal currents (Chough et al. 2002).

Figure 5. Yellow Sea Tidal Currents. Source: Chough et al. (2002).

In addition to atmospheric forcing, the temperature and salinity in the Yellow Sea are also influenced by the introduction of relatively fresh water from the Yangtze River, by the introduction of water from the YSWC, and from eddies that spin up along the shelf. The introduction of the source water with varying temperature and salinity into the Yellow sea is valuable to this research, as alterations in these properties will affect the acoustic propagation.

F. INTERANNUAL VARIABILITY

One of the more notable phenomena dominating weather patterns is the East Asian Monsoon (EAM). The EAM is quite a complex weather system with global impact, characterized by distinct seasonal interannual variation of the East Asian Summer Monsoon (EASM), and the East Asian Winter Monsoon (EAWM) (Li and Zeng 2003; Zhu et al. 2005).

The East Asian Monsoon index (EAMI) represents the seasonal and interannual variability of the EASM and the EAWM; it was calculated based on the zonal and meridional land-sea temperature gradients throughout Asia-Pacific region (Zhu et al. 2005). The EAMI is a useful tool in predicting the EASM and EAWM onset and intensity. The initiation of an EASM is generally represented by unique rainfall patterns over the region and dominant meridional circulation. The EAWM onset is typically characterized by an Aleutian low-pressure system and a Siberian high-pressure system that prevails across the mid-latitudes and dominate zonal flow pattern. By mapping the interannual variability of the EAMI from 1979 through 2003, Zhu et al. (2005) were able to define strong and weak years for both the EASM and the EAWM. The EASM was strong in four years (1981, 1985, 1990, and 1999) and weak in five years (1980, 1983, 1991, 1995, and 1996). The EAWM was strong in six years (1983, 1991, 1992, 1995, 1996, and 2003) and weak in five years (1979, 1985, 1989, 1999, and 2001).

Research has shown that onset and duration of these monsoons vary, and the seasonal and annual precipitation across the region also varies. Wang and Zhou (2005) were able to draw a correlation between monsoonal trends and extreme precipitation rates through China, showing that “extreme precipitation events in the Yangtze River basin increased dramatically by 10%-20% every 10 years in summer, consistent with increasing trends.” Due to the large output volume of the Yangtze into the Yellow Sea, it is important to realize the precipitation patterns and how they the impact acoustic properties. In similar efforts, Wang and Zhou (2005) were able to compare two datasets of monthly mean precipitation over the Yangtze River basin, where the summer months reached nearly 70mm, and the winters months were as low as 10–20mm. This drastic influx of freshwater to the Yellow Sea in the summer will alter the salinity and potentially the acoustic propagation.

III. THEORY OF ACOUSTIC PROPAGATION IN THE SHALLOW WATER ENVIRONMENT

The Medwin equation developed by Herman Medwin (1975) is an equation that is used to calculate the speed of sound in water when you know the temperature, salinity and depth of the water. As sound speed in water drives the acoustic path, “knowing the speed of sound in water is critical to many of the applications of acoustical oceanography” (Clay and Medwin, 1998).

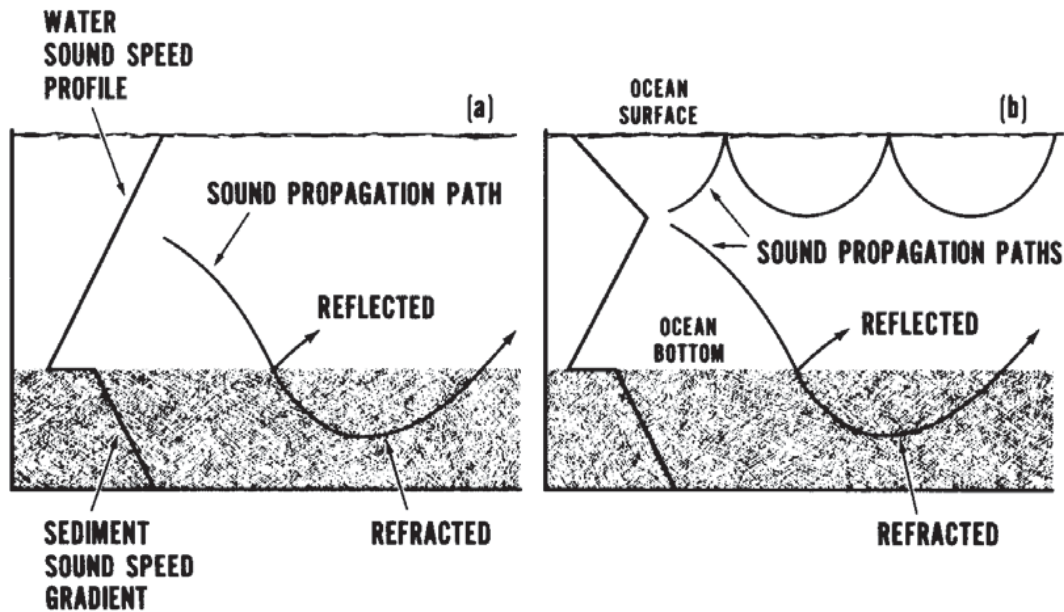
$$c = 1449.2 + 4.6T - 0.055T^2 + 0.00029T^3 + (1.34 - 0.010T)(S - 35) + .016z \quad (1)$$

where c represents the speed of sound in m/s, T represents temperature in degrees Celsius, S represents salinity in psu (practical salinity units), and z represents the depth of the water in meters. The depth is a key factor in determining the pressure, as pressure increases with depth. Sound speed in water increases as each or any combination of these factors, T , S , or z increases.

While each of these properties (T , S , z) influences sound speed, they do so with differing degrees significance. It is widely accepted that per every degree of temperature increase, sound speed increases by 4.0 m/s. For every 100m depth increase, speed increases by 1.7m/s, and for every 1ppt increase of salinity, by 1.4 m/s. Water pressure is generally omitted in calculating the speed of sound in shallow water. Because the water is not deep enough for the overlying weight to contribute in altering the pressure, it does not affect the shallow water speed of sound. This is the case for the Yellow Sea, where depth rarely exceeds 100m.

A sound speed profile (SSP) is calculated from temperature and salinity profiles and shows how the speed of sound in water varies with increasing depth. The vertical gradient of the SSP will direct the movement of the sound (Figure 6). In an environment where the SSP varies with depth, the path that the underwater sound travels will change.

The path of sound through the water column, i.e., the propagation path, is modeled in the simplest way with a ray. Each single path shown in Figure 6 is an individual ray path. Due to shallow depth of the Yellow Sea, the only expected paths are direct path, bottom bounce (reflected or refracted), or potentially surface ducts when there is a strong thermocline. According to Snell's law, as sound passes through levels of water with different acoustic properties, the ray will bend toward the region where sound moves slower, thus creating a propagation path.



a) A sound speed profile with a negative gradient will cause the sound energy to be refracted downward there by causing a bottom limited condition where energy is either reflected at the sediment water interface or refracted by the sediments. b) Positive sound speed profiles or shallow ducts result in the sound energy being propagated through the water with less interaction with the bottom (Allen, 1980).

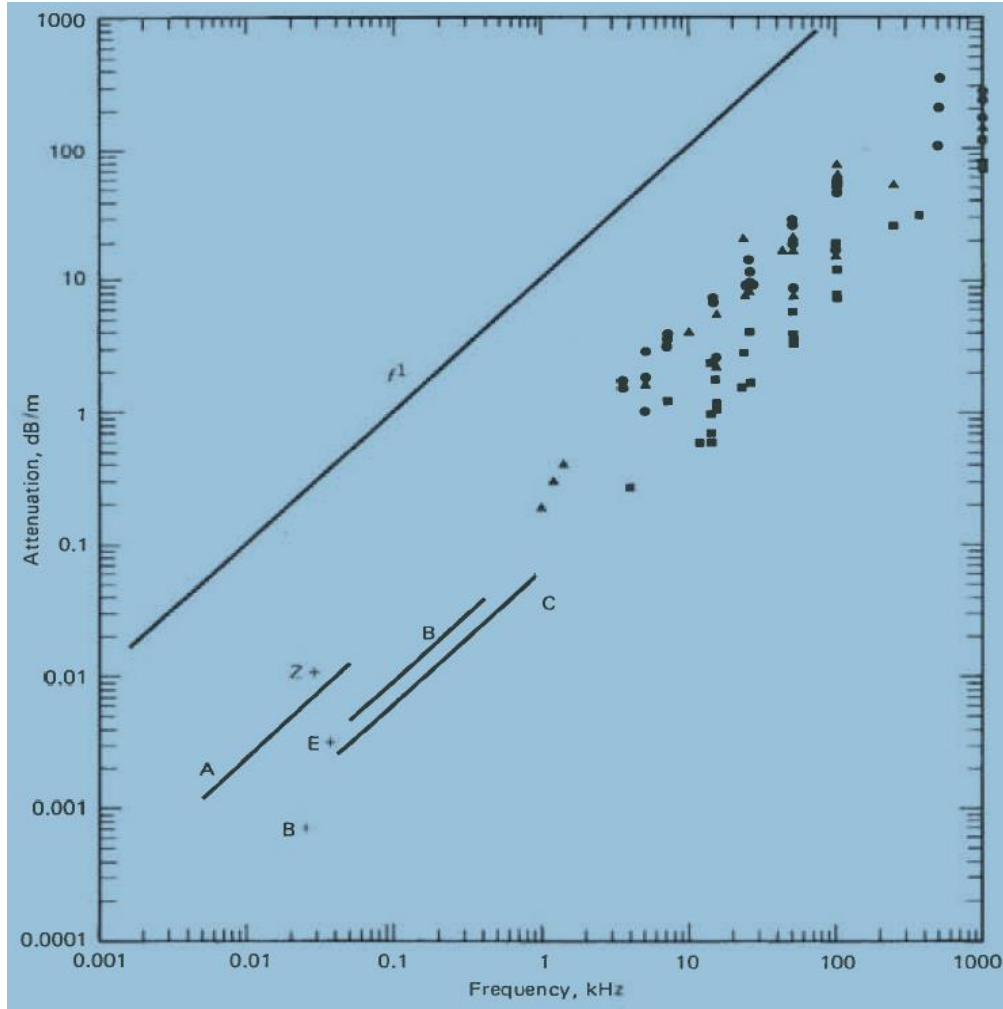
Figure 6. SPP and Propagation Paths. Source: Allen (1980).

It is important to understand that “the effect of seasonal changes in the sound speed profile in shallow water can cause severe differences in the role the ocean bottom plays in contributing to the transmission loss of sound in shallow water” (Allen 1980). The seasonal variability affects the shallow water SSP, and in turn, the effect on the transmission loss is well document in experimentation done by Chu and Cintron in 2001.

Although the sound speed profile continues to be the single most important environmental parameter in determining the interaction of sound with the geologically controlled ocean bottom, the bottom [sediment] far surpasses the oceanographic controlled sound speed profile in complexity and lack of knowledge. (Allen 1980)

In order to best account for the bottom effect, and in an effort to reduce the uncertainty, scientists have developed geoacoustic models. According to Hamilton (1980), “a ‘geoacoustic model’ is defined as a model of the real sea floor with emphasis on measured, extrapolated, and predicted values of those properties important in underwater acoustics and those aspects of geophysics involving sound transmission.” The bottom sediment composition and layers is particularly important in shallow water due to the likelihood of the sound interacting with the bottom. In addition to the source frequency, the bottom type will determine/influence attenuation by altering the reflection, absorption, and refraction of sound.

When developing or selecting a geoacoustic model it is useful for researchers to define the frequencies they will be working with, as it impacts how deep into the sediments the sound will interact. Sound interaction with the bottom will vary greatly depending on the sediment type. Sound in the water will be absorbed, scattered, or reflected in varying manners contributing to its attenuation dependence on the bottom composition being solid rock, sandy, gravel, etc.



Attenuation versus frequency in natural, saturated sediments and sedimentary strata; Symbols: circles—sands (all grades); squares—clayey silt, silty clay; triangles—mixed sizes (e.g., silty sand, sandy silt, sand-silt-clay); sand data at 500 and 1000 kHz. Low frequency data: Line labeled “f¹” indicates slope of any line having a dependence of attenuation on the first power of frequency. (Hamilton 1972).

Figure 7. Attenuation versus Frequency. Source: Hamilton (1972).

$$\alpha = k f^n \quad (2)$$

Attenuation contributes to the overall transmission loss. Attenuation from various bottom type sediments reveals a power law characteristic (Figure 7), where α is the attenuation factor (dB/m); f is the frequency (kHz); k is a constant; and n is the exponent of frequency (equation 2). The k parameter is the only source of variability in the attenuation equation and it depends on the sediment type (porosity and grain size). As

attenuation is related to frequency approximately by the first power, n has a value of one and can be neglected for these mid frequency ranges. Attenuation is represented by dB/λ with simple conversion (Equation 3).


$$(\text{dB/m})(c/f) = \text{dB}/\lambda. \quad (3)$$

In shallow water, sound of higher frequencies will experience more interaction with the bottom and thus attenuate rather quickly, not traveling a long distance. Frequency may also change the expected propagation paths in water. “For example, even in coastal waters ‘high frequency’ sound displays propagation characteristics typical of those for deep water” (Ali 1993).

Propagation loss in shallow water is affected by many parameters, far more than the deep water acoustics model requires. Transmission loss and propagation loss will be used interchangeably through this paper to address the amount of overall dissipation of the sound's energy as it passes through water. There are 24 input parameters to consider when modeling propagation loss in shallow water (Table 2). Parameters 3–13 pertain to bottom sediment characteristic of a specific layer; for each sediment layer an additional 11 inputs would be required. Water depth, SSP, and surface of the bottom type will be the key parameters applied to assess acoustic variability in this research.

Table 2. Inputs to Universal Shallow Water Propagation Model.
Adapted from Rogers (1981).

1.	Water Depth
2.	Sound Speed Profile
	A. Temperature
	B. Salinity
3.	Acoustic Attenuation in Water
4.	Density of Sediment
5.	Sound Speed in Sediment
6.	Shear Speed in Sediment
7.	Acoustic Attenuation in Sediment
8.	Shear Attenuation in Sediment
9.	Sound Speed Gradient in Sediment
10.	Shear Speed Gradient in Sediment
11.	Attenuation Gradient in Sediment
12.	Density Gradient in Sediment
13.	Thickness of Sediment Layer
14.	Sound Speed in Basement
15.	Shear speed in Basement
16.	Density of Basement
17.	Acoustic Attenuation in Basement
18.	Shear Attenuation in Basement
19.	Surface Roughness
20.	Bottom Roughness
21.	Subbottom Roughness
22.	Gas Bubbles
23.	Biological Scatterers
24.	Wind Vector


 x the number of sediment layers

IV. DATA

Four environmental datasets and one acoustic model were used to produce data on acoustic interannual variability used in this research (Allen and U.S. Navy 2012, Chu and Fan 2016b, NAVO 2006, NAVO 2009, and Porter 2011). Prior to pulling the temperature and salinity data, the bathymetry and bottom sediment data was extracted for the region of interest. Once these initial characteristics are plotted, the two foundational datasets of temperature and salinity profiles to be compared in this research, GDEM and SMG-WOD, were extracted for this region.

A. BATHYMETRY DATABASE

Bathymetry data used for this research is extracted from the NAVO database Digital bathymetric Database-Variable resolution (DBDB-V) version 5.4. The DBDB-V is produced and availed for use at three classification levels; this research utilizes the Level 0, which is unclassified data allowed for public release (NAVO 2006). NAVO specifically designed this data to be easily incorporated into bathymetric chart, or to be combined with other environmental ocean parameters for modeling purposes.

The user may select the desired resolution of bathymetry data available in in arc minutes of either 2', 1', 0.5, or 0.1'. The database design description recommends appropriate use for each resolution and the limitations each resolution contains. The 2-minute arc grid was generated by compiling information from various publicly available sources in 2004, and it is the only resolution that provides complete global coverage. The finer resolutions were developed by incorporating data from hard copy charts and converting it into a digital format and running the data through sophisticated computer algorithms (NAVO 2006). The present research uses a 0.5' resolution.

B. SEDIMENTS DATABASE

There are four openly available sediment databases: Enhanced, Standard, Reduced, and High Frequency Environmental Acoustics (HFEVA). The bottom sediment characteristics of the research area of interest can be extracted from any one of these

databases, but with varying degrees of resolution available across the globe. “The Enhanced is the actual database that is maintained by NAVO. It is suitable for researchers and developers with technical geologic knowledge, or in cases where the most geologic information is desired” (NAVO 2006). Due to the redundancy and sometimes ambiguous nature of the large enhanced dataset, it is generally considered too cumbersome for operational application. Operational or tactical use of the data is best retrieved from a subset of the total data such as HFEVA (used in the present research), reduced, or standard.

The HFEVA sediment categories are provided in Table 3. HFEVA categories range from 1–23, with two additional; 888 referring to “no data” and 999 referring to “land.” The enhanced database includes 88 and 999, but the categories range from 0102–6890. The comparison between the HFEVA and the enhanced is that, grouping many similar bottom types under one category heading for simplification. For example, within the enhanced database code 3308 is listed as clay with the additional categorization as HT (hemi pelagic and terrigenous). This corresponds to code 23 in the HFEVA database, which denotes a bottom type of clay. Depending on the field of study, it may be important to know that “pelagic and hemipelagic sediments are mostly fine-grained deposits, the product of slow deposition in typically low-energy depositional environments” which make up 50% of the Earth’s surface (Garrison 1990). However, when the bottom type is composed of small particulate matter that responds acoustically similar regardless of the origin (land/sea, organic/inorganic) then less granularity of classification is required. A complete table of the Enhanced sediment categories is in the appendix.

Each sediment dataset with a focus on the Yellow Sea is plotted in order to determine which dataset is most appropriate for this research. The baseline resolution extracted was 1. Individual sediment plots were also mapped at resolutions of 0.5° and 5.0° for comparison to the 1° resolution sediment data to see if there were significant differences necessitating resolutions other than 1°.

Table 3. HFEVA Sediment Categories. Source: NAVO (2006).

HFEVA Standard Sediment Type	HFEVA Category
Rough Rock	1
Rock	2
Cobble or Gravel or Pebble	3
Sandy Gravel	4
Very Coarse Sand	5
Muddy Sandy Gravel	6
Coarse Sand or Gravelly Sand	7
Gravelly Muddy Sand	8
Medium Sand or Sand	9
Muddy Gravel	10
Fine Sand or Silty Sand	11
Muddy Sand	12
Very Fine Sand	13
Clayey Sand	14
Coarse Silt	15
Gravelly Mud or Sandy Silt	16
Medium Silt or Sand-Silt-Clay	17
Sandy Mud or Silt	18
Fine Silt or Clayey Silt	19
Sandy Clay	20
Very Fine Silt	21
Silty Clay	22
Clay	23
<i>No data</i>	888
<i>Land</i>	999

C. GEOACOUSTIC PARAMETERS

The geoacoustic parameters will change based on the bottom type as determined from the sediment database. The pertinent geoacoustic parameters to this research are the attenuation coefficient and, the compressional sound speed, and the sediment density. The attenuation coefficient is calculated at each location (sediment type), as discussed in Chapter III. The compressional sound speed (sound speed ratio) and the density are available in Table 4. The geoacoustic parameters are part of the input data required to run the acoustic model.

Table 4. Geoacoustic Parameters Index. Source: Cintron (2001).

Bottom Sediment Composition	Bulk Grain Size Index	Long (32 Char) Name	Density gm/cm ³	Sound Speed Ratio	Wave Number Ratio
BOULDER	-9	Rough Rock	2.5	2.5	0.0137
ROCK	-7	Rock	2.5	2.5	0.0137
GRAVEL	-3	Gravel, Cobble or Pebble	2.5	1.8	0.0137
	-1	Sandy Gravel	2.492	1.337	0.01705
	-0.5	Very Coarse Sand	2.401	1.3067	0.01667
	0.0	Muddy Sandy Gravel	2.314	1.2778	0.01630
	0.5	Coarse Sand	2.231	1.2503	0.01638
	1.0	Gravelly Muddy Sand	2.151	1.2241	0.01645
SAND	1.5	Sand or Medium Sand	1.845	1.1782	0.01624
	2.0	Muddy Gravel	1.615	1.1396	0.01610
	2.5	Silty Sand or Fine Sand	1.451	1.1073	0.01602
	3.0	Muddy Sand	1.339	1.0800	0.01728
	3.5	Very Fine Sand	1.268	1.0568	0.01875
	4.0	Clayey Sand	1.224	1.0364	0.02019
	4.5	Coarse Silt	1.195	1.0179	0.02158
	5.0	Sandy Silt	1.169	0.9999	0.01261
	5.5	Medium Silt	1.149	0.9885	0.00676
SILT	6.0	Silt	1.149	0.9873	0.00386
	6.5	Fine Silt	1.148	0.9861	0.00306
MUD	7.0	Sandy Clay	1.147	0.9849	0.00242
	7.5	Very Fine Silt	1.147	0.9837	0.00194
	8.0	Silty Clay	1.146	0.9824	0.00163
CLAY	9.0	Clay	1.145	0.9800	0.00148
	10.0		1.145	0.9800	0.00148

D. SMG-WOD

SMG-WOD is one of the many databases developed from the overarching World Ocean Database (WOD) maintained by NOAA (WOD 2016). The current version of WOD, WOD13, has expanded from the earlier databases, which contained only six variables over 40 layer depth, into a massive open source database with 148 layer depths and over 20 variables (Boyer et al. 2013). The WOD13 database contains a “collection of scientifically quality-controlled ocean profile and plankton data that includes measurements of temperature, salinity, oxygen, phosphate, nitrate, silicate, chlorophyll, alkalinity, pH, pCO₂, TCO₂, Tritium, $\Delta^{13}\text{Carbon}$, $\Delta^{14}\text{Carbon}$, $\Delta^{18}\text{Oxygen}$, Freons, Helium, $\Delta^3\text{Helium}$, Neon, and plankton” (Boyer et al. 2013). In Table 5, the source instruments by which all of these data are collected are itemized.

The datasets of particular interest to ocean acoustics are OSD (ocean station data), CTD (conductivity, temperature, depth), and XBT (expendable bathythermograph); as these datasets provide measurements of temperature, salinity, or both. Instruments such as the DRB (drifting buoy) are useful for recording sea surface temperature, but may also be used to characterize the thermocline structure if they are equipped with long enough thermistor chains extending from the buoy.

Table 5. WOD13 Datasets and the Instruments Sources that Contribute Data.
Source: Boyer et al. (2013).

DATASET	SOURCE
OSD	Bottle, low-resolution Conductivity-Temperature-Depth (CTD), low-resolution XCTD data, and plankton data
CTD	High-resolution Conductivity-Temperature-Depth (CTD) data and high-resolution XCTD data
MBT	Mechanical Bathythermograph (MBT) data, DBT, micro-BT
XBT	Expendable (XBT) data
SUR	Surface only data (bucket, thermosalinograph)
APB	Autonomous Pinniped Bathythermograph - Time-Temperature-Depth recorders attached to elephant seals
MRB	Moored buoy data from TAO (Tropical Atmosphere-Ocean), PIRATA (moored array in the tropical Atlantic), MARNET, and TRITON (Japan-JAMSTEC)
PFL	Profiling float data
DRB	Drifting buoy data from surface drifting buoys with thermistor chains
UOR	Undulating Oceanographic Recorder data from a Conductivity/Temperature/Depth probe mounted on a towed undulating vehicle
GLD	Glider data

Over the years, as the amount of data in the WOD has grown immensely, it became necessary to create various filters on the data, allowing researchers to pull only the pertinent data they required. One such popular dataset is the World Ocean Atlas (WOA), which used the unevenly distributed WOD data to create gridded climatological monthly fields of oceanographic data. Locarnini et al. (2013) developed the gridded dataset for temperature data, and Zweng et al. (2013) developed the dataset for salinity. The WOA is accessible via the NOAA website (WOA 2016).

A new dataset, referred to as SMG-WOD throughout the rest of this paper, has been generated using the Optimal Spectral Decomposition method (thereafter OSD-method). The OSD-method had been used in ocean data analysis, where it proved

successful in drawing out ocean phenomena that had not previously been apparent (Chu et al. 2005; Chu et al. 2007; Chu 2011), but it may also be used in ocean data assimilation (Chu et al. 2015). This method makes use of the topography and lateral boundary conditions, and is different from previous ocean data interpolation methods, for example optimal interpolation (OI), because it does not require a background error covariance matrix (Chu and Fan 2016a). As it is dependent on the lateral boundary condition, the SMG-WOD dataset does not contain data for geographically closed bodies of water. The effectiveness of OSD used in this manner was tested on data using the Parallel Ocean Program (POP) model (Smith 2002).

SMG-WOD maintains spatial resolution for temperature and salinity as found in the WOA2013, but allows for greater time resolution (synoptic versus climatological).

Table 6. SMG-WOD Depth Layers. Source: Rodriguez (2016).

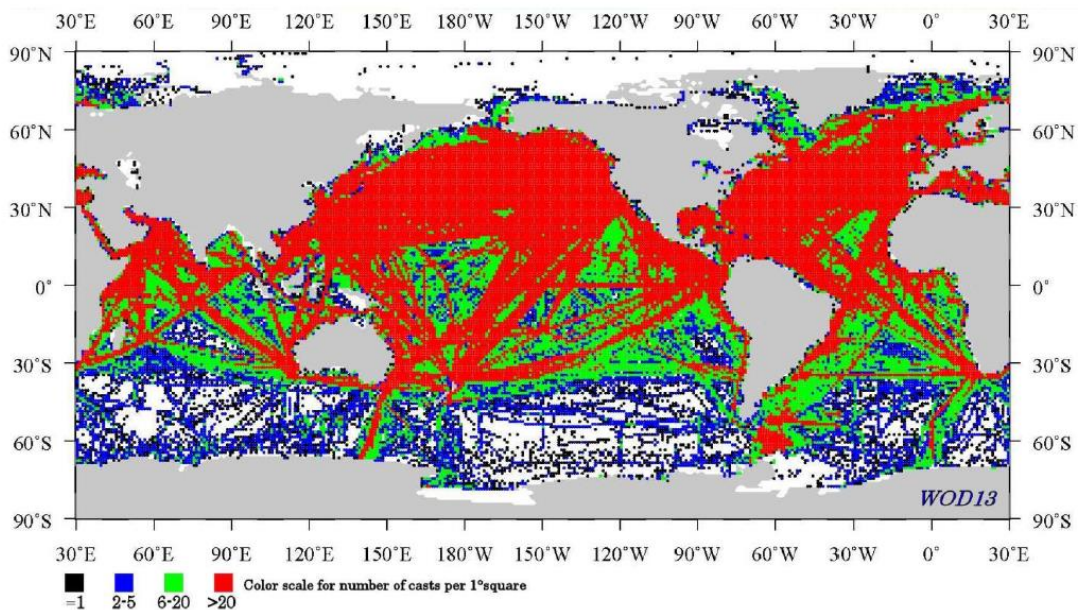
Layer	Depth (m)	Layer	Depth (m)	Layer	Depth (m)
1	0	11	250	21	1200
2	10	12	300	22	1300
3	20	13	400	23	1400
4	30	14	500	24	1500
5	50	15	600	25	1750
6	75	16	700	26	2000
7	100	17	800	27	2500
8	125	18	900	28	3000
9	150	19	1000		
10	200	20	1100		

These depth layers are the same as those in the WOA13 database.

As the Yellow Sea is very shallow, it will primarily be expressed only by the first 5 layers (50m) in the SMG-WOD, extending down to layer 10 in only a few locations. In comparison, the GDEM data base containing 78 layers has much finer resolution through the first several layers. SMG-WOD can be accessed on the NOAA website(Chu and Fan 2016b).

E. GDEM

The Navy's answer to the global ocean climatology of temperature and salinity was GDEM (Generalized Digital Environmental Model). Carnes (2009) points out that "development of GDEM at the Naval Oceanographic Office began in 1975 and culminated in the first release to the Navy community in 1984." Originally, GDEM only covered the North Atlantic but attained global coverage by the early 1990s. Previous climatological databases for temperature and salinity excluded data sources that did not capture temperature and salinity at the same time, and only applied open source data. This excluded large sets of data from sources such as XBTs, but also prevented using any data that had been collected via classified means. Additionally, the WOA did not have a high enough resolution to adequately capture the Navy's needs for detailed mapping of coastal waters or inland seas. GDEM ocean climatology was designed for the Navy to specifically address these coverage gaps and limitations that are crucial to naval operations and to successful exploitation of the environment.



This coverage of WOD XBT data show the relative abundance and density of the XBT data that is available globally that is tripped from some climatological databases, but preserved in GDEM.

Figure 8. Global XBT Coverage in WOD13.

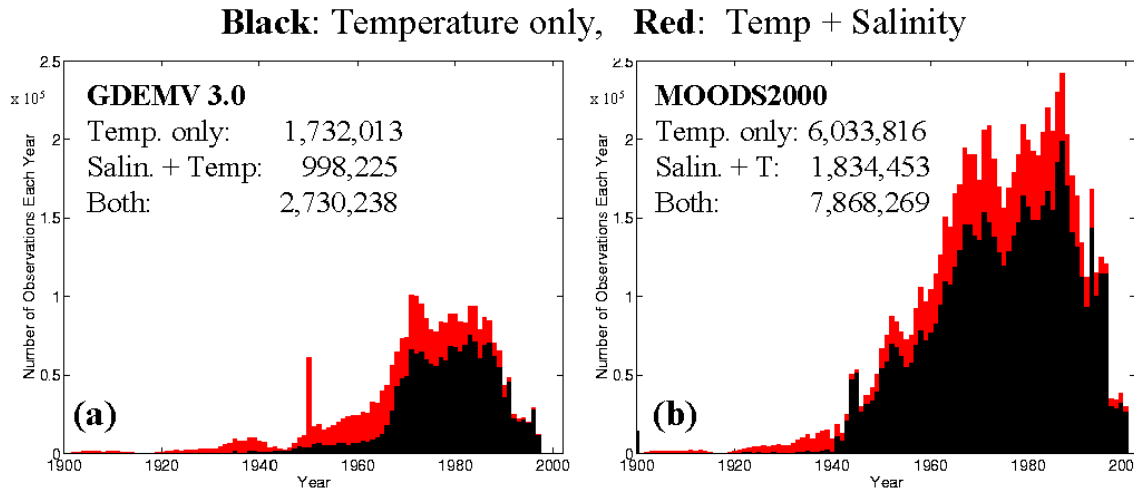
GDEM has undergone expansion and several upgrades since its initial development improving in coverage, resolution, new fields, and resolved profile computational errors. The current working version, GDEM-V 3.0, is available on the NOAA website (Allen and U.S. Navy 2012). For simplicity, this dataset shall be referred to as GDEM throughout the rest of this paper. GDEM contains global monthly climatologies of temperature, salinity, as well as temperature and salinity standard deviations (SD). The latter can be used in estimating acoustic modeling uncertainty caused by the uncertainty in SSP input.

The GDEM database was derived from temperature and salinity profiles existing as of 1995 in the Master Oceanographic Observational Data Set (MOODS). In 2001, and 2002, the profiles from MOODS were reviewed and selected by NRL to create the Modular Ocean Data Assimilation System (MODAS) (Carnes 2009). Scientists then manually edited each profile from MODAS that was to be incorporated into GDEM, mostly removing erroneous or redundant data. There is about 1/3 of MOODS data that made it into GDEM (Figure 9).

GDEM has a horizontal resolution of $1/4^{\circ}$ (or 15 arc minutes) set across world (NAVO 2009). Vertical resolution in GDEM consists of 78 layer depths, starting at the surface 0m and continuing down to 6600m (NAVO 2009). There are 14 layers depth representative of the 50m and less, a full table of GDEM depth layer and associated depth can be found in the appendix. Each profile has four dimensions: latitude, longitude, depth, and time. Sound speed is calculated upon extraction using the SeaWater library of EOS-80 seawater properties (Morgan 2003).

The first time that GDEM was ever discussed in open source literature was by Teague et al. in 1990 when they published a comparison between GDEM and WOD. At the time, GDEM has not yet expanded to global coverage and the WOD climatology was referred to as the “LC” for its publisher, Levitus climatology. Large-scale oceanographic features appeared to be similarly expressed between the two climatologies. However, when comparing the results for season variability, GDEM outperformed “LC” likely because “lower data densities used in LC formulation produced less representative data fields than in GDEM formulation” (Teague et al. 1990). Teague et al. (1990) also raise an interesting

point that GDEM is generally only accessible to the U.S. Navy and its affiliates, whereas the WOD is widely accessible and used by academics, researcher and the military alike.



The number of profiles each year from 1900 to 2000 in (a) the profile database used to construct the MODAS and GDEM-V 3.0 climatologies, and (b) the number of profiles in MOODS (Carnes 2009).

Figure 9. GDEM Database Shown as a Subset of MOODS.
Source: Carnes (2009).

THIS PAGE INTENTIONALLY LEFT BLANK

V. METHODS

A. EOF ANALYSIS

Empirical orthogonal function (EOF) decomposition, also more commonly referred to as principal component analysis (PCA), has been used by atmospheric scientists for nearly a century and only more recently been applied by oceanographers. First applied in the 1940s by meteorologists, the original requirement was to reduce large numbers of variables contained in observational or model data down to only a few variables without degrading variability of the data (Hannachi 2004; Hannachi et al. 2007). Variable reduction is done by finding a linear combination of existing variables. This data compression was required due to the inability of earlier computing and storage systems to handle very large datasets. Today, EOF continues to be a valuable technique for pattern recognition, revealing the amount of variability per mode in a system. Most textbooks addressing multivariate statistical analysis will provide at least a basic introduction to EOF.

EOF application to determine the spatial and/or temporal variability of a dataset is first accomplished by subtracting the mean, leaving only the anomalies. By applying EOF, vectors are developed that are linear combinations of the anomalies (Wilks 2011). The first EOF, or the first mode, will contain the largest degree of variability and so on with increasing modes until no significant variability is expressed. The summation of each of the EOFs will add to the total variability of the dataset as each EOF stands individually without dependence or correlation to other EOFs (Wilks 2011).

EOF allows the researcher to separate the spatial and temporal variability. This research applies an EOF approach similar to the one used by Kumar et al. (2014), where subtidal velocities and temperature variability with depth from deployed several stations was determined. In this research the EOF is adapted to decompose sound speed anomalies, \tilde{c} , into a series over a set of orthogonal modes, so that vertical variability is represented by EOFs ($\varphi^{(n)}(z)$) and the temporal variability is represented by coefficients

$(A^{(n)}(t))$, also referred to as principal components PCs (Equation 4). The number of modes is equal to N , and the $n=1$ refers to the first mode containing the most variance.

$$\tilde{c}(z, t) = \sum_{n=1}^N A^{(n)}(t) \phi^{(n)}(z) \quad (4)$$

The time variability can then be expressed as time series with A representing the coefficients (amplitudes).

The sound speed anomalies $\tilde{c}(z_k, t_m, \tau_s)$ are calculated as departures of sound speed profiles from their climatological monthly means as follows

$$\tilde{c}(z_k, t_m, \tau_s) = c(z_k, t_m, \tau_s) - \bar{c}(z_k, t_m), \quad (5)$$

where $k = 1..K, K = 28$ is an index over vertical levels; $m = 1..M, M = 12$ is an index over months; $s = 1945..2014, S = 70$ is an index over years, and $\bar{c}(z_k, t_m)$ are the climatological monthly means:

$$\bar{c}(z_k, t_m) = \frac{1}{S} \sum_{s=1945}^{2014} c(z_k, t_m, \tau_s) \quad (6)$$

The time dependency of sound speed anomalies (Equation 5) on month and year, is converted into a sequential index p , which runs from 1 to $p = 840$.

B. BELLHOP

The sound speed profiles generated from GDEM and SMG-WOD temperature and salinity fields were used to calculate acoustic transmission loss in the Yellow Sea environment via BELLHOP model. “BELLHOP is a beam tracing model for predicting acoustic pressure fields in ocean environments...BELLHOP can produce a variety of useful outputs including transmission loss, eigenrays, arrivals, and received time-series” (Porter 2011). A BELLHOP overview by Rodriguez (2008) further delineated that “Bellhop is designed in order to perform two-dimensional acoustic ray tracing for a given sound speed profile $c(z)$ or a given sound speed field $c(r; z)$, in ocean waveguides with at

or variable absorbing boundaries.” The bottom absorbing boundary is of particular interest in the research due the shallow water depths of the Yellow Sea.

There are several considerations for selecting BELLHOP as the acoustic model for this research. BELLHOP is an open source, which makes it more easily accessible for those who wish to expand upon this research or provide validation. Ray tracing is also a widely accepted method for accessing acoustic propagation.

Ray tracing is one of the oldest methods for modeling sound propagation in the ocean. Newer so-called full-wave methods have supplanted ray tracing in many areas, however, ray models are still widely used... Their principal strength is for high-frequency problems—full wave models are often intolerably slow for such problems (Porter and Liu 1994).

Ray tracing models perform exceptionally well in cases uses active sonar and for imaging of acoustics in the ocean. Modeling acoustic transmission with ray profiles is a common method for studying and understanding how sounds energy propagates within a given sound channel (Porter 2011).

Dong et al. (2014) performed a comparison of BELLHOP’s transmission loss values with those of RAM, range- dependent acoustic model. RAM, known for its rapid and accurate acoustic modeling, was developed at NRL by Collins (Zingarelli and King 2003). The result of Dong et al. (2014) study was that BELLHOP was observed to perform with strong agreement, thus strengthening the case further for the use of BELLHOP.

The next step beyond ray tracing is Gaussian beam tracing, which in general produces a more accurate depiction of transmission loss (Porter 2011). In a simple ray trace, we see that frequency does not matter, that is, the ray is independent of the source frequency. As the model becomes more accurate via beam tracing, the source frequency is very important. In the transmission plots in this research, the transmission loss models are frequency dependent.

The sediment type is of such importance that it is a parameter taken into calculation in BELLHOP. The sediment type translates into a bottom reflectivity coefficient. Porter (2011) explains, that “to specify an arbitrary bottom reflection

coefficient to characterize the bottom ... one must provide a bottom reflection coefficient file with angle-reflection pairs defining the reflectivity.” This is just one of the many environmental inputs into BELLHOP made in order to produce a ray trace and further calculate transmission loss for ocean acoustics (Figure 10).

The temperature and salinity data is pulled from GDEM and formatted to meet the input requirements for BELLHOP. This data is then transformed into a SSP for each selected grid point. The same location temperature and salinity data is pulled from SMG-WOD where OSD has been applied. This data at each location is pulled monthly for an average of all 70 years. The EOF between each of SMG-WOD data and GDEM data from the same gridpoint will be run to determine variability. This first pass through the data is essentially treating the SMG-WOD data as climatological monthly means to see how it compares to the true climatology of GDEM.

Transmission loss in decibels, dB, is calculated from the pressure field. While pressure is not a direct input parameter for BELLHOP it is generated from the depths input. The conversion for pressure, p , to dB is $20\log_{10}(|p|)$.

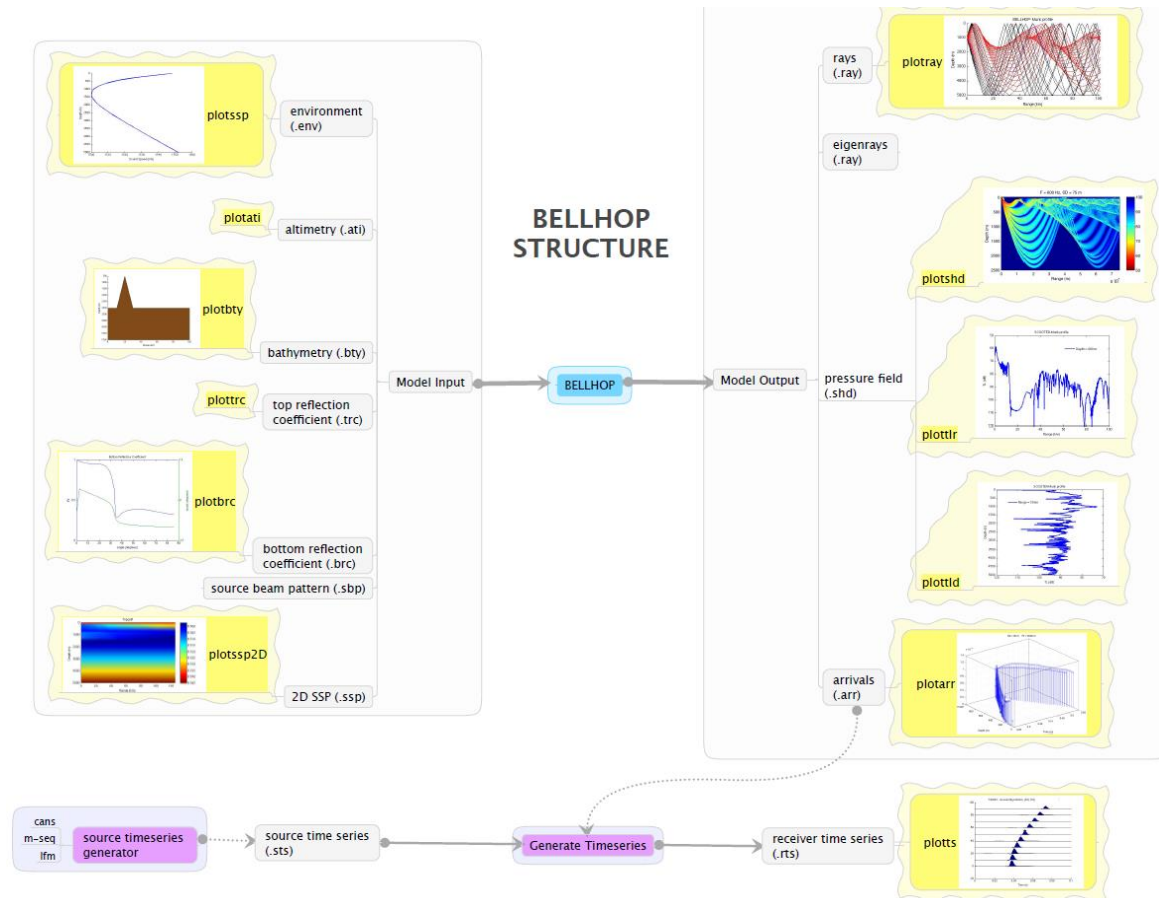
Transmission loss can be plotted in three different ways in BELLHOP. The user may select run criteria to plot transmission loss as coherent, incoherent, or semi-coherent depending on the desired detail of the acoustic field. Coherent transmission loss runs provided the most acoustic detail of the interference patterns, but it also takes the longest to run. When such fine-patterned interference is not required, the user should select incoherent transmission loss, essentially an averaged transmission loss across a band of frequencies. Incoherent should not be used for deterministic forecasts. The third option, semi-coherent is essentially a combination of the previous two; it captures some but not all of the effects from interference.

A combination of BELLHOP TL runs will be modeled at various months, frequencies, and source to receiver depth pairing. The two alternating source and receiver depths that will be used for this shallow body of water are 8m and 20m (Table 7).

Table 7. Bellhop TL Runs.

location	receiver depth (m)	source depth (m)	frequency (Hz)	month
A, B, C, D, E, F, O	20	20	3500	01
				08
	8	8	3500	01
				08
	20	8	3500	01
				08
	8	20	3500	01
				08

each run 360° at 10° increments



The left side of this figure shows all the input sources that can be provided to BELLHOP. The right side shows all of the model output products.

Figure 10. Bellhop Structure. Source: Porter (2011).

C. QUANTIFYING UNCERTAINTY

In an effort to estimate the acoustic uncertainty and possibly pinpoint the sources variability, researchers have applied methods such as Polynomial Chaos Expansions or the Monte Carlo Method (Emerson et al. 2015; LePage 2006; Lermusiaux et al. 2002). Upon reviewing the results these methods will be considered for applicability to this research.

Uncertainty of the transmission loss, as modeled in BELLHOP, will also be assessed for each binning of data. As this research aims to reveal interannual variability of sound speed and ultimately the acoustics in the Yellow Sea, a comparison of the TL range variability will give insight as to which dataset provides greater reliability. Histograms will be used to capture the frequently occurring TL ranges in addition to the extent of the outlying TL ranges by year.

D. MATLAB

The computing, modeling (including BELLHOP) and algorithms applied in thesis will be run in MATLAB. MATLAB, Matrix Laboratory, is a computer programming environment that was developed by MATHWORKS in 1984 and has since undergone many revisions to facilitate numerical computing. MATLAB codes designed to work with other conventional computer programs such as C++, Java, FORTRAN, and Python allowing the user to integrate between these coding languages. The advantages of MATLAB are that it is easy to use; it is platform independent; it comes with many functions predefined; its visualization and plotting capability are device independent; and it has an interactive graphical user interface (GUI) (Chapman 2009). MATLAB is used in most academic environments, as it allows relatively inexperienced programmers to develop and execute complicated data analysis.

VI. RESULTS AND DISCUSSION

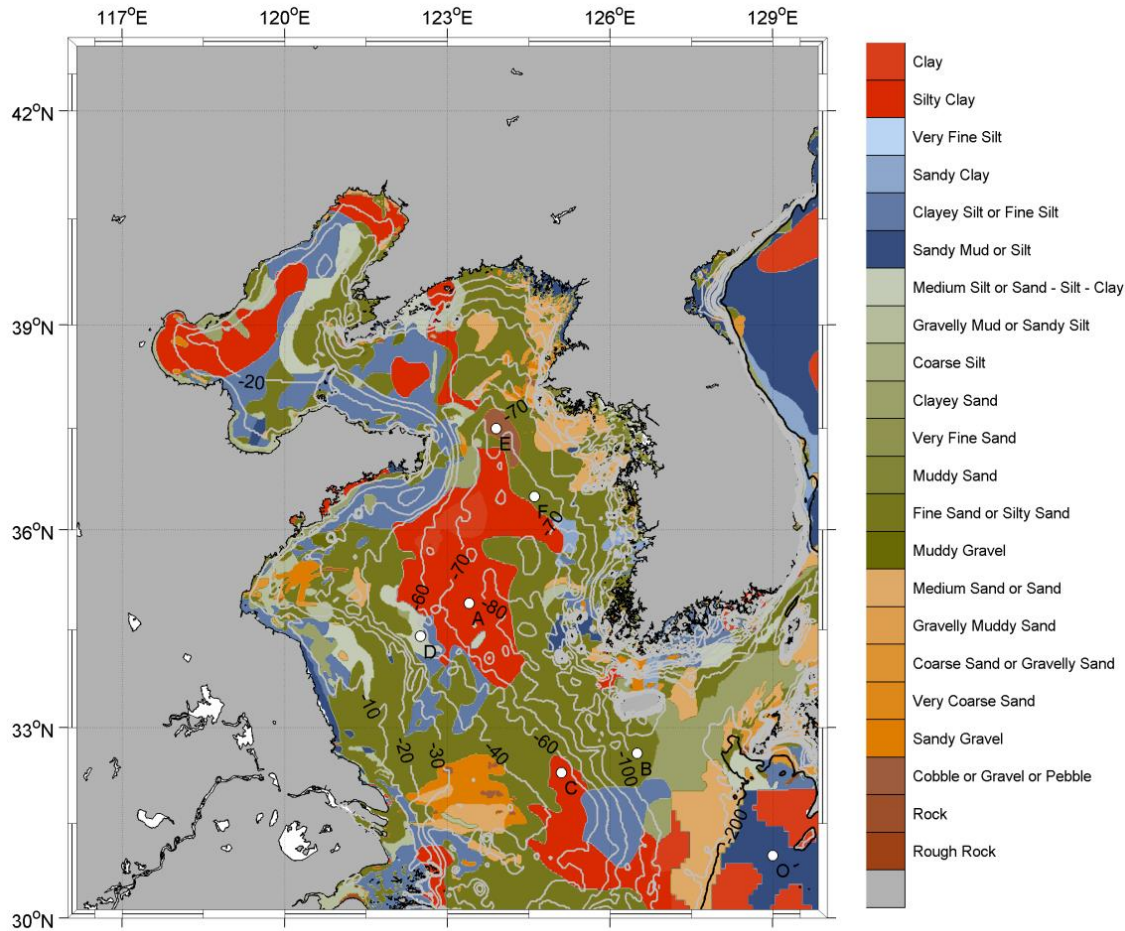
A. LOCATIONS: BOTTOM SEDIMENTS AND BATHYMETRY

Sediments plots for the Yellow Sea were made from each of the four sediment databases: Enhanced, Standard, HFEVA, and Reduced. Although the databases differ in the number of sediments they classify, the contours defining the boundaries of different sediments within the Yellow Sea were consistent throughout all databases. For instance, where one dataset calls select region granules, another may call it cobble, gravel, or pebble, with the same location and coverage. Therefore, while the classification names of the bottom sediment differ, the size of the particles and density will have the same effect on acoustics due to bottom attenuation, reflection and refraction. The HFEVA sediment database was determined to be the most appropriate sediment database for this research, and its output is displayed in Figure 11. The HFEVA database resolution allows the user to discriminate between various bottom types without extensive details.

The bottom sediment chart with the bathymetry overlaid was used to select six locations for acoustic propagation modeling within the Yellow Sea. The locations were chosen to ensure a variety of bottom types, and/or depths as shown in Table 8. The TL ranges can then be compared between bottom types and depths when climatological data versus synoptic monthly data are used to model the acoustic environment.

For ease of reference, the selected locations are labeled A through F and will be referenced as such throughout the rest of this research. Figure 11 shows the spatial layout of the points within the Yellow Sea and the specifics are found in Table 8. Location A is selected due to being the center of the Yellow Sea; it is 70–80m deep and has a silty clay bottom. Location B is directly south of Cheju Island and is the deepest location at just over 100m with a bottom type of fine sand. Location C is selected because it has the same bottom type as point A, but it is more shallow (40–50m) than location A and closer to the edge of the Yellow Sea where there will be greater interaction with water from the ECS. Location D is chosen for its bottom type of gravelly mud and same depth as location C, 40–50m. Location E is the most northern location with a depth of 60–70m and a rocky,

cobble or gravel, bottom; points north of E and in the Bohai Sea were considered but were outside of the SMG-WOD dataset, as can be seen from the temperature and salinity data (Figure 13 and 16). Location F was selected because it shares the bottom type with location B, but it is further north and has a shallower depth at 70–80 m.



The Yellow Sea basin's bottom sediment structure comprises silty clay, fine sand with several patches of the other sediments, as shown in the legend. There is large variation in the bottom sediment at the mouth of the Yangtze River.

Figure 11. HFEVA Sediments with Bathymetry Overlay in the Yellow Sea.

Location O was selected for reference because it is outside of the Yellow sea and nearly twice as deep as most locations within the Yellow Sea. Because location O is so much deeper, it will have more levels of data within SMG-WOD to resolve profiles.

Table 8. Locations A through O by Depth and Bottom Type.

<u>Location</u>	<u>Latitude °N, Longitude, °E</u>	<u>Depth (m)</u>	<u>Bottom Sediment Type</u>
A	123.4, 34.9	70-80	silty clay
B	126.5, 32.6	>100	fine sand
C	125.1, 32.3	40-50	silty clay
D	122.5, 34.3	40-50	gravelly mud
E	123.9, 37.5	60-70	cobble or gravel
F	124.6, 36.5	70-80	fine sand
O	129.0, 31.0	>200	sandy mud

B. TEMPERATURE AND SALINITY DATA FOR GDEM AND SMG-WOD

In order to understand the variability of the acoustic propagation within the Yellow Sea the temperature and salinity variability is analyzed. Surface temperature and salinity are compared for seasonal variability first, and then by thermohaline variability with depth. By comparing the temperature and salinity between GDEM and SMG-WOD the different horizontal and vertical resolutions and the impact to defining features is quite clear and will be further discussed.

1. Temperature

The images for surface temperature are displayed to capture the seasonal range of temperatures observed in the Yellow Sea as observed in GDEM (Figure 12) and compared to a single year of SMG-WOD (Figure 13). Comparison of these figures illuminates the differences in the horizontal resolution of the two datasets. As August is the observed warmest SST month, August SSTs for each decade starting at 1945 until the end of the dataset were reviewed for any obvious signs of warming in the later years; however, the variations were insignificant.

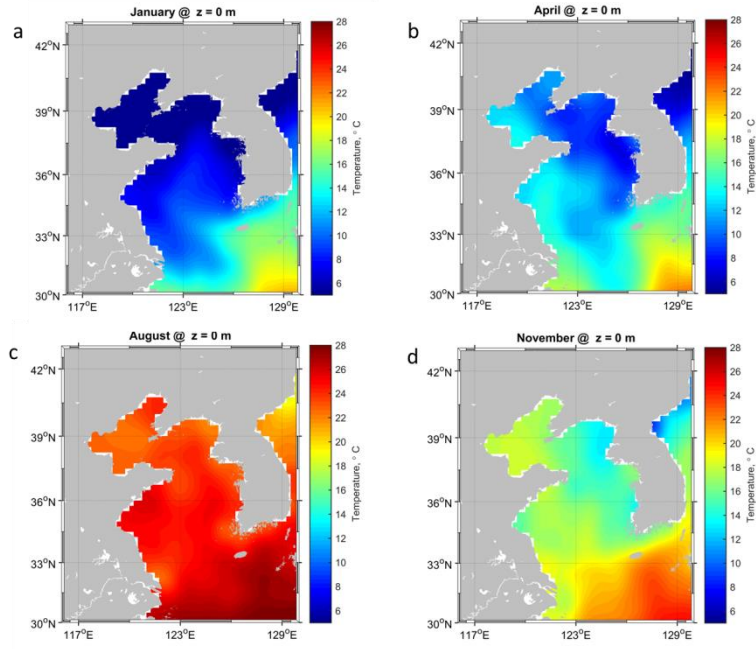


Figure 12. Seasonal Variability of GDEM SST in the Yellow Sea.

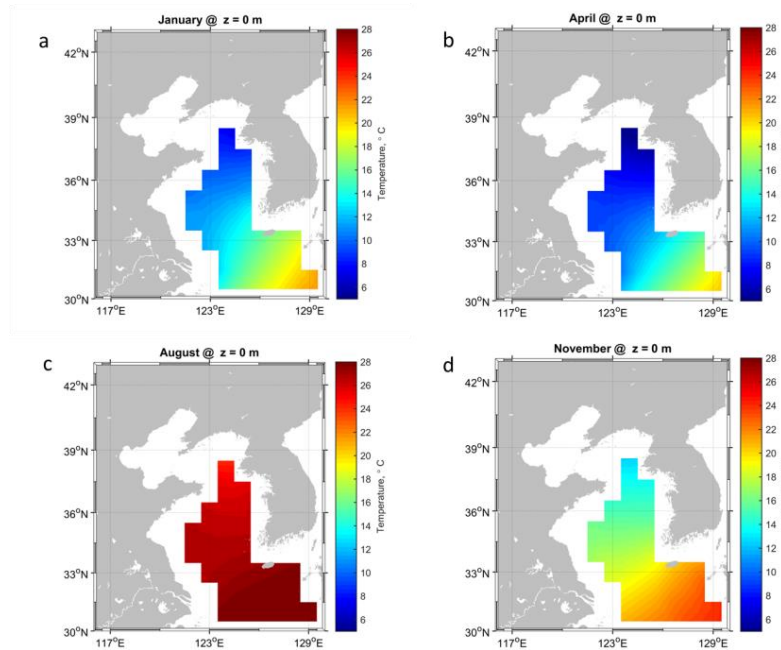
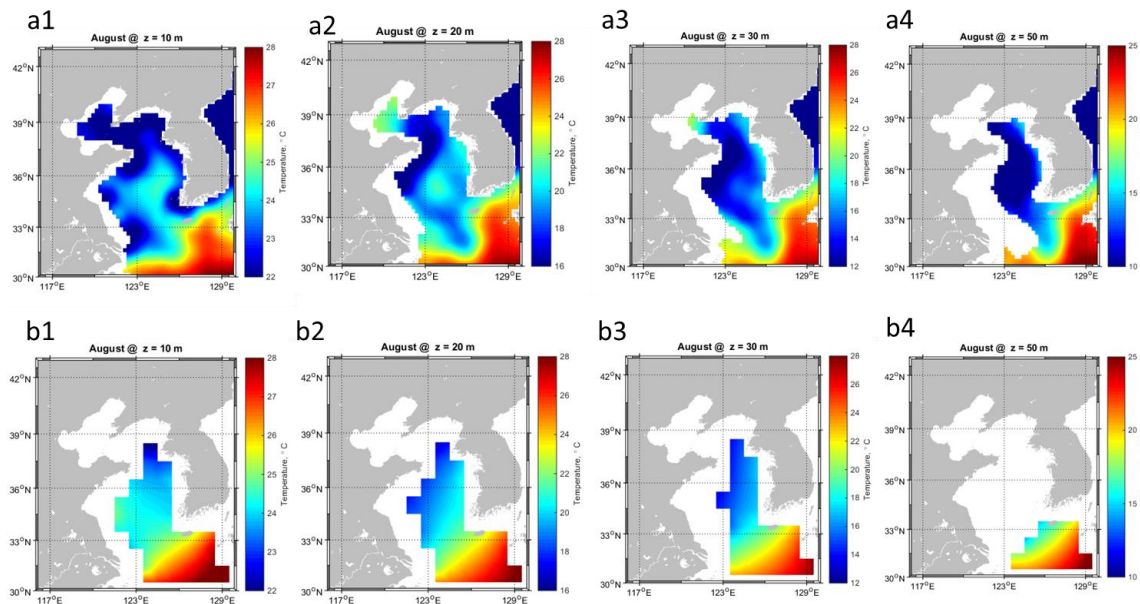


Figure 13. SMG-WOD (1945) Seasonal Variability of SST in the Yellow Sea.

The thermal structure variability with depth was analyzed by plotting temperature at 10Z, 20Z, 30Z, and 50Z for a single month (Figure 14). For visual comparison, the GDEM levels are selected to match the levels available in SMG-WOD. The temperature color bars for depth are adjusted per level to draw out features, but consistent at each level between SMG-WOD and GDEM.

The higher vertical and horizontal resolution of GDEM resolves a cold front extension from center of the Yellow Sea southward, and strengthening with depth. This front, while the general location is in the same position in the SMG-WOD figures, is much less pronounced. SMG-WOD has difficulty resolving this feature due to the limited vertical resolution in SMG-WOD, and thus less data levels for such shallow water. A comprehensive collection of temperature images by years can be found in the Appendix B.



a1-a4) GDEM temperature in August, 0m-50m descending from left to right
b1-b4) SMG-WOD temperature in August, 0m-50m descending from left to right.

Figure 14. GDEM and SMG-WOD (1945) Temperature Variation with Depth.

2. Salinity

The images for salinity at the surface are displayed to capture the seasonal range of temperatures observed in the Yellow Sea as observed in GDEM (Figure 15) and compared to a single year of SMG-WOD (Figure 16). Comparison of these figures illuminates the differences in the horizontal resolution of the two datasets. As August is the observed warmest SST month, August SSTs for each decade, starting at 1945 and until the end of the dataset, were reviewed for any obvious signs of warming in the later years, however the variations were insignificant.

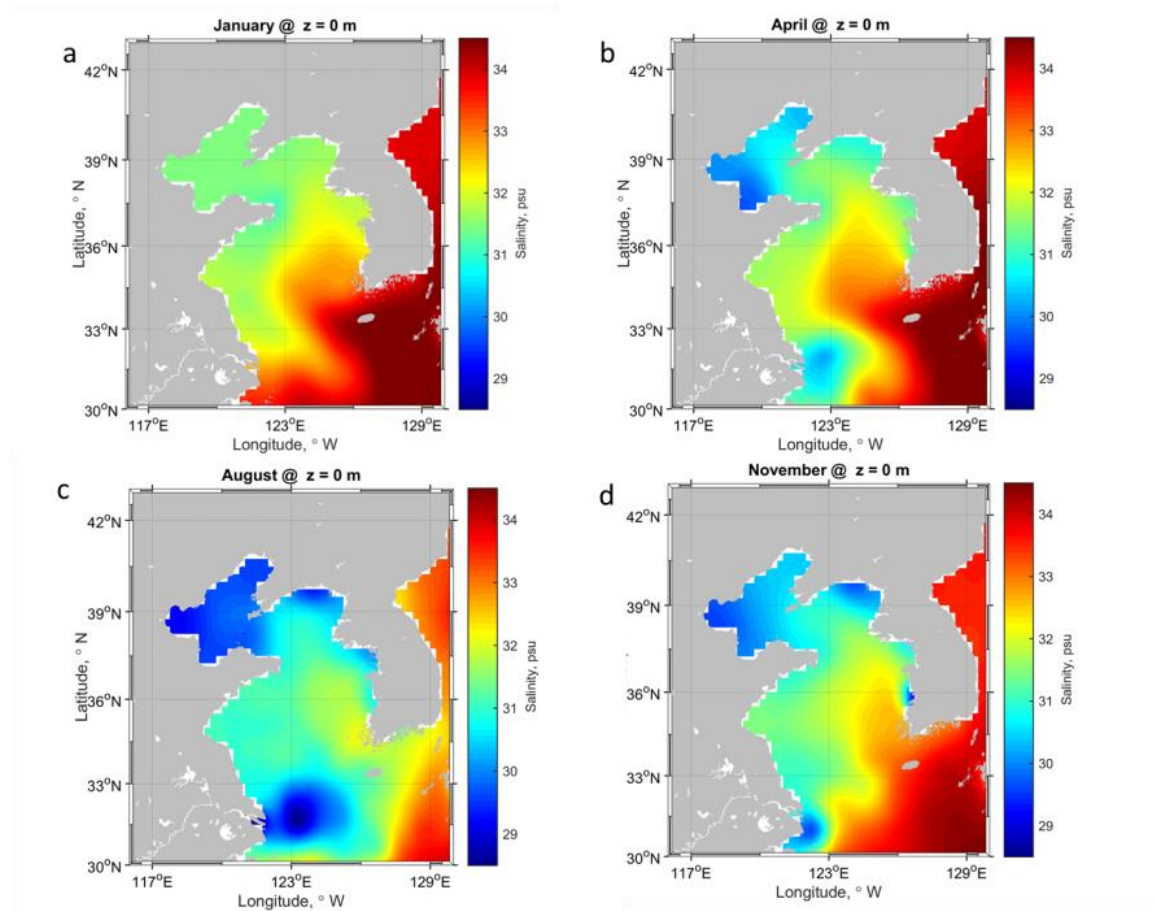


Figure 15. GDEM Seasonal Salinity.

The haline structure variability with depth was analyzed by plotting salinity at 10Z, 20Z, 30Z, and 50Z for a single month (Figure 17). For visual comparison, the GDEM levels are selected to match the levels available in SMG-WOD. As with the temperature figures, the salinity color bars for depth are adjusted per level to draw out features, but consistent at each level between SMG-WOD and GDEM.

GDEM greater vertical resolution resolves a cold water extension from center of the Yellow sea temp front strengthening with depth. This front, while the general location is in the same position in the SMG-WOD figures, is much less pronounced. SMG-WOD has difficulty resolving this feature due to the limited vertical resolution in SMG-WOD, and thus less data levels for such shallow water. A comprehensive collection of salinity images by years can be found in the Appendix B.

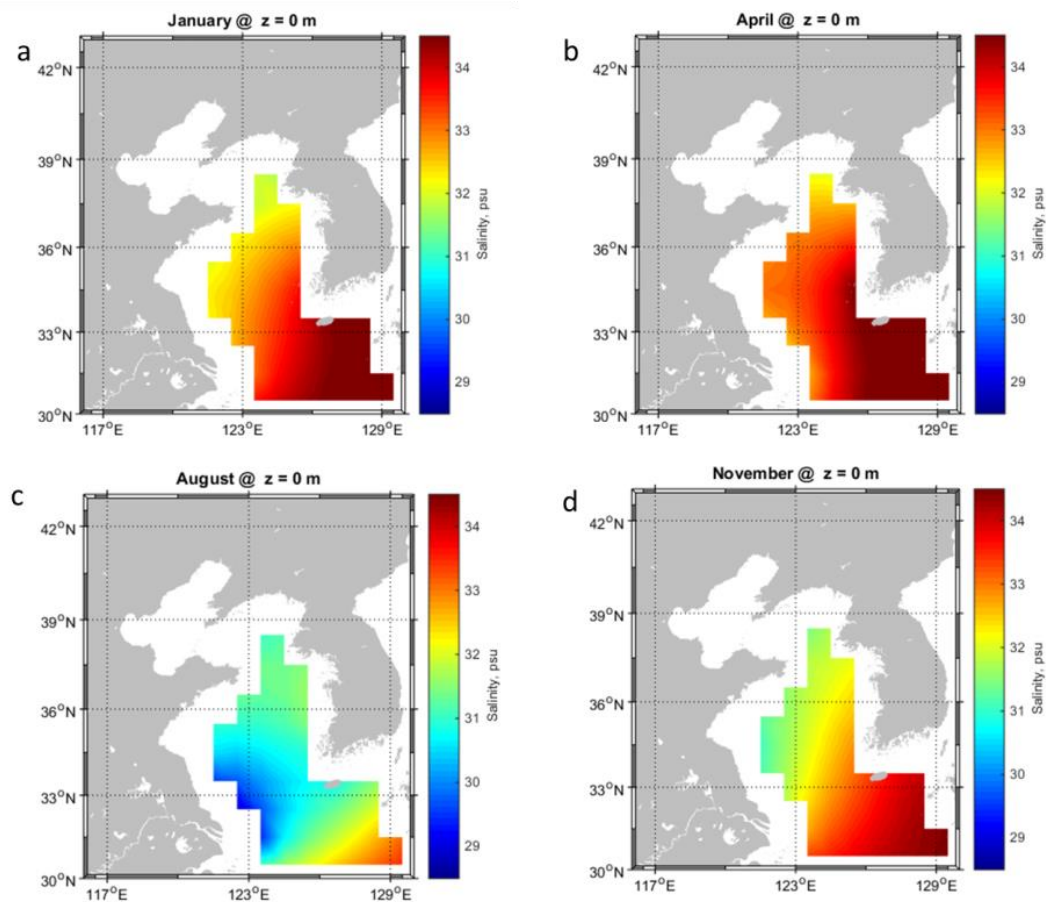
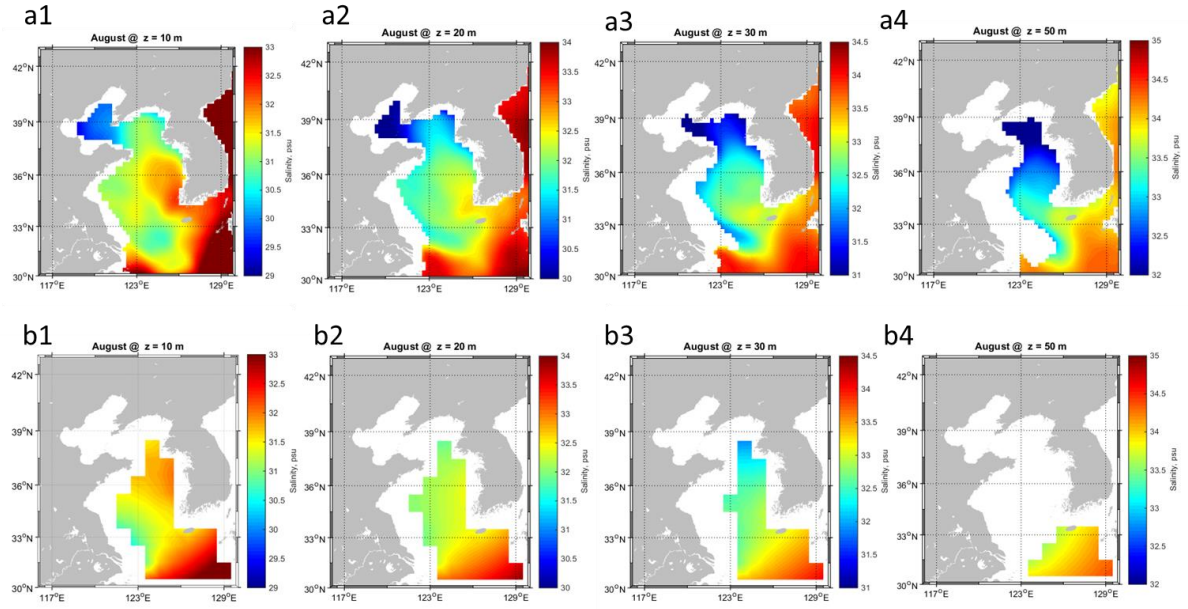


Figure 16. SMG-WOD (2014) Seasonal Salinity.



a1-a4) GDEM Salinity in August, 0m-50m descending from left to right
b1-b4) SMG-WOD Salinity in August, 0m-50m descending from left to right

Figure 17. GDEM and SMG-WOD (2014) Salinity Variation with Depth.

C. SOUND SPEED PROFILES

The temperature and salinity data for each dataset were used to create the SSPs at each location. The SSP is indicative of how the sound will propagate in the water, and as such, it is the first step toward detecting inter-annual acoustic variability. The SSPs total (annual) mean, monthly means, variations in SSP shape, as well as sound speed variability within both the datasets are analyzed below.

1. Mean SSPs

The total and monthly means calculated over GDEM and SMG-WOD datasets are shown in Figures 18 and 19 for two locations, A and C. The winter months have nearly vertical SSPs, which correspond to the isothermal conditions in the Yellow Sea as a result of enhanced surface mixing during winter as seen in (Fralick 1994, Chu et al. 2005; Hsu et al. 2000). While approximately uniform, the SSPs in winter exhibit a weak positive

gradient due to pressure effect. This may have an important acoustic implication creating a surface channel.

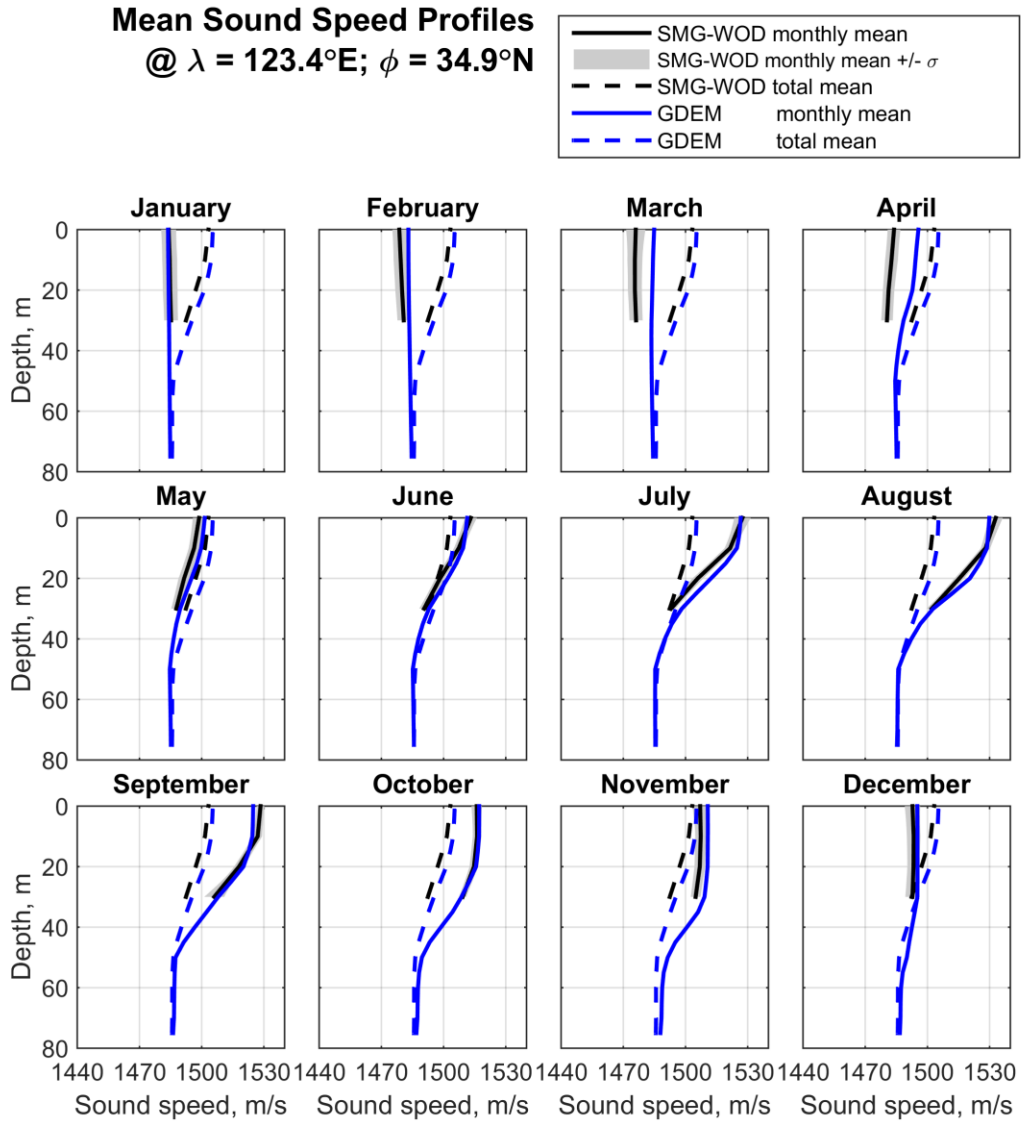
During summer, the SSPs at all locations show a rather sharp shift of the upper SSP to the right. Even more importantly, the summer SSPs exhibit a layered structure as expected for a temperature-driven shallow-water SSP. The upper layer is either uniform or has a weak negative gradient of sound velocity with depth. Warming of the surface causes the temperature to decrease with depth faster; this effect now dominates over the pressure effect in the upper layer. The thermocline causes more pronounced sound velocity gradient in the summer SSPs between 10 and 50 m at location A, and between 10 and 25 m at location C. Note that the thicker thermocline at location A allows for better resolution in the SMG-WOD database than at location C. Below the thermocline, summer SSPs are mostly driven by pressure effect and are either uniform or have a slightly positive vertical gradient. The standard deviation plotted with the SMG-WOD SSP monthly mean is very small, indicating that annual SSPs tend to be close to the mean.

SMG-WOD SSPs for all means at location A appear truncated at 30m depth when compared with GDEM, which extends to 70m (Figure 18). This is due to the differing resolutions between the datasets, where SMG-WOD resolves to 10 m must be shallower bathymetry within the same resolution grid as location A. In location C (Figure 19), the SSP means for SMG-WOD extend all the way down matching the same as GDEM.

The sound speed in the upper water column varies up to a maximum of 30 m/s faster than the mean in the summer months, with the greatest departure from the mean seen in August across all locations. This is important, as it sets the parameters for which months to run TL, from winter months, January with the nearly vertically uniform structure, and from summer, August where there is the strongest departure from the mean.

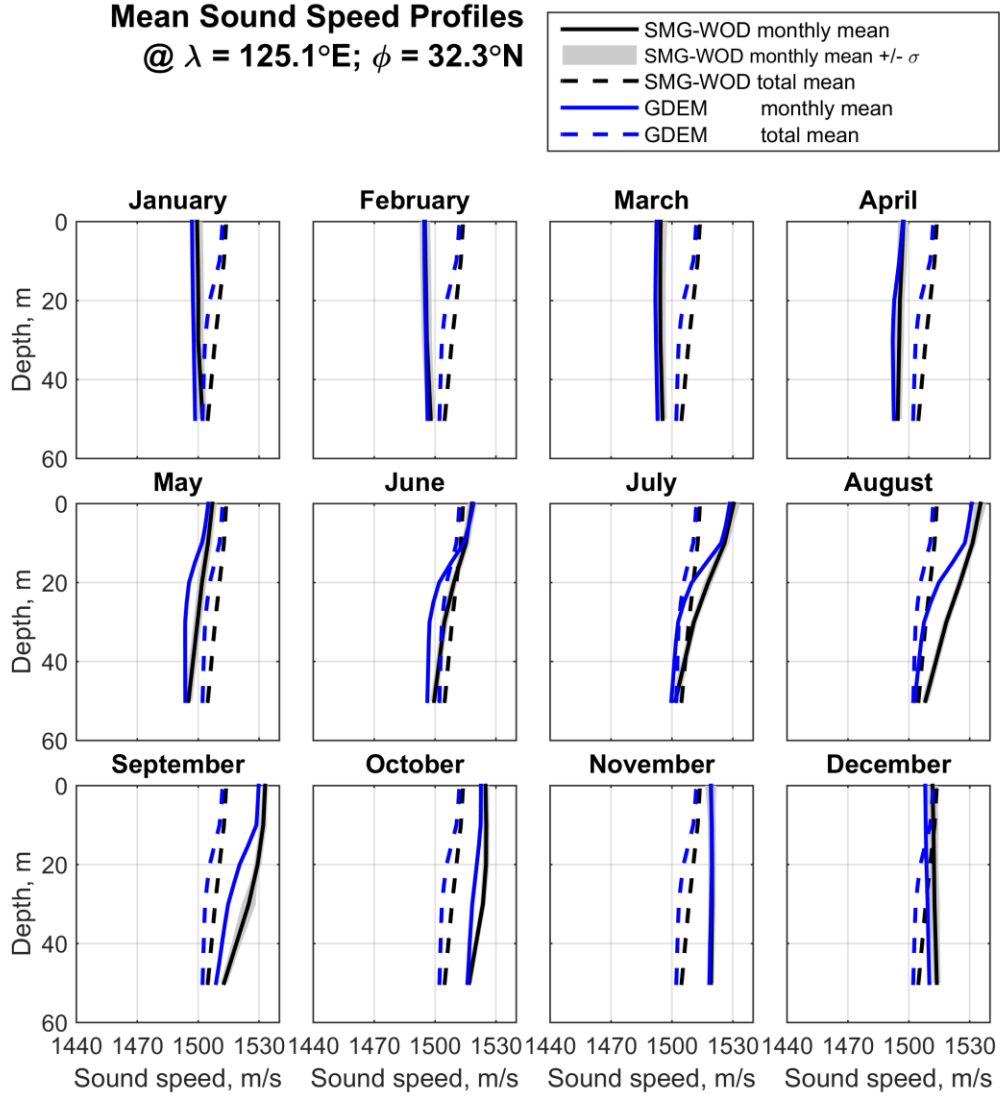
While the monthly means for the datasets extend away from the total time mean in the summer to the right (faster sound speed) and back closer and past the total time to the left in the winter, the overall position of the SSP monthly means generally move

together. However, in some locations there is a notable split, such as seen in August and September for location C (Figure 19). The SMG-WOD and GDEM monthly means are very close and nearly directly on top of each other in the winter months, but with a clear departure from each other around the 20–30m depth in the summer. The mean SSPs figures for all locations are in Appendix C.



SMG-WOD monthly mean and total mean for SSPs (black) with \pm one standard deviation overlay in gray. GDEM monthly mean and total mean for SSPs (blue).

Figure 18. Location A: SMG-WOD and GDEM Mean SSPs.



SMG-WOD monthly mean and total mean for SSPs (black) with \pm one standard deviation overlay in gray. GDEM monthly mean and total mean for SSPs (blue).

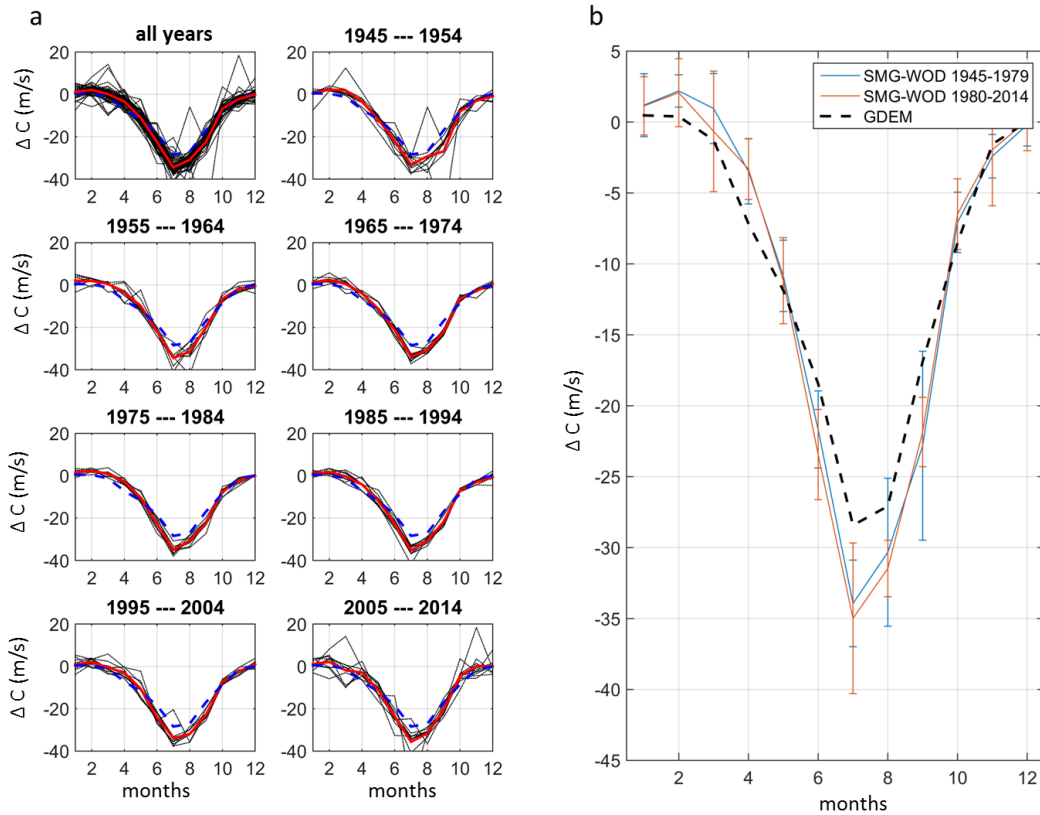
Figure 19. Location C: SMG-WOD and GDEM Mean SSPs.

2. SSP Structural Variation

The value of sound speed difference from bottom depth of the SSP (30m) to the surface 0m is used to study the SSP structural changes or (Cmax)- (Cmin) which will be referred to as ΔC , where delta is the difference and C is for sound speed. An isothermal structure will result in a SSP profile with nearly no gradient, the value of ΔC will be at or near zero. A SSP with a steep slope or gradient in the SSP will have a larger ΔC value;

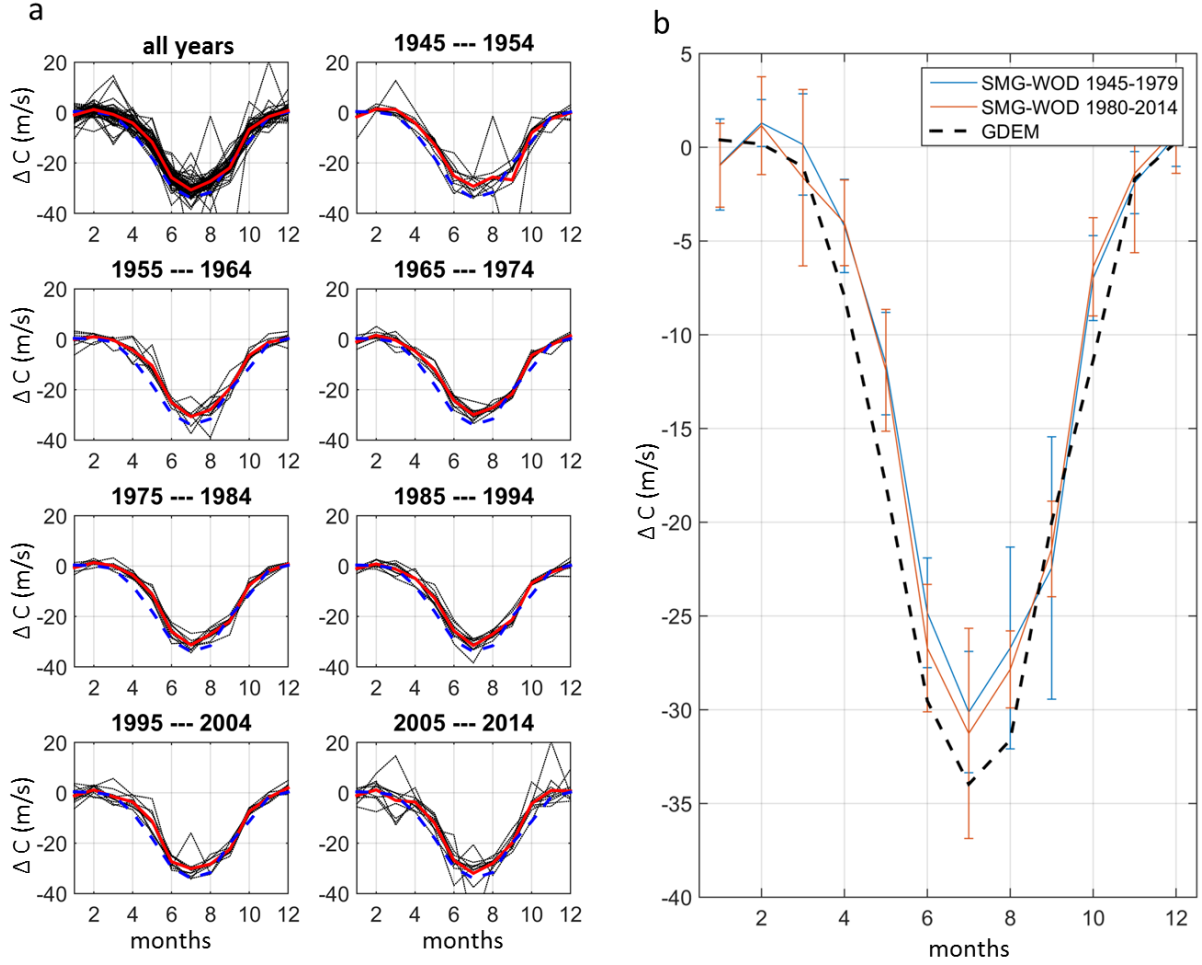
this is expected to be found in the warmer summer months. The SMG-WOD dataset was binned into 10-year means to cover all 70 years of data and draw out the years expressing the greatest change in sound speed, ΔC , by month for all locations and GDEM is overlaid in a dashed line. In some locations, the GDEM ΔC is more than several m/s less than SMG-WOD ΔC (Figure 20).

At location F, the GDEM ΔC is extends past that of SMG-WOD (Figure 21) indicating that the SSP structural variability that exists in SMG-WOD is not always the same with reference to GDEM, but that variability is location dependent. In most locations the mean SMG-WOD ΔC is nearly the same as the GDEM ΔC as can be seen in the Appendix C.



a) Structural variation of the SSPs (Cmax-Cmin) binned in all years and by 10yr binning; SMG-WOD years as indicated (black), SMG-WOD mean (red), GDEM mean (blue dash), b) (Cmax-Cmin) mean of the first half of the SMG-WOD dataset (blue), (Cmax-Cmin) mean of the second half of the SMG-WOD dataset (orange), and (Cmax-Cmin) of GDEM (black dash).

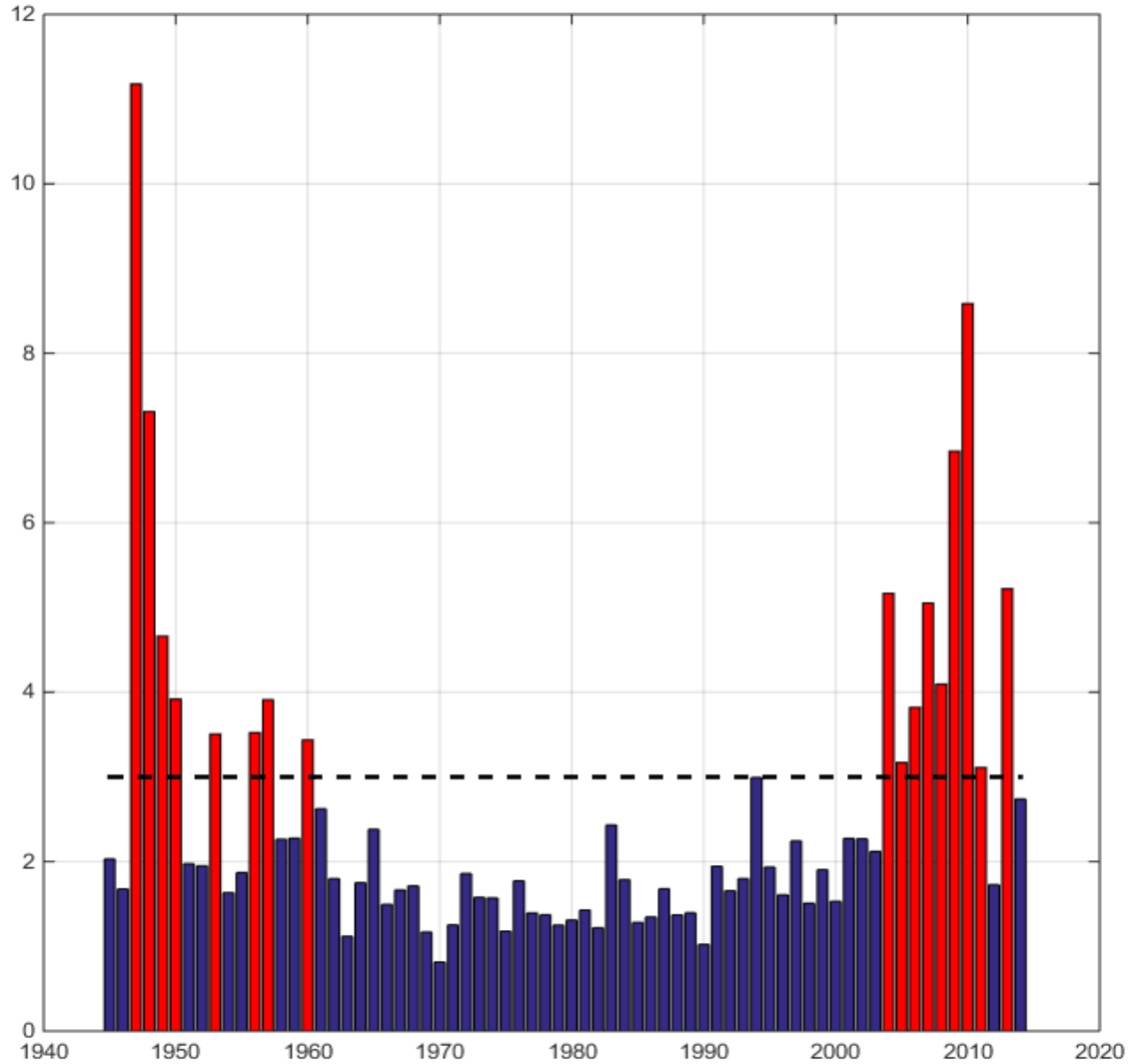
Figure 20. Location A: SSP Structural Variation.



a) Structural variation of the SSPs ($C_{max}-C_{min}$) binned in all years and by 10yr binning; SMG-WOD years as indicated (black), SMG-WOD mean (red), GDEM mean in (blue dash), b) ($C_{max}-C_{min}$) mean of the first half of the SMG-WOD dataset (blue), ($C_{max}-C_{min}$) mean of the second half of the SMG-WOD dataset (orange), and ($C_{max}-C_{min}$) of GDEM (black dash).

Figure 21. Location F: SSP Structural Variation.

The variations in sound speed profile structure is seen by binning the SMG-WOD data in to 10 year increments where the greatest variability is in the first ten years of the dataset (1945-1954) and the last 10 years of the dataset (2005-2014) (Figures 20a and 21a). Another way to represent this is by plotting the standard deviation by year (Figure 22). The standard deviation plot draws the attention to years when ΔC departs from its mean by at least three standard deviations, plotted in red.



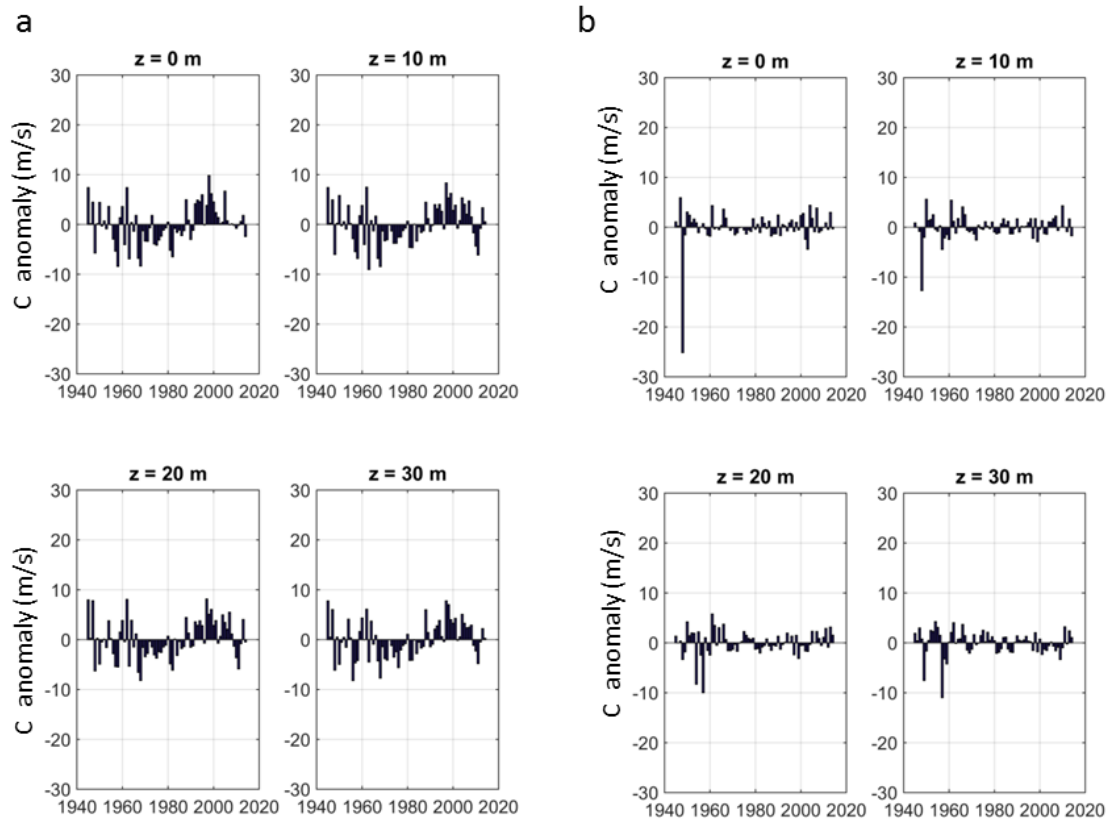
ΔC by year, years exceeding 3 standard deviations from the SMG-WOD mean are highlighted in red.

Figure 22. Location A: Standard Deviation of SMG-WOD ΔC .

3. SSP Anomaly at Depth

Another way to analyze the SSPs for inter-annual variability is by looking at anomaly of the sound speed, c , at various depths. The magnitude of the anomaly from the SMG-WOD total mean SSP profile indicates the strength of the anomaly, and the value positive or negative) indicates This is to measure the value of m/s from the mean SSP.

The SSP anomalies for each year of SMG-WOD data is plotted with depth from the surface and at 10m, 20m, and 30m. the SSP anomalies for location F are representative of all the location, each have the same general pattern (Figure 23). In the winter months, there is a larger anomaly than seen in the summer months. The winter anomalies at all locations follow a trend at all depths of being variable between positive and negative in the first 1/3 of the dataset, all negative in the middle years, and all positive in the last 1/3 of the dataset.



SMG-WOD SSP anomalies with depth zero at the surface down to 50m, a) January, b) August.

Figure 23. Location F: SSP Anomalies.

Cumulative variance across all locations was analyzed by developing a method to quantify the total anomalies per year. Starting from January and working through month

by month, the anomaly at each level was tested against a particular threshold from the mean it was given a critical value of 1, so that the maximum critical number (N_{cr}) any single month could receive is an N_{cr} 4. As each year has twelve months assessed for the anomalies exceeding a given threshold, the maximum N_{cr} possible for any year is 48. This provides a way to compare the sound speed anomalies with depth at all locations and is color coded by month. N_{cr} at location F is shown in Figure 23; in this case, the threshold that each anomaly had to meet or exceed was 4 in order to be counted. All location were relatively similar with the exception of location O. Due the greater depth at location O, the first 4 levels (0m, 10m, 20m, and 30m) do not capture the full structure of the SSP which extends much deeper, thus the very low N_{cr} .

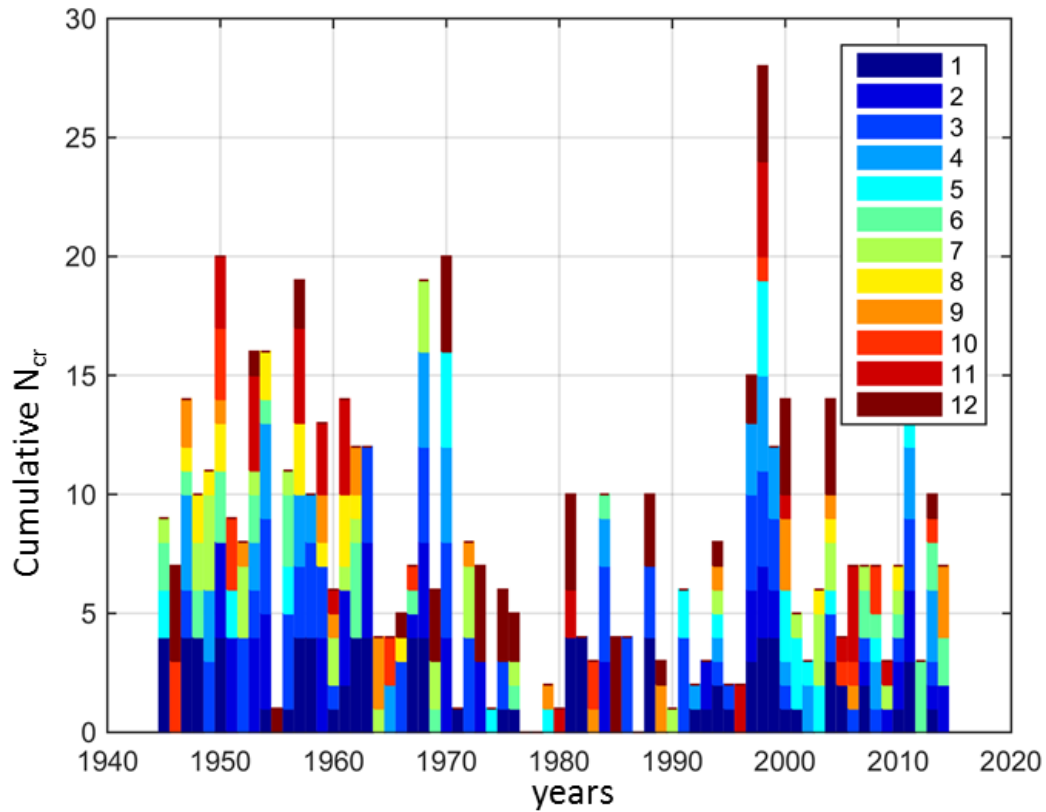
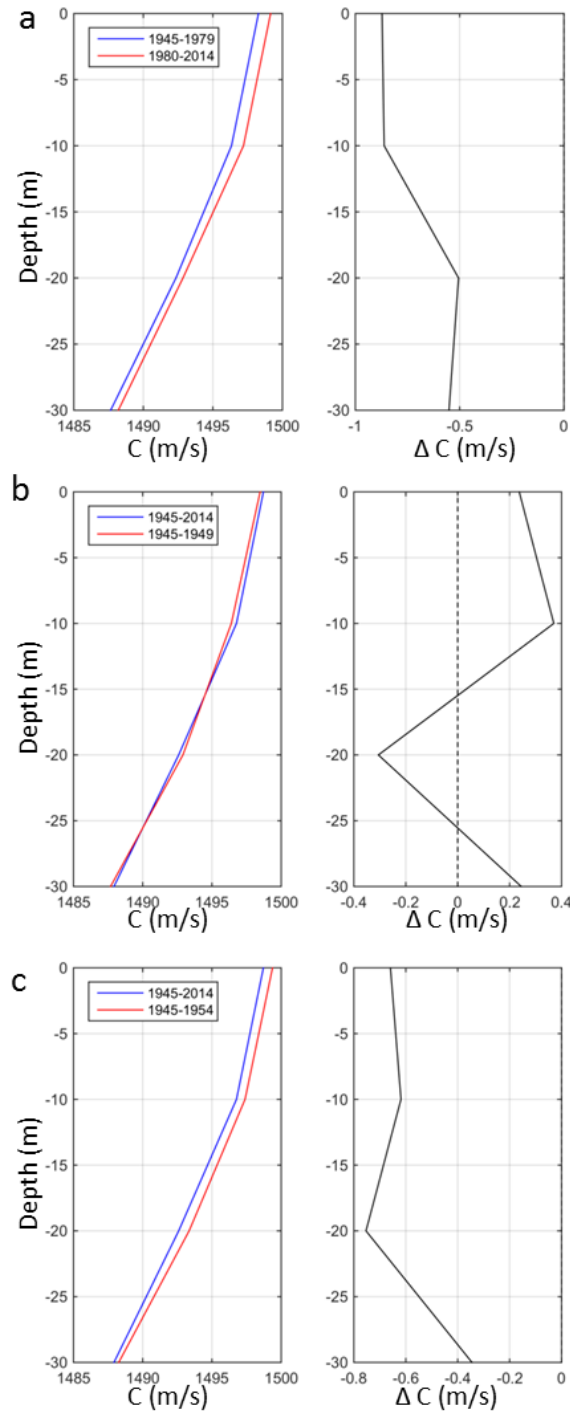


Figure 24. Location F: Cumulative N_{cr} for SSP Anomalies.

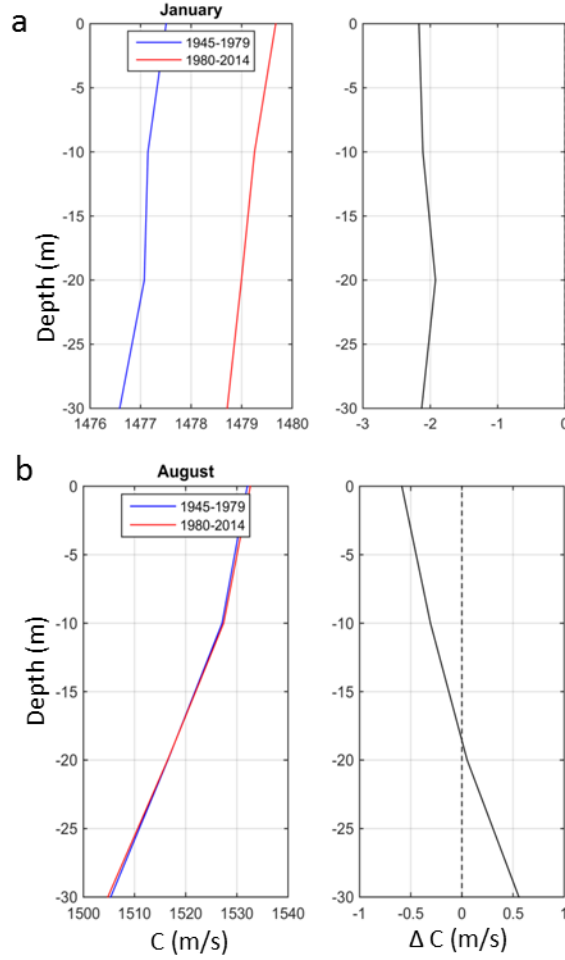
In order to investigate possible trends the SMG-WOD data binned into different year grouping and the SSPs of the means were compared and repeated at all locations. Once such binning was done by dividing the dataset in half with the earlier years, 1945–1979 averaged together and the later years, 1980–2014 averaged and the SSPs plotted together (Figure 24). At the first, the later part of the dataset would appear to have faster sound speeds that correspond to the years typically associated with global warming however, when the data is binned in different year groups, that trend does not hold true. The SSP from the first ten years of the dataset plotted with the SSP from the entire dataset would need to be slower sound speed than the overall average, but instead there is nearly the same spread showing the first 10 years SSP as faster the overall SSP (Figure 24c). While the magnitude of the difference in SSPs varied slightly between locations, the overall pattern remained the same.

The SMG-WOD dataset divided into the first half of dataset and the second half of the dataset plotted by season reveals a significant separation of the SSPs in the winter months as compared to the summer months. In January, the SSP for second half of the dataset is to the right, roughly 2m/s faster than the SSP of first half of the dataset (Figure 25) as observed at all location. However, in August the SSPs for the divided dataset are nearly identical. This faster sound speeds in winter are indicative of warmer winter waters in the later years, but with an overall average in SSPs remaining the same across the dataset.



Location F, all months, a) first half of the dataset (blue), second half of the data set (red); b) first 5 years of the dataset (red), the entire dataset(blue); c) first 10 years of the dataset (red), the entire dataset (blue) F.

Figure 25. Various Binning SMG-WOD Data to Compare ΔC .



Location F, a) January, first half of the dataset (blue), second half of the data set (red);
b) August, first half of the dataset (blue), second half of the data set (red).

Figure 26. Compare ΔC by Month.

D. EOF ANALYSIS

EOF was performed on the SMG-WOD data including all years from 1945 to 2014 in order to assess inter-annual variability. The seasonal variability is first removed because it is the dominant variance and prevents the interannual signal from standing out. The EOF modes represent the spatial component of the SSPs, which capture maximum variance. The ECs are the time-dependent amplitudes. Due to the limited vertical resolution, the number of data points contributing to the EOF SSP structure is quite limited. The PC, is either positive or negative and when multiplied by the corresponding

EOF SSP profile for each mode the resulting profile expresses the deviation from the mean SSP profile for each particular mode. The PC amplitudes after removing seasonality are quite small and so there is no distinguishable temporal trend.

The variance contained in the first three modes of EOFs for all location is shown in Table 9. The subsequent modes were very minimal and not significant to the analysis of identifying patterns in the data.

Locations A and C are shown as they have the same bottom type of different depths, because location C has one more level of data available within SMG-WOD, the EOF is able to calculate an additional mode (Figures 27 and 28). Essentially, the number of modes that can be calculated corresponds to the number of inputs, in this case, level of sound speed data.

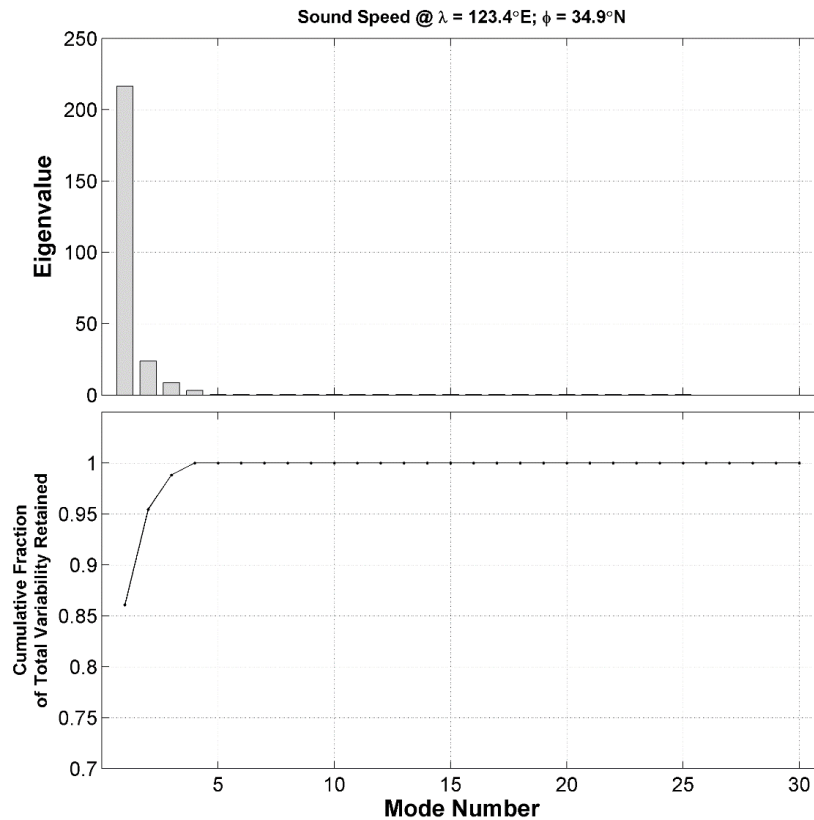


Figure 27. Location A: Eigenvalues and Mode Variance.

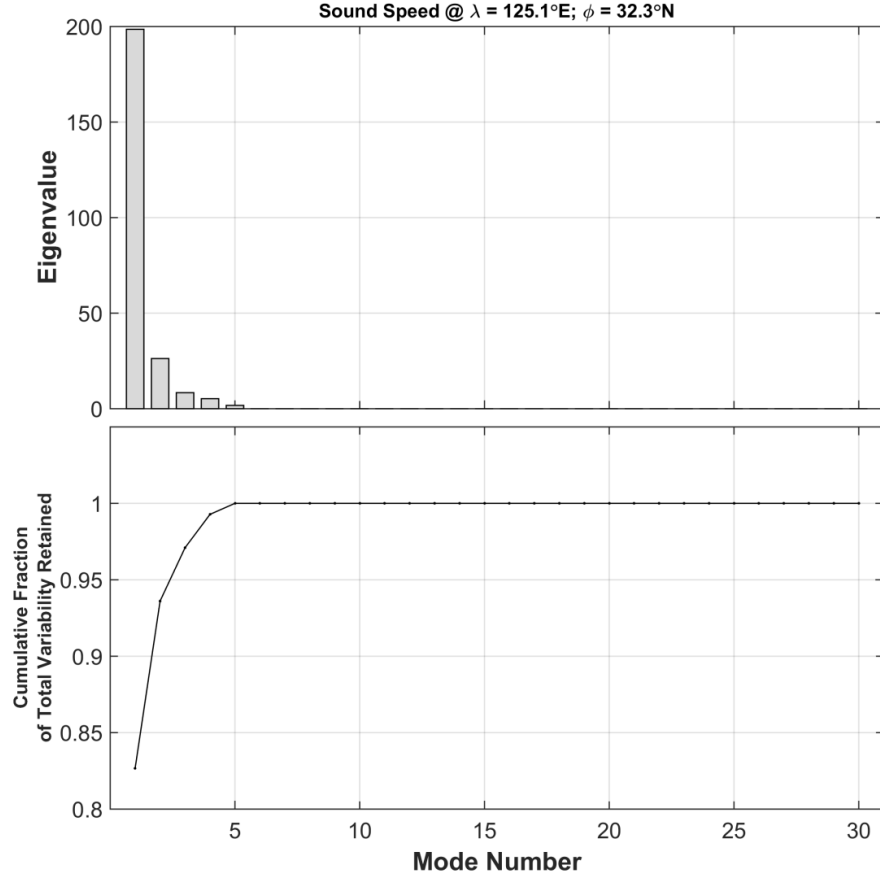


Figure 28. Location C: Eigenvalues and Mode Variance.

The variances in the interannual SSP for deeper waters just outside of the Yellow Sea are represented by EOF where ϕ is the latitude of 31.0°N , and λ is longitude of 129°E , which is location O. This is the deepest location surveyed within this research at greater than 200m and the EOF modes run until the 9th EOF before capturing the entire variability of the SSP (Figure 29). This is two times greater than at most locations within the Yellow Sea, which max out around 4–5 modes as seen in location A and C (Figures 27 and 28). Greater vertical resolution in the deeper water may account for the greater modes resolved by the EOF, but also that in deeper water the gradient of the SSP change is more slight and elongated through the water column than observed for very shallow water there the change is velocity is much sharper.

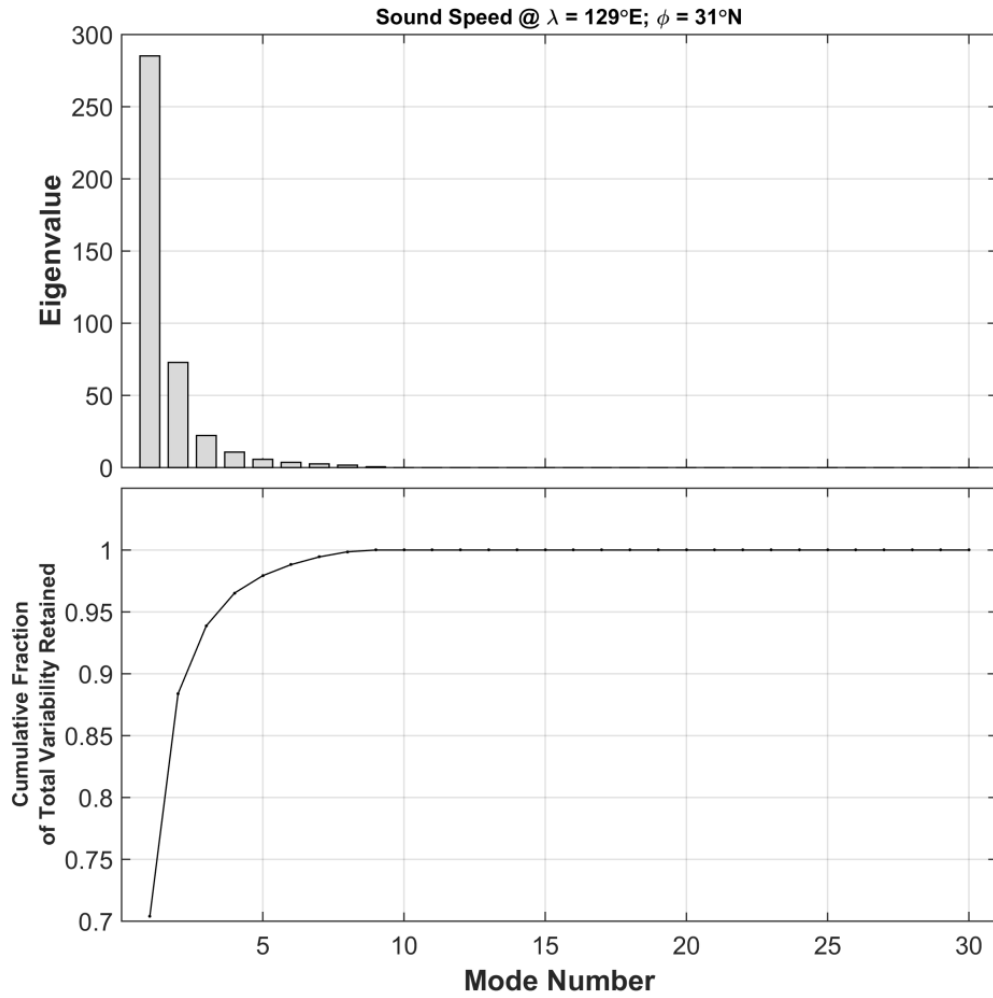


Figure 29. Location O: Eigenvalues and Mode Variance.

Table 9. Variances of the Leading EOF modes of Synoptic Monthly Anomaly at All Locations.

Location	Mode 1 % Variance	Mode 2 % Variance	Mode 3 % Variance	Cumulative Variance
A	86.07	9.38	3.36	98.81
B	79.74	12.82	4.30	96.86
C	82.68	10.93	3.49	97.10
D	90.69	7.86	1.45	100.00
E	85.95	9.45	3.38	98.78
F	86.08	9.38	3.34	98.80
O	70.41	17.99	5.48	93.88

Locations A through F reveal that 95% of the cumulative variance is captured within the first three EOF modes. Location O, although following a similar pattern where model contains the majority of the variance, is the only location below with a cumulative variance within the first three modes of 93.88%. Location D is unique in that all possible variability of the SSPs, 100% of the cumulative interannual variance is expressed with the first three modes. The EOF data for all locations can be found in Appendix D.

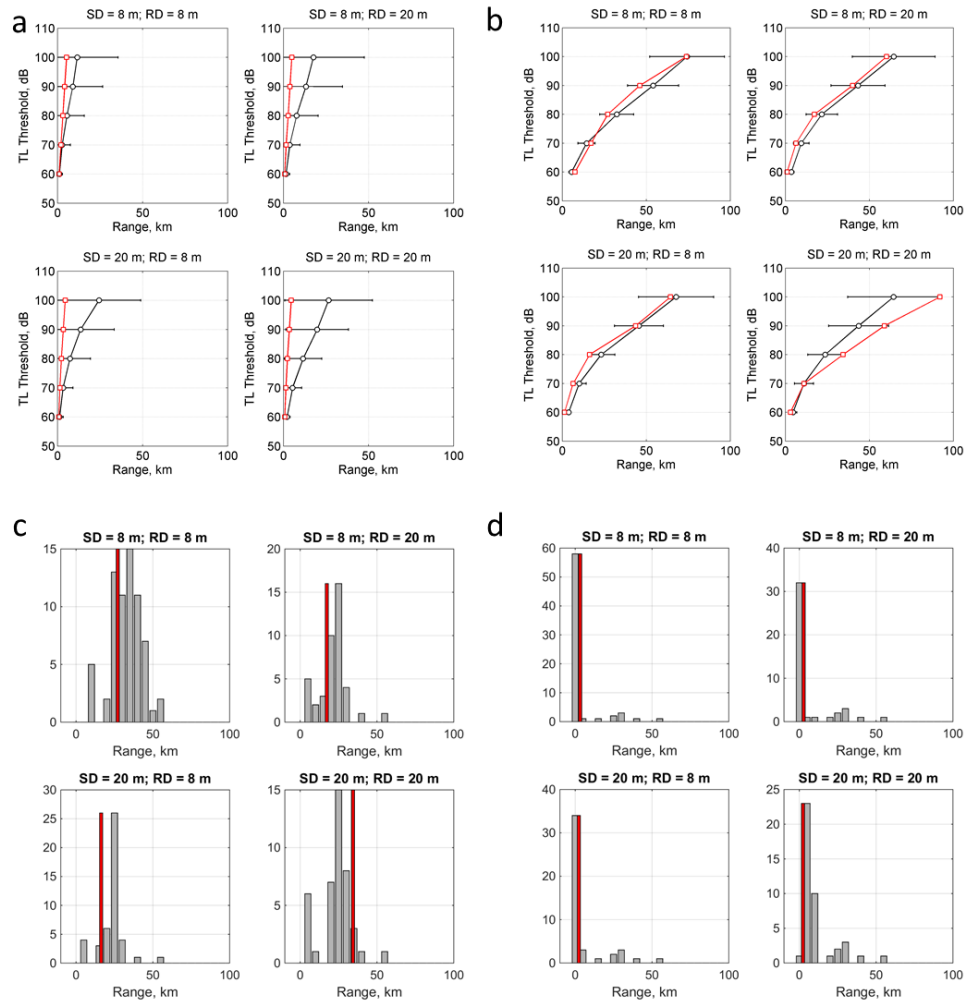
E. TRANSMISSION LOSS ANALYSIS

Frequency is one of the multiple parameters that can be accounted for in the BELLHOP model. The frequency is typically a significant actor in acoustic propagation, however due to the shallow nature of the Yellow Sea this did not have a large impact on the transmission loss. TL was initially tested at 3500 Hz and then at 500Hz for multiple locations, months, and source/receiver configurations. The reduction of frequency did not significantly alter the TL ranges, which is most likely an effect of the shallow water. Frequency was set at 3500Hz for all subsequent TL runs. As determined from the SSP profiles, the greatest deviation from the total mean SSP profile occurred in August, and the least variation in January across all locations. TL was modeled for both SMG-WOD and GDEM at each location, 360° at 10° intervals, with varying combinations of source depth (SD) to receiver depth (RD) (8m to 8m, 8m to 20m, 20m to 20m).

In order to quantify the propagation ranges to allow for comparison, TL thresholds were established across all profiles. TL plotted as dB loss versus range, with thresholds set at 60dB, 70dB, 80dB, 90dB, and 100 dB Loss in order to analyze the difference in rates of TL across various locations in a quantitative manner. The mean and maximum TL range values for all bearings, and all source to receiver depths are listed by dataset and by month (Table 10–13). The 80dB threshold was selected for all histogram runs.

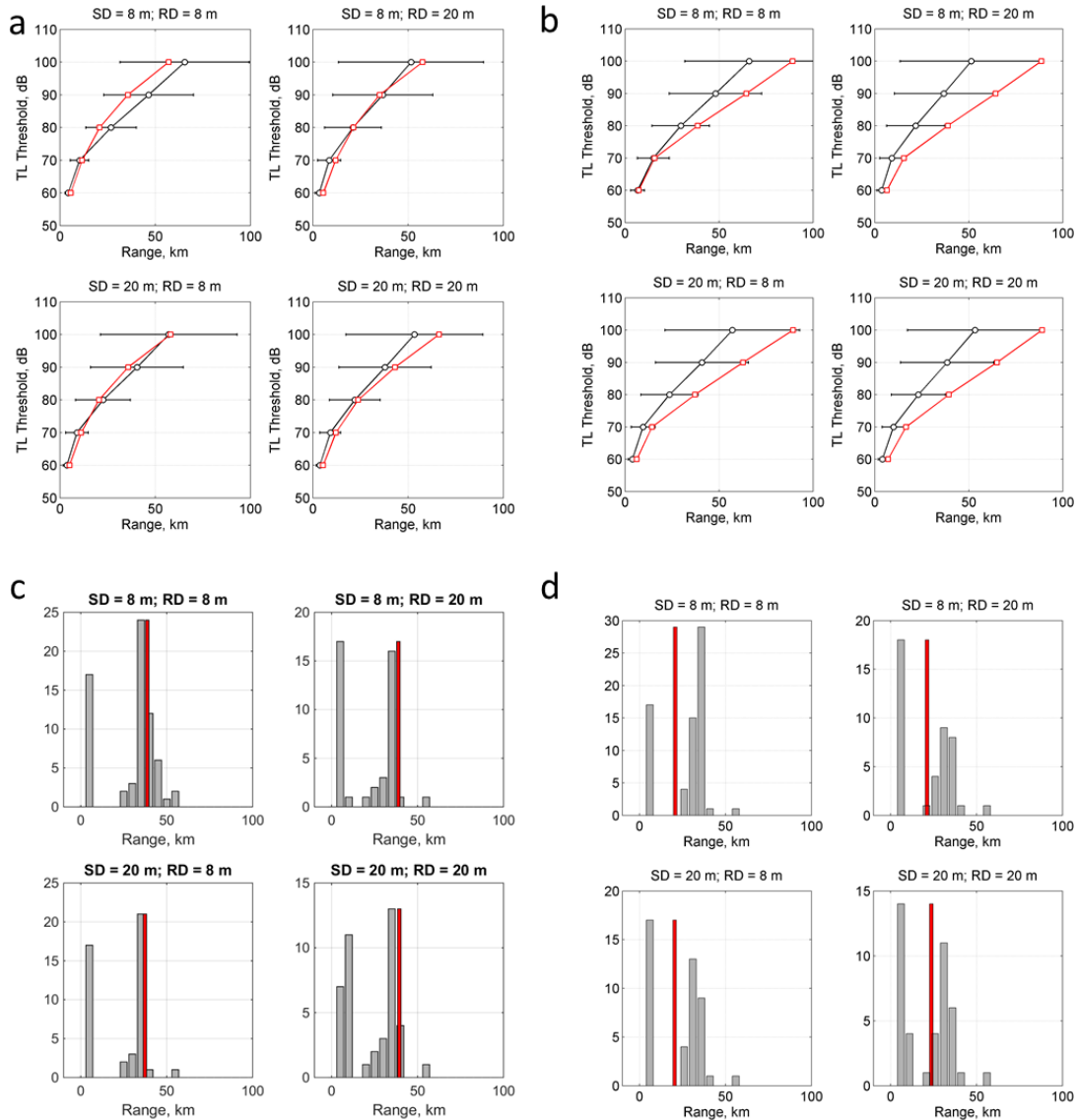
As observed at all locations, slight variations between the ranges for In all locations the SMG-WOD propagation extends beyond the GDEM ranges in August for all source to receiver combinations. The only case where this is not observed in August is at location E, with a source and receiver both at 20m (Figure 31a). In January, GDEM

exhibits longer ranges in at least one or more of the sources to receiver combinations (Figure30). The separation between GDEM and SMG-WOD is much more pronounced in August for location as compared with other locations. All transmission loss plots per location can be found in Appendix F.



TL loss at varying thresholds of 60dB-100dB, SMG-WOD (black) and GDEM (red) a) August, b) January: Histogram of 80dB threshold c) August, d) January.

Figure 30. Figure 30. TL Location A.

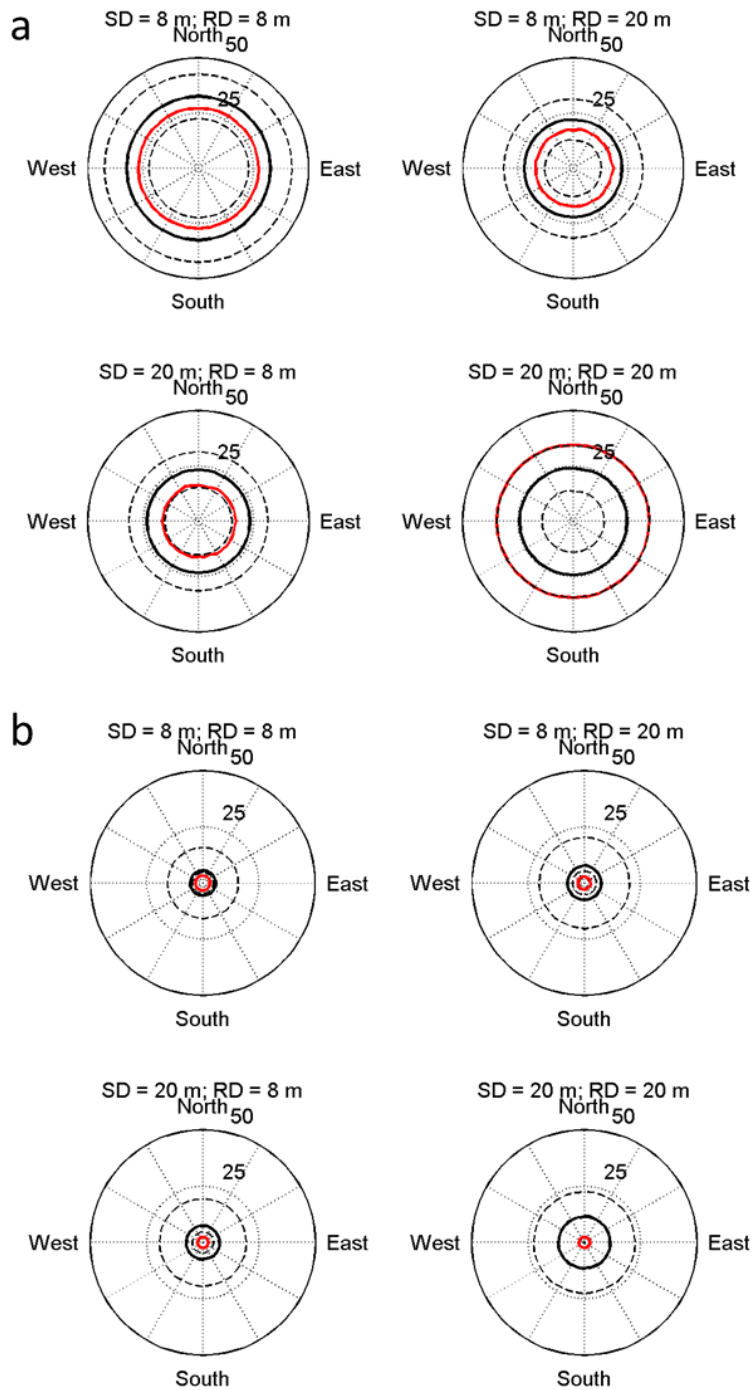


a) August, b) January: TL loss at varying thresholds of 60dB-100dB, SMG-WOD (black) and GDEM (red), c) August, d) January: Histogram of 80dB threshold.

Figure 31. TL Location E.

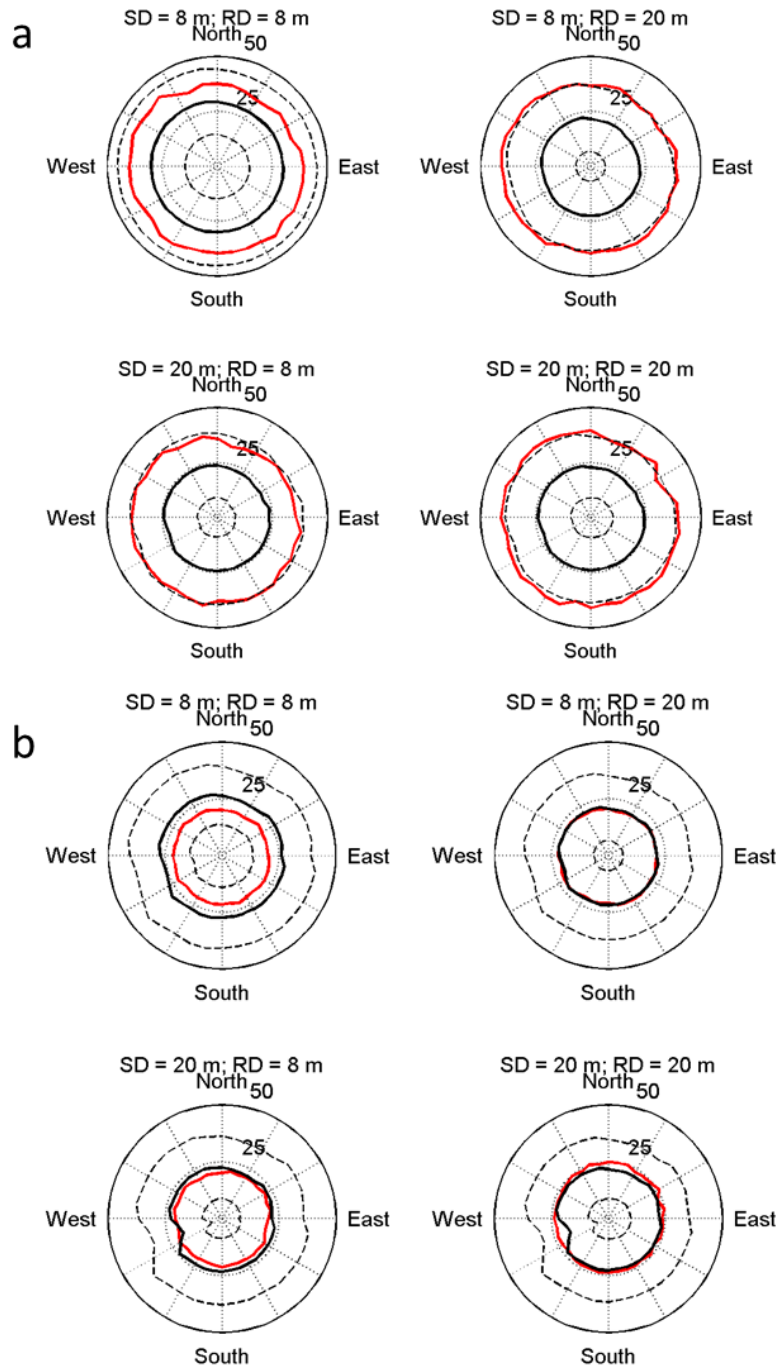
Another useful way to visualize the TL versus range is to express the data in polar coordinate plots that show the extent of the propagation ranges. The polar plots provide a clear picture of how much of the area surrounding the sounds source gets ensounded. The Polar plots also give a sense for how drastically reduced the propagation ranges are in summer compared to the longer ranges in winter. Location is representative of how most

of the locations modeled the ranges, with SMG-WOD generally showing further ranges, other than at the 20m source depth to 20m receiver depth when GDEM models longer ranges in winter (Figure 32). As with the range plots and histograms, location E with the gravel bottom type, models farther GDEM ranges in winter as well (Figure 33). There is a significant amount of variability in the propagation range dependent on the depth of the source as well as the receiver which means not only does the bottom type affect the propagation range, but the juxtaposition of the sensors as well. Propagation polar plots for all locations can be found in Appendix G.



Propagation ranges for plotted for SMG-WOD (black) and GDEM (red) the dashed line is one standard deviation for SMG-WOD. a) January b) August.

Figure 32. Location A: Polar Plots of Propagation Range.



Propagation ranges for plotted for SMG-WOD (black) and GDEM (red) the dashed line is one standard deviation for SMG-WOD. a) January b) August.

Figure 33. Location E: Polar Plots of Propagation Range.

A total histogram was compiled for all locations, all bearings, and all source and receiver depth combinations at threshold of 80dB (Figure 34). This total histogram reveals a few key features allowing for comparison of the datasets. In both SMG-WOD and GDEM, the maximum shifts from 20–40km in the winter to 0–10km in the summer. The SMG-WOD has a bi-modal structure revealing two maxima. In January, the second SMG-WOD maximum is more prominent and more heavily weighted toward longer ranges than the GDEM maximum. In August, the dominant maximum of the SMG-WOD shifts left and is in line with the GDEM maximum for shorter ranges. The GDEM mean TL data is not a classical histogram in the sense that it does not capture the randomness of multiple years (GDEM is a climatological database), but it does show variability which suggests the sensitivity of BELLHOP to the input of source and receiver depth and how varying these will produce different ranges.

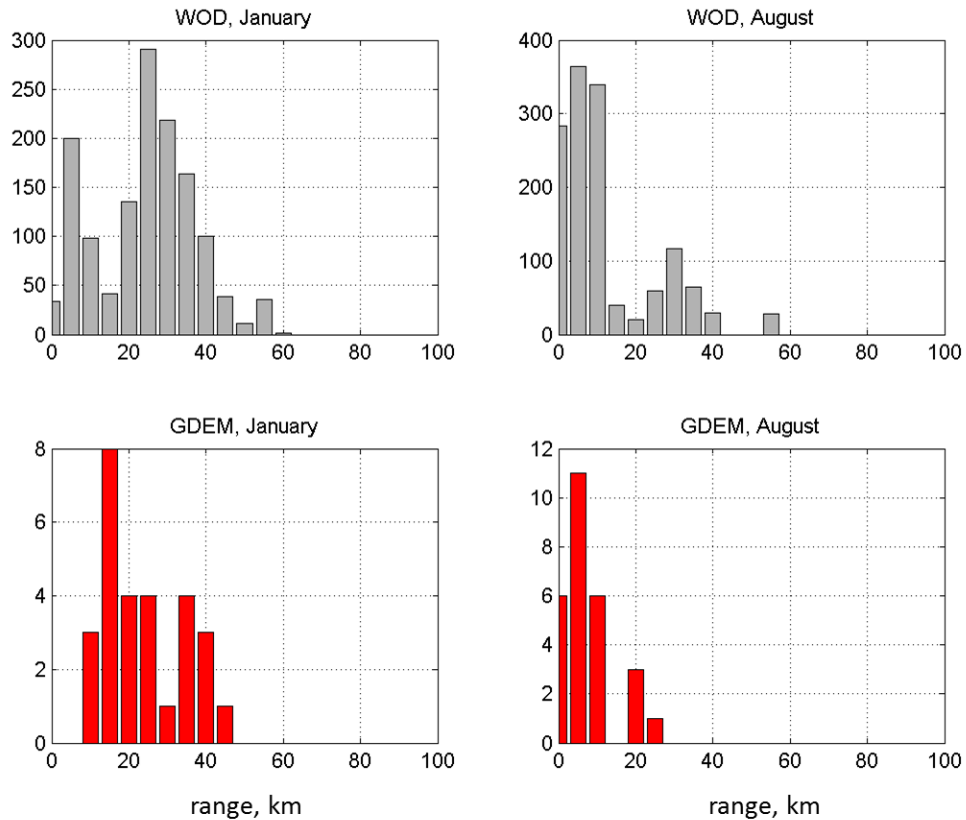


Figure 34. Total TL GDEM and SMG-WOD.

Table 10. Transmission Loss Values SMG-WOD January.

threshold (dB)	range (km)	Location						
		A	B	C	D	E	F	O
60	mean	4.5142	4.4062	3.6771	5.0928	4.8623	3.6476	2.6214
	max	10.5967	9.9216	9.9216	11.4932	12.5317	11.4225	9.9216
70	mean	11.6788	12.2127	11.3663	12.9979	11.4653	9.1267	8.4181
	max	31.7003	31.1898	31.1898	32.9935	31.1898	31.1898	31.1898
80	mean	26.14.19	27.3951	25.1847	27.2414	25.2152	20.3387	18.0278
	max	53.9514	58.6182	54.7512	55.0608	53.9514	53.9514	53.9514
90	mean	47.6035	48.0953	43.9857	46.6375	41.9877	34.8001	31.4071
	max	87.9457	81.9004	84.5373	79.7884	77.0103	82.453	74.5893
100	mean	68.1388	69.7172	63.9175	68.2433	58.127	48.7102	44.9997
	max	92.3192	91.9653	91.9653	91.9653	91.9653	91.9653	91.9653

Table 11. Transmission Loss Values GDEM January.

threshold (dB)	range (km)	Location						
		A	B	C	D	E	F	O
60	mean	3.2627	4.5386	2.8798	3.2001	6.7946	3.4232	1.413
	max	7.5583	7.9578	5.6569	5.5768	7.3418	4.4929	2.8922
70	mean	10.2989	11.2539	9.8557	10.4596	15.5678	9.0209	4.9732
	max	17.1218	16.4182	16.6187	17.6548	16.6254	11.0515	8.0957
80	mean	23.7641	22.8042	23.0009	28.6708	38.5399	18.2543	10.5838
	max	34.3483	32.9114	35.9501	46.157	39.379	23.4702	18.0085
90	mean	47.2287	43.7958	45.2065	46.0015	64.13	34.3497	20.968
	max	59.0338	57.6121	57.4838	61.5141	64.9756	42.3332	38.0115
100	mean	72.6501	63.1721	64.2717	60.2321	89.0296	54.3492	37.7323
	max	92.0613	74.2362	76.5833	73.0217	89.3854	63.7604	55.7593

Table 12. Transmission Loss Values SMG-WOD August.

threshold (dB)	range (km)	Location						
		A	B	C	D	E	F	O
60	mean	1.457	3.5422	1.5666	2.2522	3.8924	2.6188	2.2326
	max	9.9216	9.9216	9.9216	9.9216	9.9216	9.9216	9.9216
70	mean	3.6554	7.9692	3.569	4.9789	9.4116	6.1479	6.0618
	max	31.1898	31.1898	31.1898	31.1898	31.1898	31.1898	31.1898
80	mean	7.7223	14.6942	7	9.9708	23.6079	11.7726	12.4431
	max	53.9514	53.9514	53.9514	53.9514	53.9514	53.9514	53.9514
90	mean	13.2845	24.4461	11.5323	16.3627	41.2092	19.0684	20.81
	max	74.5893	74.5893	74.5893	74.5893	74.5893	74.5893	74.5893
100	mean	18.9952	36.9348	15.1487	21.3142	58.0341	25.4549	29.4261
	max	91.9653	91.9653	91.9653	91.9653	91.9653	91.9653	91.9653

Table 13. Transmission Loss Values GDEM August.

threshold (dB)	range (km)	Location						
		A	B	C	D	E	F	O
60	mean	0.8339	2.8091	0.79208	1.427	5.4375	2.3219	0.84981
	max	0.98235	3.2964	0.96651	1.722	5.7659	2.6349	0.89771
70	mean	1.6139	6.106	1.3259	2.4962	11.7526	4.4197	3.4008
	max	2.0368	6.7257	1.5941	2.8337	12.1603	4.5578	3.4304
80	mean	2.671	10.2964	1.9617	4.1585	21.588	7.2814	6.8195
	max	3.1903	11.1137	2.1844	4.4257	23.7492	7.9183	6.8517
90	mean	3.7663	15.8272	2.6948	6.3945	37.4626	11.7533	12.3378
	max	4.2478	16.7245	2.8533	7.8383	43.1782	14.7736	12.3965
100	mean	4.8602	23.1134	3.5924	8.2717	59.7458	16.4812	23.5609
	max	5.358	25.1659	3.9414	10.2709	66.2201	21.7788	23.8398

VII. CONCLUSION

This research shows that inter-annual variability exists in the Yellow Sea and that the acoustic propagation in this environment is sensitive to this variability. It has been confirmed through analysis of the SSPs variability and the resultant variability in TL ranges. Due to the inter-annual variability, it is desirable to use a dataset such as SMG-WOD, which provides the option of breaking out data by year, as opposed to the climatological average in GDEM.

The spatial resolution, both horizontal and vertical, plays an important role in capturing the acoustic variability. This can be an issue for the current version of the SMG-WOD, which is a global one with 1° horizontal resolution, and has 28 vertical levels of 10 m vertical resolution in the upper part of the water column. The GDEM database has the horizontal resolution of $1/4^\circ$ horizontal resolution and 78 vertical levels of 2m vertical resolution in the upper part of the water column. Familiarity with the difference in these databases and the how they may be best applied is very important for the Navy's Meteorology and Oceanography METOC community. As the impact of resolution shortfalls is determined, the METOC community may request updated datasets.

It is therefore recommended to create a region-specific dataset, which would have the functionality of SMG-WOD, but with the vertical and horizontal resolution of GDEM. Note that the Optimal Spectral Decomposition method used to create the SMG-WOD database is capable of producing as high spatial resolution as raw data allow for. Besides, the OSD basis functions do not depend on measurements but only on the basin configuration and bathymetry. This makes it possible to calculate fine resolution basis functions for a specific basin just once, and then use them as soon as new data for the current year(s) become available or for any historical data.

Although ranges are overall farther in winter (January) than the summer (August) for both datasets, the propagation ranges are overall larger in GDEM than SMG-WOD in the winter. In the summer, where ranges are significantly reduced in both datasets due to

the warming in shallow waters of the Yellow Sea, the SMG-WOD tends to display a spread of TL ranges that is generally farther than the summer TL ranges for GDEM.

The overall average TL ranges between the two datasets same, but because SMG-WOD models individual years we can see the several extended ranges for acoustic transmission that break out well past the GDEM TL ranges, not by a mere one or two km but in some cases twice the average TL range such that 20km detection range may jump to 40 km depending in the environment at the time.

This research also reveals the sensitivity of BELLHOP; it is sensitive enough to produce different TL results based on the variations of source and receiver depths when given the same SSP input. BELLHOP is also sensitive to the attenuation values for the bottom sediment, as location E had the hardest, most reflective bottom type and the in both datasets it modeled the longest ranges as opposed to most of the other locations being silty clay or mud and BELLHOP modeled significantly shorter ranges.

For a general study, either database would be relevant because the average TL ranges are very close, but for tactical naval application, this research shows that in shallow water, the TL range variations between the two datasets can be significant. Just a few km extension of TL range can greatly increase the entire ensonification coverage area, which is crucial for sonar operators on submarines or ships, or of unmanned. This research shows that TL ranges may vary up to 10km or further, depending on the combination of source depth to receiver depth, which is important since submarines are not fixed in a vertical position. As the submarine varies its depth, it can greatly affect its detection vulnerability, or based on the season, it may choose to avoid an entire shallow operating area where ranges are poor.

This research is very specific to the Yellow Sea as it such a shallow body of water, and while it may produce results comparable to other shallow bodies of water such as the Arabian Gulf, it would provide greater insight to actually conduct this same study but in multiple other ocean. For deeper oceans, the resolution differences between the datasets may not impact the results, and the SSPs will have different structures. As no correlation was found between the SSP variability and any published indices, a beneficial

future area of research would be to pair an oceanographic study of acoustic variability with a meteorological study to develop and test various EAMIs and the search for a correlation to acoustics. It would also be valuable to expand upon this research by comparing in situ TL data ranges to the projection of SMG-WOD and GDEM ranges in order to see how the real world matches up to the models.

THIS PAGE INTENTIONALLY LEFT BLANK

APPENDIX A. COMPLETE SEDIMENT LIST

Table 14. Sediment Type Definitions from the Enhanced database.
Source: NAVO (2006).

Type	<i>Enhanced Categories Description</i>	Enhanced	Standard	Reduced	HFEVA
PT	Sand	102	1125	25	9
PT	Silt	105	1105	52	18
PT	Silty Clay	107	1107	50	7
PT	Clay	108	1108	8	23
PT	Gravel	112	1112	62	3
PT	Sandy Mud	196	1104	25	96
PT	Mud	197	1107	50	7
PC	Sand	202	1225	25	9
PC	Silty Sand	203	1203	24	11
PC	Sandy Silt	204	1204	53	16
PC	Silt	205	1205	52	18
PC	Clayey Silt	206	1206	50	19
PC	Silty Clay	207	1207	50	22
PC	Clay	208	1208	8	23
PC	Sand - Silt - Clay	209	1209	52	17
PC	Marl	211	1208	8	23
PC	Gravel	212	1212	62	3
PC	Gravelly Sand	220	1220	21	7
PC	Coarse Sand	222	1222	22	7
PC	Medium Sand	223	1223	23	9
PC	Sandy Clay	242	1242	25	20
PC	Ooze	310	1208	8	23
PS	Silt	405	1105	52	18
PS	Silty Clay	407	1107	50	7
PS	Clay	408	1108	8	23
PS	Ooze	510	1108	8	23
PS	Mud	511	1105	52	17
P	Clayey Silt	706	1106	50	19
P	Silty Clay	707	1107	50	22
P	Clay	708	1108	8	23
V	Sand	802	1102	23	9
V	Silt	805	1105	52	18
V	Silty Clay	807	1107	50	7
O	NO DATA	888	888	888	888
L	LAND	999	999	999	999
T	Rock	1101	1101	1	2
T	Sand	1102	1102	23	9
T	Silty Sand	1103	1103	25	11
T	Sandy Silt	1104	1104	25	16
T	Silt	1105	1105	52	18

Type	<i>Enhanced Categories Description</i>	Enhanced	Standard	Reduced	HFEVA
T	Clayey Silt	1106	1106	50	19
T	Silty Clay	1107	1107	50	22
T	Clay	1108	1108	8	23
T	Sand - Silt - Clay	1109	1109	24	17
T	Gravel	1112	1112	62	3
T	Sandy Gravel	1113	1113	63	4
T	Silty Gravel	1114	1114	63	10
T	Muddy Sandy Gravel	1115	1114	63	6
T	Clayey Gravel	1116	1116	63	10
T	Muddy Gravel	1117	1116	63	10
T	Gravelly Muddy Sand	1118	1120	63	8
T	Gravel - Silty Sand	1119	1113	63	8
T	Gravelly Sand	1120	1120	21	7
T	Very Coarse Sand	1121	1121	21	5
T	Coarse Sand	1122	1122	22	7
T	Medium Sand	1123	1123	23	9
T	Fine Sand	1124	1124	24	11
T	Very Fine Sand	1125	1125	25	13
T	Clayey Sand	1126	1126	25	14
T	Gravel - Shell	1128	1112	62	3
T	Gravelly Silt	1130	1130	21	16
T	Gravelly Silt - Shell	1131	1130	21	16
T	Gravelly Sandy Silt	1132	1130	21	16
T	Gravelly Mud	1133	1130	21	16
T	Gravel - Sand - Mud	1134	1113	63	6
T	Rock - Sand - Mud	1135	1161	61	3
T	Rock - Gravel - Mud	1136	1161	61	3
T	Rock - Gravel - Sand	1137	1161	61	3
T	Rock - Gravel - Sand - Mud	1138	1161	61	3
T	Gravelly Clay	1140	1140	21	21
T	Sand - Clay - Shell	1141	1102	23	9
T	Sandy Clay	1142	1142	25	20
T	Coarse Sand - Shell	1146	1113	63	4
T	Very Fine Silt	1150	1150	50	21
T	Fine Silt	1151	1151	51	19
T	Medium Silt	1152	1152	52	17
T	Coarse Silt	1153	1153	53	15
T	Rough Rock	1154	1101	1	1
T	Mud over Rock	1155	1101	1	2
T	Silty Clay - Shell	1156	1130	21	16
T	Boulders	1160	1160	60	2
T	Cobbles (Stones) - Shell	1161	1161	61	3
T	Pebbles - Shell	1162	1162	62	3
T	Granules	1163	1163	63	3
T	Sand - Silt - Clay - Shell	1164	1112	62	16
T	Gravel - Sand - Shell	1165	1161	61	3
T	Shell	1166	1162	62	3

Type	<i>Enhanced Categories Description</i>	Enhanced	Standard	Reduced	HFEVA
T	Rock - Gravel - Sand - Shell	1167	1161	61	3
T	Sand - Shell	1168	1113	63	4
T	Rock - Gravel	1170	1101	1	2
T	Rock - Coral	1171	1101	1	1
T	Rock - Sand	1172	1101	1	2
T	Rock - Mud	1173	1101	1	2
T	Mud - Shell	1174	1114	63	10
T	Gravel - Sand	1175	1113	63	4
T	Gravel - Mud	1176	1114	63	10
T	Clayey Sand - Shell	1177	1120	21	7
T	Soft Mud	1178	1106	50	21
T	Hard Mud	1179	1106	50	19
T	Silty Sand - Shell	1181	1121	21	5
T	Gravelly Sand - Shell	1182	1113	63	4
T	Medium Sand - Shell	1183	1120	21	5
T	Fine Sand - Shell	1184	1120	21	7
T	Sandy Gravel - Shell	1185	1113	63	4
T	Clayey Silt - Shell	1186	1130	21	16
T	Silt - Shell	1187	1130	21	16
T	Silty Gravel - Shell	1188	1114	63	10
T	Sandy Silt - Shell	1189	1113	21	8
T	Muddy Tidal Flats	1190	1153	53	15
T	Sandy Tidal Flats	1191	1123	23	9
T	Sandy Muddy Tidal Flats	1192	1109	24	17
T	Sand Dune	1193	1102	23	9
T	Sand - Mud	1194	1109	24	17
T	Muddy Sand	1195	1109	24	12
T	Sandy Mud	1196	1104	25	18
T	Mud	1197	1105	52	18
T	Clay - Shell	1198	1140	21	10
T	Stiff Mud	1199	1106	50	19
C	Rock	1201	1201	1	2
C	Sand	1202	1202	23	9
C	Silty Sand	1203	1203	25	11
C	Sandy Silt	1204	1204	25	16
C	Silt	1205	1205	52	18
C	Clayey Silt	1206	1206	50	19
C	Silty Clay	1207	1207	50	22
C	Clay (Marl)	1208	1208	8	23
C	Sand - Silt - Clay	1209	1209	24	17
C	Ooze	1210	1208	8	23
C	Marl	1211	1208	8	23
C	Gravel (Shell Detritus)	1212	1212	62	3
C	Sandy Gravel	1213	1213	63	4
C	Silty Gravel	1214	1214	63	10
C	Muddy Sandy Gravel	1215	2114	63	6
C	Clayey Gravel	1216	1216	63	10

Type	<i>Enhanced Categories Description</i>	Enhanced	Standard	Reduced	HFEVA
C	Muddy Gravel	1217	1216	63	10
C	Gravelly Muddy Sand	1218	1220	63	8
C	Gravel - Silty Sand	1219	1213	63	8
C	Gravelly Sand	1220	1220	21	7
C	Very Coarse Sand	1221	1221	21	5
C	Coarse Sand	1222	1222	22	7
C	Medium Sand	1223	1223	23	9
C	Fine Sand	1224	1224	24	11
C	Very Fine Sand	1225	1225	25	13
C	Clayey Sand	1226	1226	25	14
C	Oolite	1227	1223	23	9
C	Gravel - Shell	1228	1212	62	3
C	Gravelly Silt	1230	1230	21	16
C	Gravelly Silt - Shell	1231	1230	21	16
C	Gravelly Sandy Silt	1232	1230	21	16
C	Gravelly Mud	1233	1230	21	16
C	Gravel - Sand - Mud	1234	1213	63	6
C	Rock - Sand - Mud	1235	1261	61	3
C	Rock - Gravel - Mud	1236	1261	61	3
C	Rock - Gravel - Sand	1237	1261	61	3
C	Rock - Gravel - Sand - Mud	1238	1261	61	3
C	Gravelly Clay	1240	1240	21	21
C	Sand - Clay - Shell	1241	1202	23	9
C	Sandy Clay (Sandy Marl)	1242	1242	25	20
C	Coral Debris - Sand	1243	1212	62	3
C	Coral Debris - Sand - Shell	1244	1212	62	3
C	Coral Debris - Shell	1245	1212	62	3
C	Coarse Sand - Shell	1246	1213	63	4
C	Coral Debris - Sand - Mud	1247	1212	62	6
C	Coral Debris - Mud - Shell	1248	1212	62	6
C	Coral Debris - Mud	1249	1212	62	6
C	Very Fine Silt	1250	1250	50	21
C	Fine Silt	1251	1251	51	19
C	Medium Silt	1252	1252	52	17
C	Coarse Silt	1253	1253	53	15
C	Rough Rock	1254	1201	1	1
C	Mud over Rock	1255	1201	1	2
C	Silty Clay - Shell	1256	1230	21	16
C	Coral Debris - Sand - Mud - Shell	1257	1212	62	3
C	Coral Debris	1258	1212	62	3
C	Coral	1259	1201	1	1
C	Boulders	1260	1260	60	2
C	Cobbles (Stones) - Shell	1261	1261	61	3
C	Pebbles - Shell	1262	1262	62	3
C	Granules	1263	1263	63	3
C	Sand - Silt - Clay - Shell	1264	1212	62	16

Type	<i>Enhanced Categories Description</i>	Enhanced	Standard	Reduced	HFEVA
C	Gravel - Sand - Shell	1265	1261	61	3
C	Shell	1266	1262	62	3
C	Rock - Gravel - Sand - Shell	1267	1261	61	3
C	Sand - Shell	1268	1213	63	4
C	Rock - Gravel	1270	1201	1	2
C	Rock - Coral	1271	1201	1	1
C	Rock - Sand	1272	1201	1	2
C	Rock - Mud	1273	1201	1	2
C	Mud - Shell	1274	1214	63	10
C	Gravel - Sand	1275	1213	63	4
C	Gravel - Mud	1276	1214	63	10
C	Clayey Sand - Shell	1277	1220	21	7
C	Soft Mud	1278	1206	50	21
C	Hard Mud	1279	1206	50	19
C	Silty Sand - Shell	1281	1221	21	5
C	Gravelly Sand - Shell	1282	1213	63	4
C	Medium Sand - Shell	1283	1220	21	5
C	Fine Sand - Shell	1284	1220	21	7
C	Sandy Gravel - Shell	1285	1213	63	4
C	Clayey Silt - Shell	1286	1230	21	16
C	Silt - Shell	1287	1230	21	16
C	Silty Gravel - Shell	1288	1214	63	10
C	Sandy Silt - Shell	1289	1213	21	8
C	Muddy Tidal Flats	1290	1253	53	15
C	Sandy Tidal Flats	1291	1223	23	9
C	Sandy Muddy Tidal Flats	1292	1209	24	17
C	Sand Dune	1293	1202	23	9
C	Mud - Sand	1294	1209	24	17
C	Muddy Sand	1295	1209	24	12
C	Sandy Mud	1296	1204	25	18
C	Mud	1297	1205	52	18
C	Clay - Shell	1298	1240	21	10
C	Stiff Mud	1299	1206	50	19
S	Silt	1405	1105	52	18
S	Clay	1408	1108	8	23
S	Ooze	1510	1108	8	23
S	Mud	1511	1105	52	17
V	Sand	1802	1102	23	9
V	Silt	1805	1105	52	18
V	Gravel	1812	1112	62	3
V	Sandy Gravel	1813	1113	63	4
V	Gravelly Sand	1820	1120	21	7
V	Rough Rock	1854	1101	1	1
V	Boulders	1860	1160	60	2
V	Rock - Gravel	1870	1101	1	2
V	Rock - Sand	1872	1101	1	2
V	Gravel - Sand	1875	1113	63	4

Type	<i>Enhanced Categories Description</i>	Enhanced	Standard	Reduced	HFEVA
UC	Silt	2205	1205	52	18
UC	Clayey Silt	2206	1206	50	19
UC	Silty Clay	2207	1207	50	22
UC	Clay	2208	1208	8	23
UC	Sand - Silt - Clay	2209	1209	24	17
UC	Marl	2211	1208	8	23
US	Silt	2405	1105	52	18
US	Clay	2408	1108	8	23
UC	Ooze	2210	1208	8	23
U	Silty Sand	2603	1103	25	11
U	Sandy Silt	2604	1104	25	16
U	Silt	2605	1105	52	18
U	Clayey Silt	2606	1106	50	19
U	Silty Clay	2607	1107	50	22
U	Clay	2608	1108	8	23
U	Sand - Silt - Clay	2609	1109	24	17
U	Fine Sand	2624	1124	24	11
U	Gravel - Sand	2675	1113	63	4
U	Gravelly Sand - Shell	2682	1113	63	5
HC	Rock	3201	1201	1	2
HC	Sand	3202	1202	23	9
HC	Silty Sand	3203	1203	25	11
HC	Sandy Silt	3204	1204	25	16
HC	Silt	3205	1205	52	18
HC	Clayey Silt	3206	1206	50	19
HC	Silty Clay	3207	1207	50	22
HC	Clay (Marl)	3208	1208	8	23
HC	Sand - Silt - Clay	3209	1209	24	17
HC	Ooze	3210	1208	8	23
HC	Gravel (Shell Detritus)	3212	1212	62	3
HC	Sandy Gravel	3213	1213	63	4
HC	Silty Gravel	3214	1214	63	10
HC	Muddy Sandy Gravel	3215	1214	63	6
HC	Clayey Gravel	3216	1216	63	10
HC	Muddy Gravel	3217	1216	63	10
HC	Gravelly Muddy Sand	3218	1220	63	8
HC	Gravel - Silty Sand	3219	1213	63	8
HC	Gravelly Sand	3220	1220	21	7
HC	Very Coarse Sand	3221	1221	21	5
HC	Coarse Sand	3222	1222	22	7
HC	Medium Sand	3223	1223	23	9
HC	Fine Sand	3224	1224	24	11
HC	Very Fine Sand	3225	1225	25	13
HC	Clayey Sand	3226	1226	25	14
HC	Gravel - Shell	3228	1212	62	3
HC	Gravelly Silt	3230	1230	21	16
HC	Gravelly Silt - Shell	3231	1230	21	16

Type	<i>Enhanced Categories Description</i>	Enhanced	Standard	Reduced	HFEVA
HC	Gravelly Sandy Silt	3232	1230	21	16
HC	Gravelly Mud	3233	1230	21	16
HC	Gravel - Sand - Mud	3234	1213	63	6
HC	Rock - Sand - Mud	3235	1261	61	3
HC	Rock - Gravel - Mud	3236	1261	61	3
HC	Rock - Gravel - Sand	3237	1261	61	3
HC	Rock - Gravel - Sand - Mud	3238	1261	61	3
HC	Gravelly Clay	3240	1240	21	21
HC	Sand - Clay - Shell	3241	1202	23	9
HC	Sandy Clay (Sandy Marl)	3242	1242	25	20
HC	Coral Debris - Sand	3243	1212	62	3
HC	Coral Debris - Sand - Shell	3244	1212	62	3
HC	Coral Debris - Shell	3245	1212	62	3
HC	Coarse Sand - Shell	3246	1213	63	4
HC	Coral Debris - Sand - Mud	3247	1212	62	6
HC	Coral Debris - Mud - Shell	3248	1212	62	6
HC	Coral Debris - Mud	3249	1212	62	6
HC	Very Fine Silt	3250	1250	50	21
HC	Fine Silt	3251	1251	51	19
HC	Medium Silt	3252	1252	52	17
HC	Coarse Silt	3253	1253	53	15
HC	Rough rock	3254	1201	1	1
HC	Mud over Rock	3255	1201	1	2
HC	Silty Clay - Shell	3256	1230	21	16
HC	Coral Debris - Sand - Mud - Shell	3257	1212	62	3
HC	Coral Debris	3258	1212	62	3
HC	Boulders	3260	1260	60	2
HC	Cobbles (Stones) - Shell	3261	1261	61	3
HC	Pebbles - Shell	3262	1262	62	3
HC	Granules	3263	1263	63	3
HC	Sand - Silt - Clay - Shell	3264	1212	62	16
HC	Gravel - Sand - Shell	3265	1261	61	3
HC	Shell	3266	1262	62	3
HC	Rock - Gravel - Sand - Shell	3267	1261	61	3
HC	Sand - Shell	3268	1213	63	4
HC	Rock - Gravel	3270	1201	1	2
HC	Rock - Coral	3271	1201	1	1
HC	Rock - Sand	3272	1201	1	2
HC	Rock - Mud	3273	1201	1	2
HC	Mud - Shell	3274	1214	63	10
HC	Gravel - Sand	3275	1213	63	4
HC	Gravel - Mud	3276	1214	63	10
HC	Clayey Sand - Shell	3277	1220	21	7
HC	Soft Mud	3278	1206	50	21
HC	Hard Mud	3279	1206	50	19
HC	Silty Sand - Shell	3281	1221	21	5

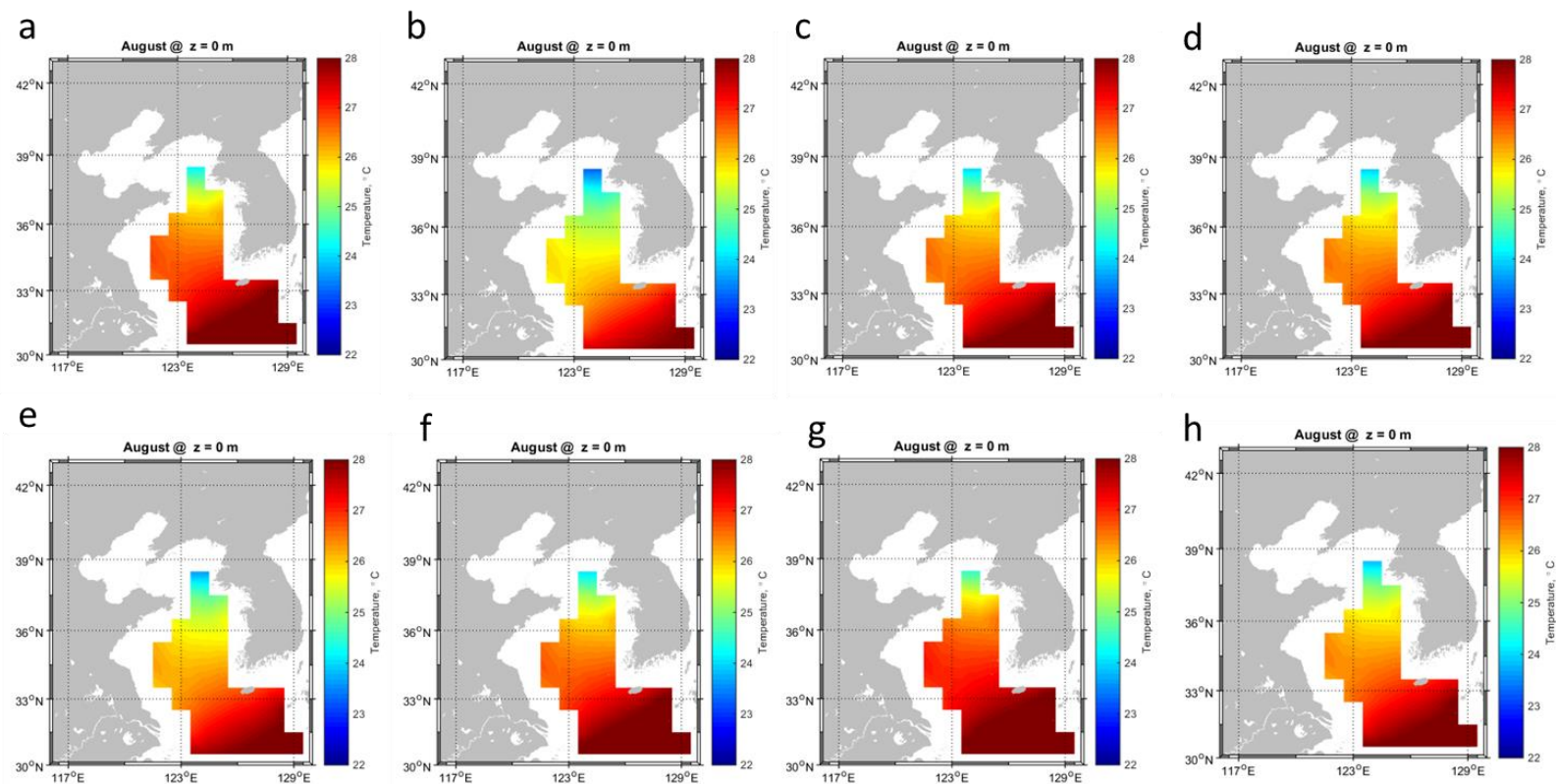
Type	<i>Enhanced Categories Description</i>	Enhanced	Standard	Reduced	HFEVA
HC	Gravelly Sand - Shell	3282	1213	63	4
HC	Medium Sand - Shell	3283	1220	21	5
HC	Fine Sand - Shell	3284	1220	21	7
HC	Sandy Gravel - Shell	3285	1213	63	4
HC	Clayey Silt - Shell	3286	1230	21	16
HC	Silt - Shell	3287	1230	21	16
HC	Silty Gravel - Shell	3288	1214	63	10
HC	Sandy Silt - Shell	3289	1213	21	8
HC	Sand - Mud	3294	1209	24	17
HC	Muddy Sand	3295	1209	24	12
HC	Sandy Mud	3296	1204	25	18
HC	Mud	3297	1205	52	18
HC	Clay - Shell	3298	1240	21	10
HC	Stiff Mud	3299	1206	50	19
HT	Rock	3301	1101	1	2
HT	Sand	3302	1102	23	9
HT	Silty Sand	3303	1103	25	11
HT	Sandy Silt	3304	1104	25	16
HT	Silt	3305	1105	52	18
HT	Clayey Silt	3306	1106	50	19
HT	Silty Clay	3307	1107	50	22
HT	Clay	3308	1108	8	23
HT	Sand - Silt - Clay	3309	1109	24	17
HT	Gravel	3312	1112	62	3
HT	Sandy Gravel	3313	1113	63	4
HT	Silty Gravel	3314	1114	63	10
HT	Muddy Sandy Gravel	3315	1114	63	6
HT	Clayey Gravel	3316	1116	63	10
HT	Muddy Gravel	3317	1116	63	10
HT	Gravelly Muddy Sand	3318	1120	63	8
HT	Gravel - Silty Sand	3319	1113	63	8
HT	Gravelly Sand	3320	1120	21	7
HT	Very Coarse Sand	3321	1121	21	5
HT	Coarse Sand	3322	1122	22	7
HT	Medium Sand	3323	1123	23	9
HT	Fine Sand	3324	1124	24	11
HT	Very Fine Sand	3325	1125	25	13
HT	Clayey Sand	3326	1126	25	14
HT	Gravel - Shell	3328	1112	62	3
HT	Gravelly Silt	3330	1130	21	16
HT	Gravelly Silt - Shell	3331	1130	21	16
HT	Gravelly Sandy Silt	3332	1130	21	16
HT	Gravelly Mud	3333	1130	21	16
HT	Gravel - Sand - Mud	3334	1113	63	6
HT	Rock - Sand - Mud	3335	1161	61	3
HT	Rock - Gravel - Mud	3336	1161	61	3
HT	Rock - Gravel - Sand	3337	1161	61	3

Type	<i>Enhanced Categories Description</i>	Enhanced	Standard	Reduced	HFEVA
HT	Rock - Gravel - Sand - Mud	3338	1161	61	3
HT	Gravelly Clay	3340	1140	21	21
HT	Sand - Clay - Shell	3341	1102	23	9
HT	Sandy Clay	3342	1142	25	20
HT	Very Fine Silt	3350	1150	50	21
HT	Fine Silt	3351	1151	51	19
HT	Medium Silt	3352	1152	52	17
HT	Coarse Silt	3353	1153	53	15
HT	Rough rock	3354	1101	1	1
HT	Mud over Rock	3355	1101	1	2
HT	Silty Clay - Shell	3356	1130	21	16
HT	Boulders	3360	1160	60	2
HT	Cobbles (Stones) - Shell	3361	1161	61	3
HT	Pebbles - Shell	3362	1162	62	3
HT	Granules	3363	1163	63	3
HT	Sand - Silt - Clay - Shell	3364	1112	62	16
HT	Gravel - Sand - Shell	3365	1161	61	3
HT	Shell	3366	1162	62	3
HT	Rock - Gravel - Sand - Shell	3367	1161	61	3
HT	Sand - Shell	3368	1113	63	4
HT	Rock - Gravel	3370	1101	1	2
HT	Rock - Coral	3371	1101	1	1
HT	Rock - Sand	3372	1101	1	2
HT	Rock - Mud	3373	1101	1	2
HT	Mud - Shell	3374	1114	63	10
HT	Gravel - Sand	3375	1113	63	4
HT	Mud - Gravel	3376	1114	63	10
HT	Clayey Sand - Shell	3377	1120	21	7
HT	Soft Mud	3378	1106	50	21
HT	Hard Mud	3379	1106	50	19
HT	Silty Sand - Shell	3381	1121	21	5
HT	Gravelly Sand - Shell	3382	1113	63	4
HT	Medium Sand - Shell	3383	1120	21	5
HT	Fine Sand - Shell	3384	1120	21	7
HT	Sandy Gravel - Shell	3385	1113	63	4
HT	Clayey Silt - Shell	3386	1130	21	16
HT	Silt - Shell	3387	1130	21	16
HT	Silty Gravel - Shell	3388	1114	63	10
HT	Sandy Silt - Shell	3389	1113	21	8
HT	Sand - Mud	3394	1109	24	17
HT	Muddy Sand	3395	1109	24	12
HT	Sandy Mud	3396	1104	25	18
HT	Mud	3397	1105	52	18
HT	Stiff Mud	3399	1106	50	19
HV	Clayey Gravel	3816	1116	63	17
HV	Rock - Gravel - Sand - Shell	3867	1161	61	3
HV	Muddy Sand	3895	1109	24	12

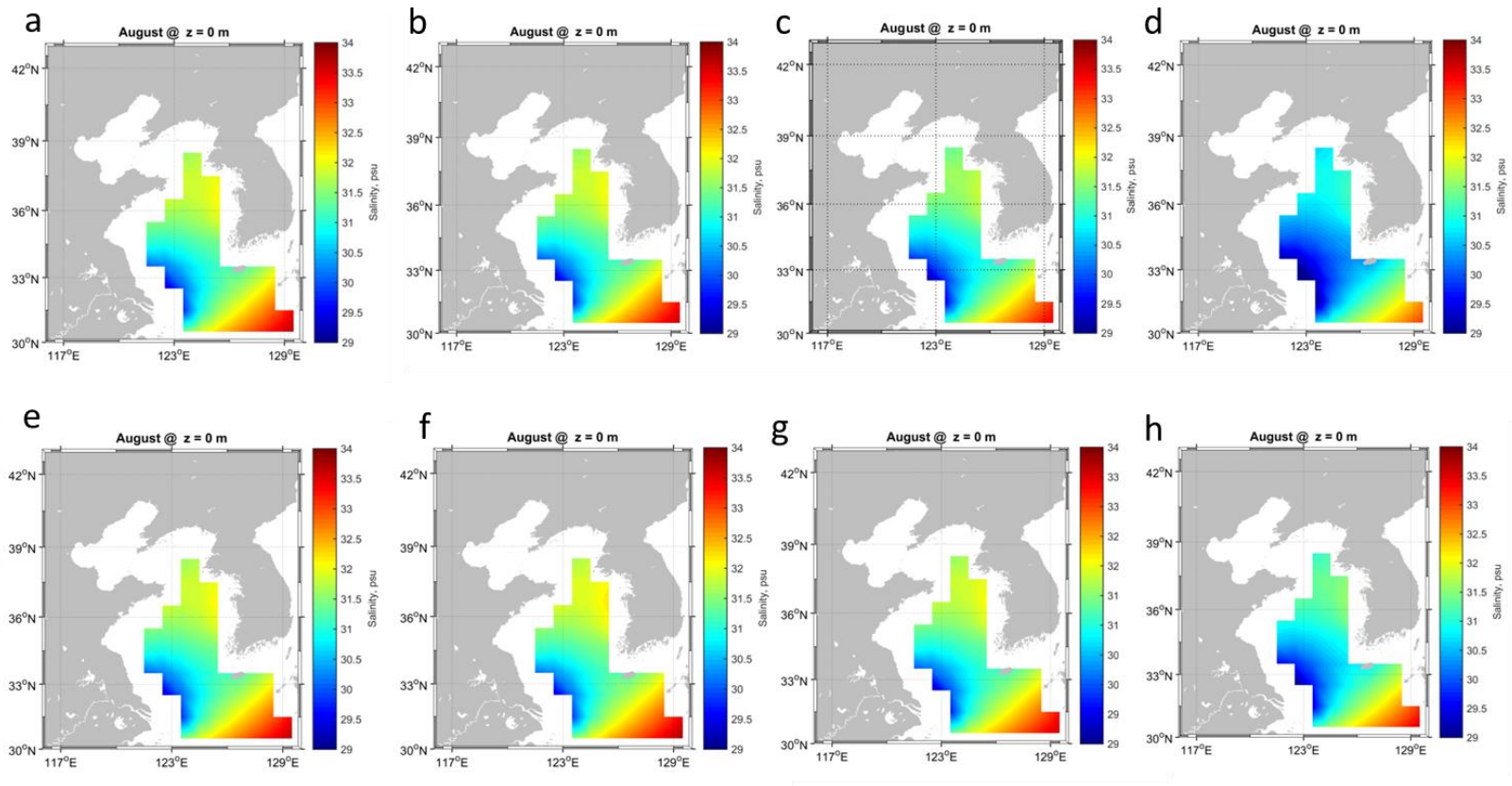
Type	<i>Enhanced Categories Description</i>	Enhanced	Standard	Reduced	HFEVA
HV	Sandy Mud	3896	1104	25	18
HV	Mud	3897	1105	52	18
HS	Ooze	3510	1108	8	23
N	Oceanic Rock Outcrops	4000	1101	1	1
N	Continental Rock Outcrops	5000	1101	1	2
N	Hard Bottom	5069	1101	1	3
A	Marsh	6845	1109	24	18
A	Mangrove	6850	1109	24	11
A	Intratidal	6855	1109	24	9
A	Supratidal Zone	6860	6860	21	999
A	Salt Dome	6865	6865	61	3
A	Gypsum	6870	6870	61	3
A	Peat	6875	1102	23	12
A	Rock Outcrop	6880	1101	1	2
A	Rubble	6885	1162	61	1
A	Manmade Features	6890	1101	1	1

A	Anomalous
C	Calcareous
H	Hemipelagic
N	Non-Depositional
L	Land
O	No Data
P	Pelagic
S	Siliceous
T	Terrigenous
U	Turbiditic
V	Volcanic

APPENDIX B. ADDITIONAL SMG-WOD TEMPERATURE AND SALINITY FIGURES



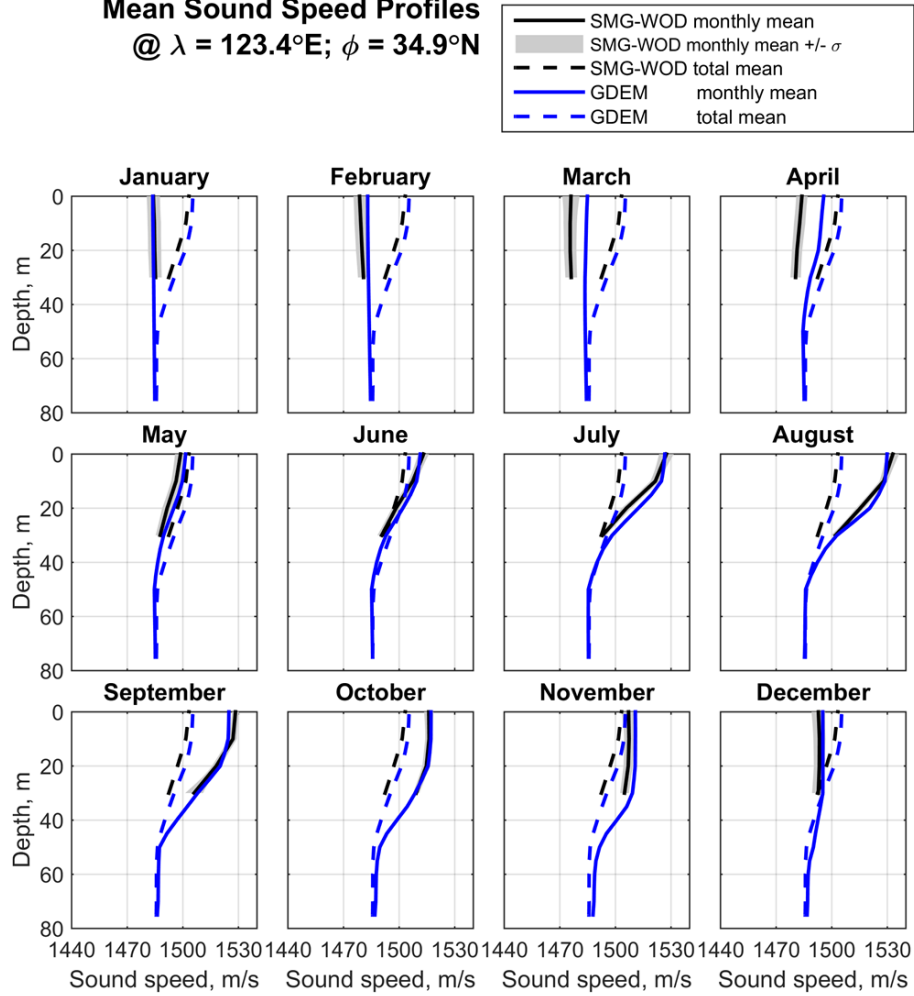
SMG-WOD SST a)1945, b) 1955, c) 1965, d) 1975, e) 1985, f) 1995, g) 2005, h) 2014.



SMG-WOD salinity at the surface a) 1945, b) 1955, c) 1965, d) 1975, e) 1985, f) 1995, g) 2005, h) 2014.

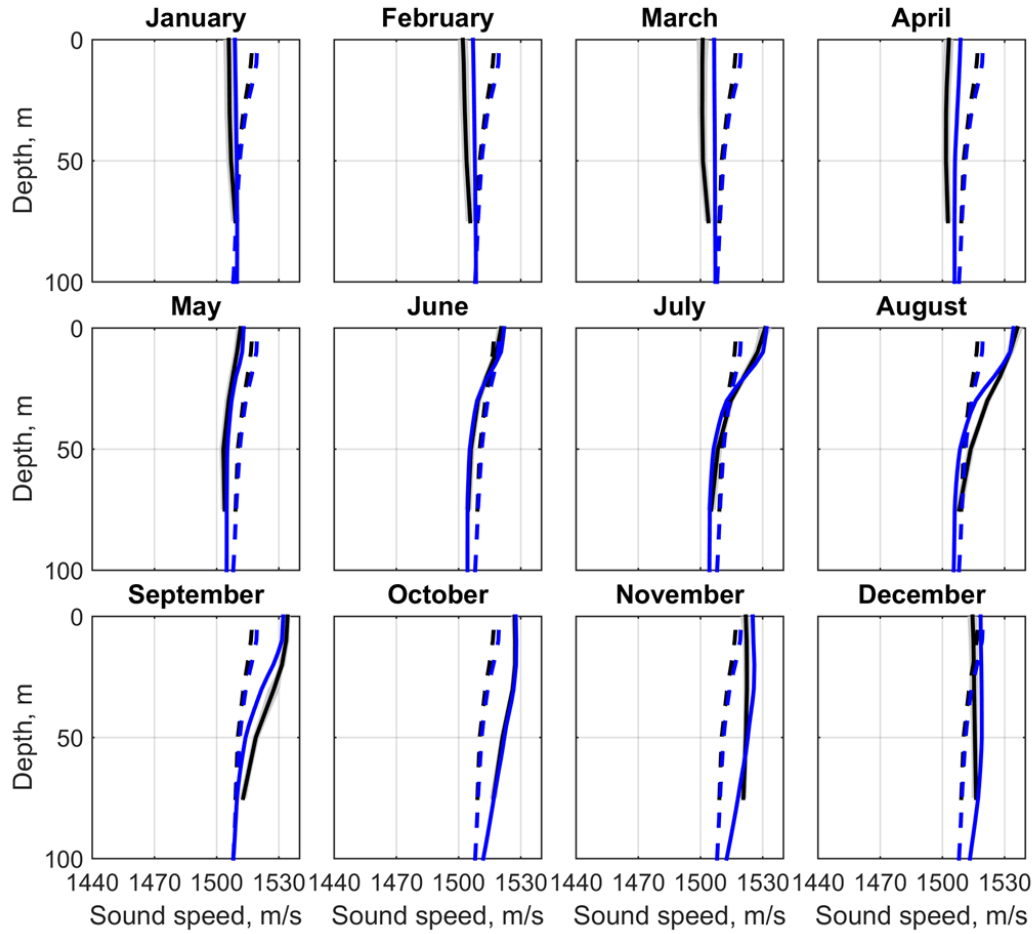
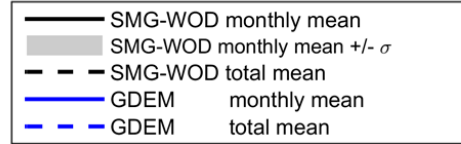
APPENDIX C. SSP MEANS

Mean Sound Speed Profiles @ $\lambda = 123.4^{\circ}\text{E}$; $\phi = 34.9^{\circ}\text{N}$



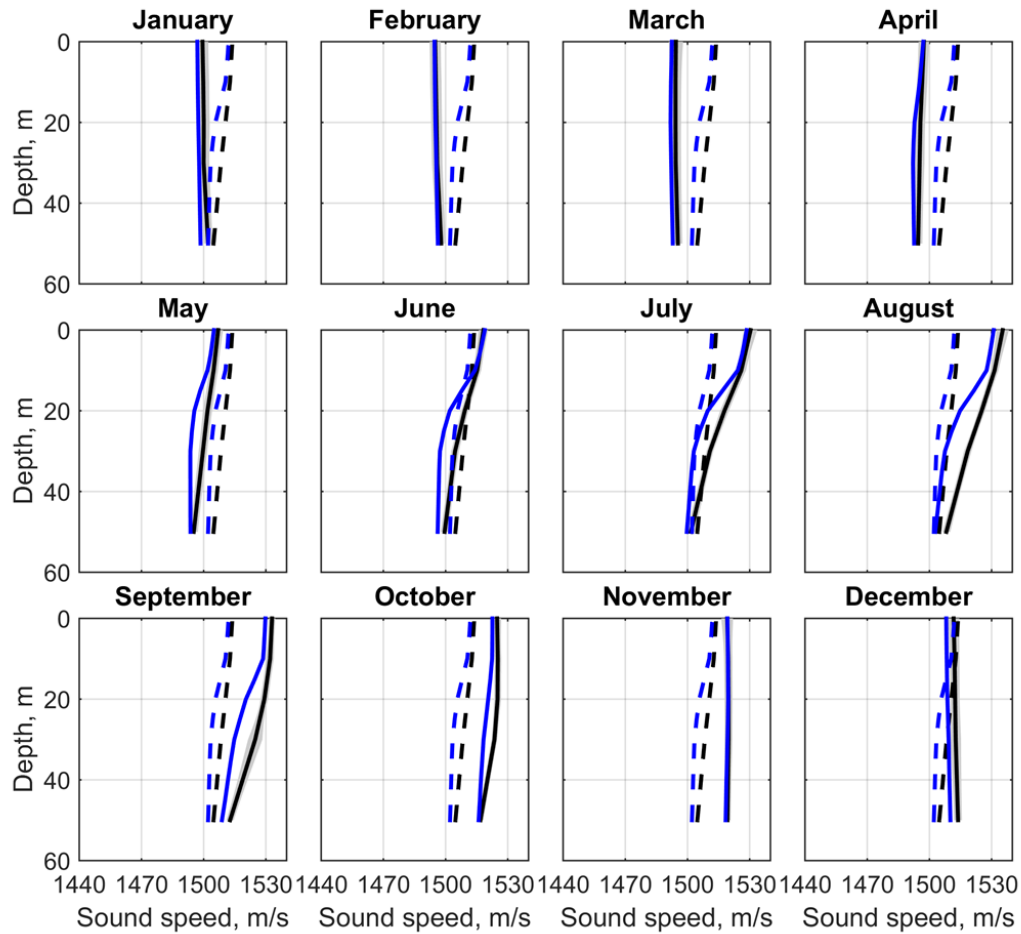
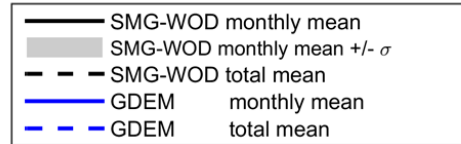
Location A (silty clay)

Mean Sound Speed Profiles **@ $\lambda = 126.5^{\circ}\text{E}$; $\phi = 32.6^{\circ}\text{N}$**



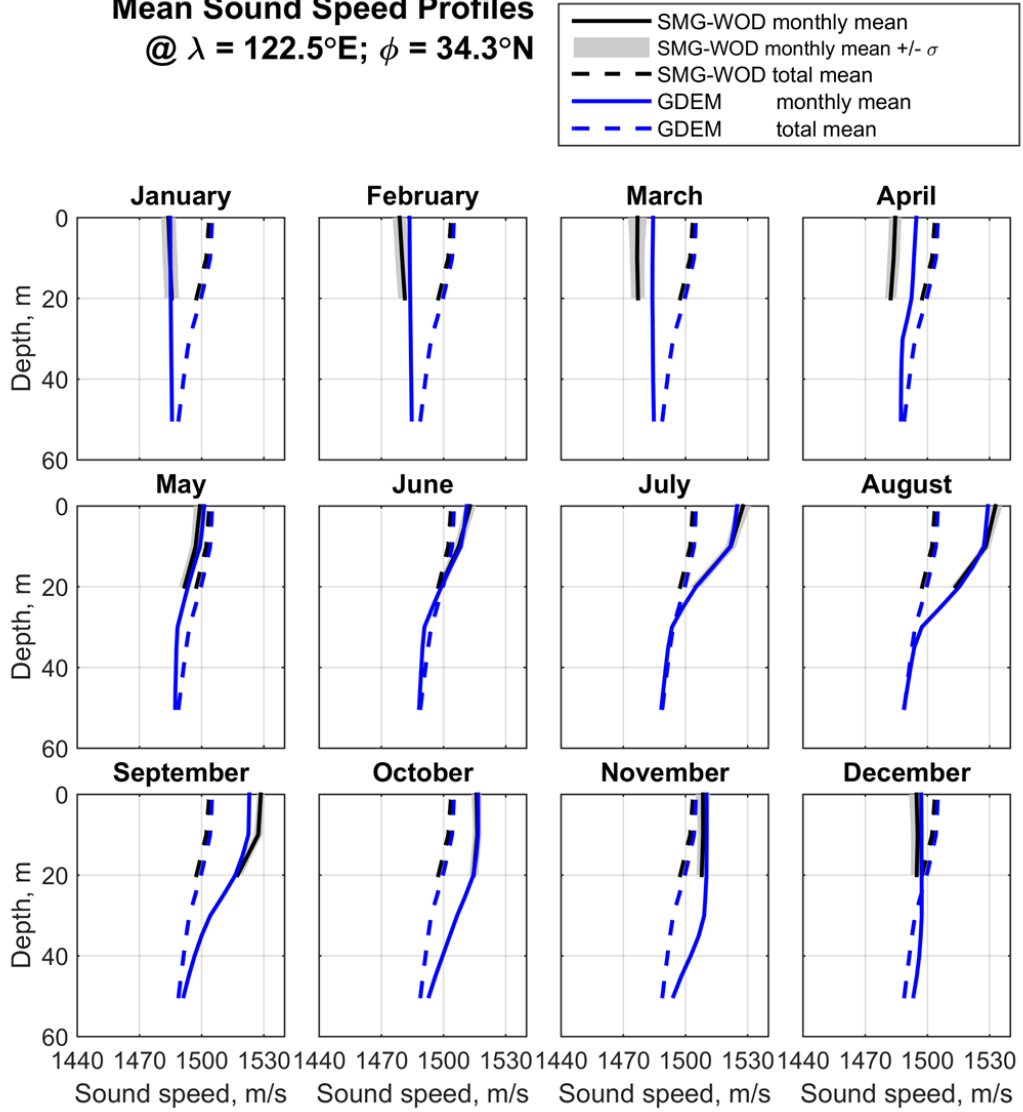
Location B (fine sand)

Mean Sound Speed Profiles **@ $\lambda = 125.1^\circ\text{E}$; $\phi = 32.3^\circ\text{N}$**



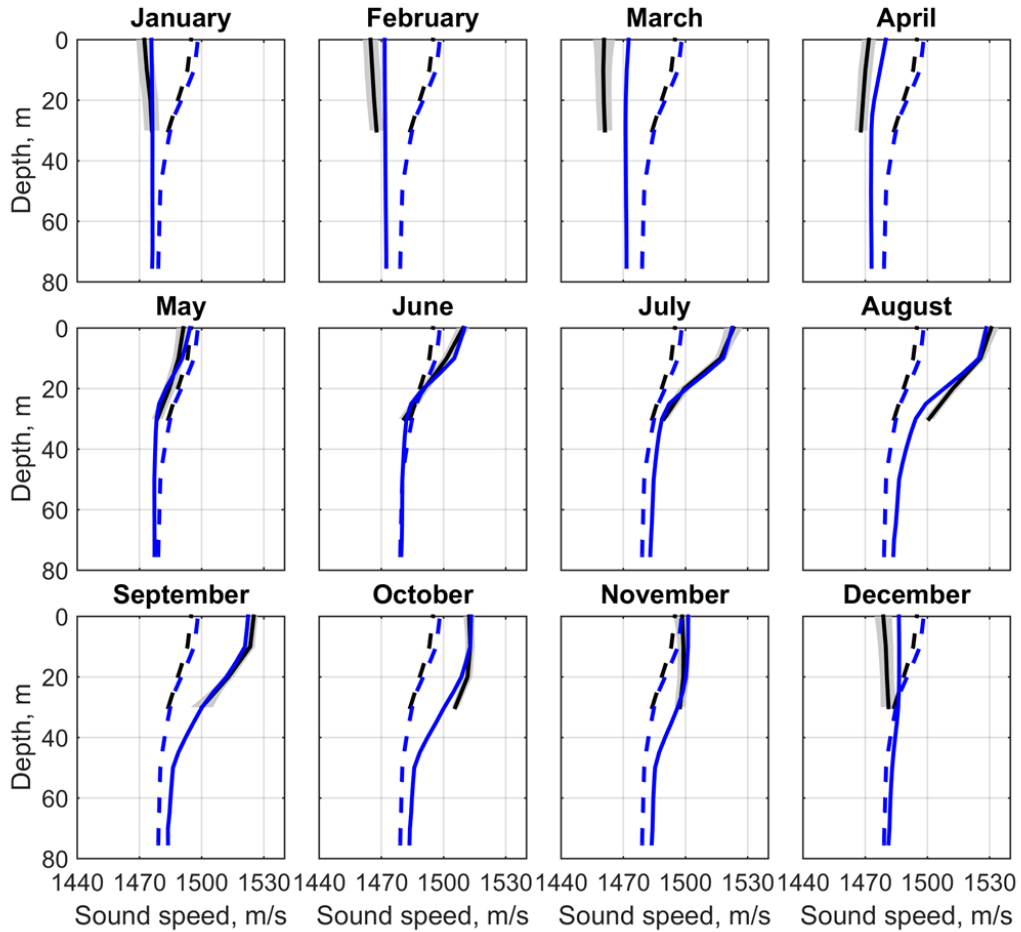
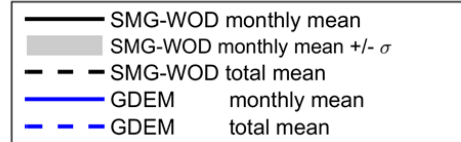
Location C (silty clay)

Mean Sound Speed Profiles **@ $\lambda = 122.5^{\circ}\text{E}$; $\phi = 34.3^{\circ}\text{N}$**



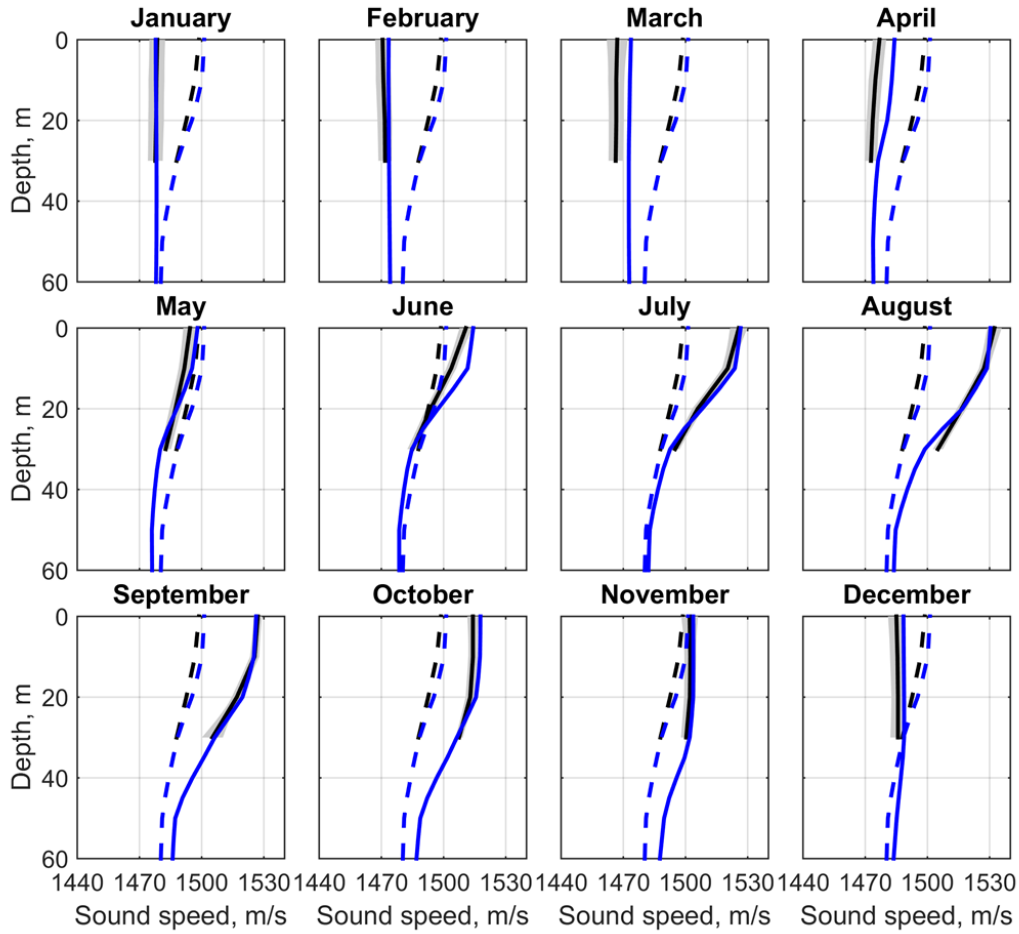
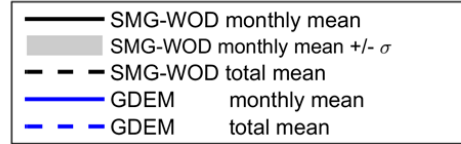
Location D (gravelly mud)

Mean Sound Speed Profiles **@ $\lambda = 123.9^\circ\text{E}$; $\phi = 37.5^\circ\text{N}$**



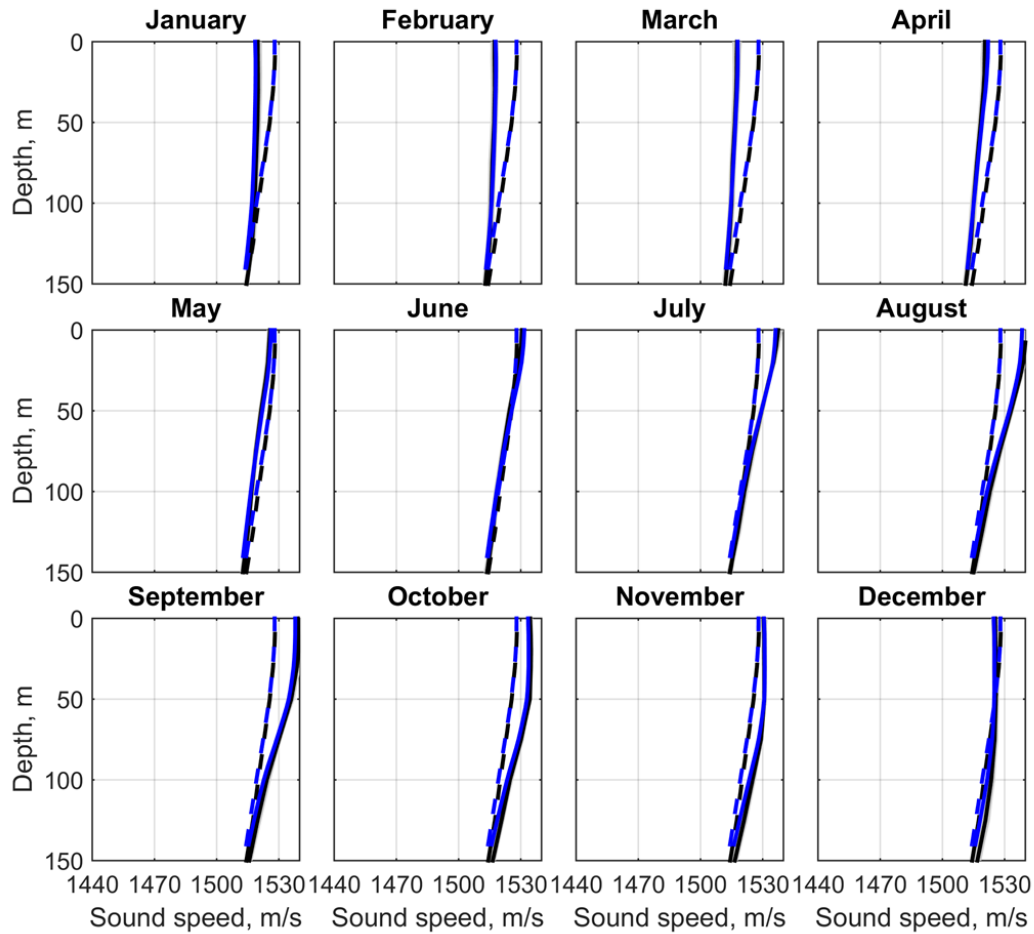
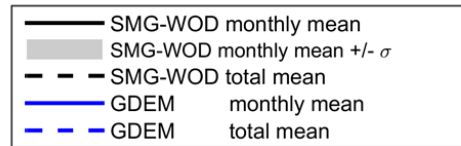
Location E (cobble or gravel)

Mean Sound Speed Profiles **@ $\lambda = 124.6^\circ\text{E}$; $\phi = 36.5^\circ\text{N}$**



Location F (fine sand)

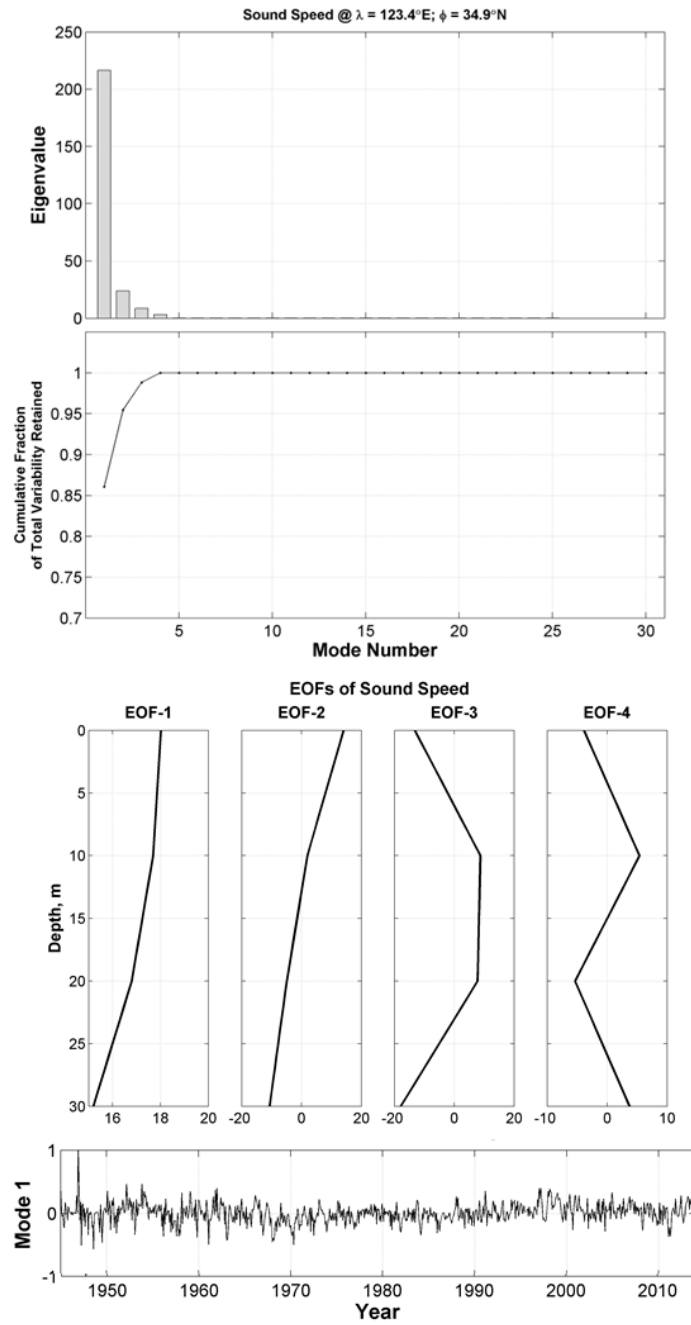
Mean Sound Speed Profiles **@ $\lambda = 129^\circ\text{E}$; $\phi = 31^\circ\text{N}$**



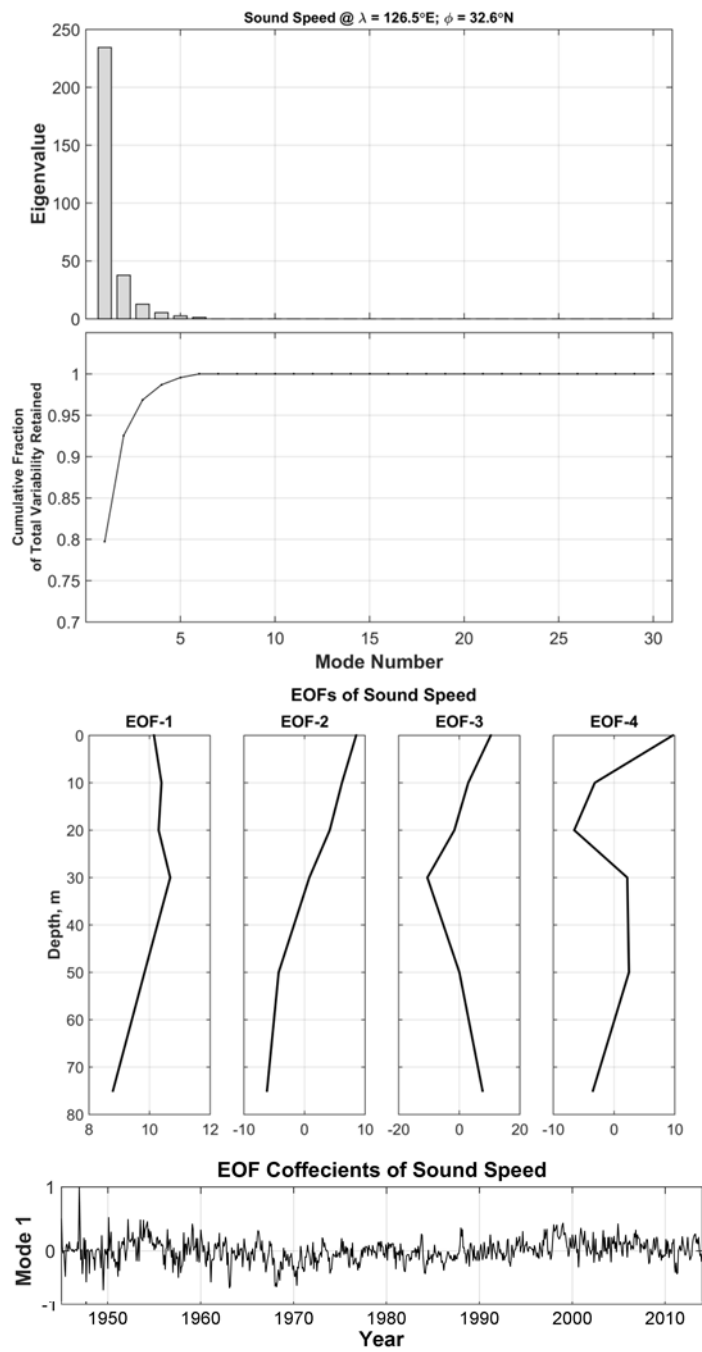
Location O (sandy mud)

THIS PAGE INTENTIONALLY LEFT BLANK

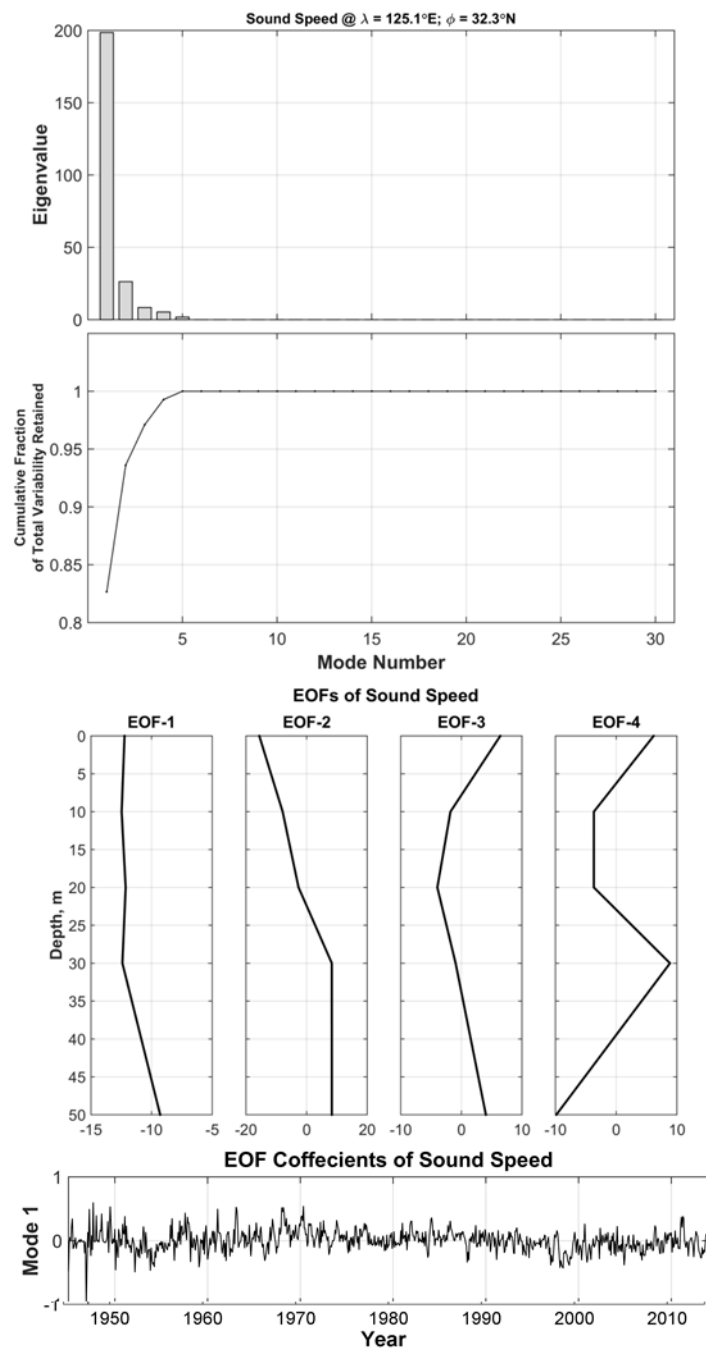
APPENDIX D. EOF



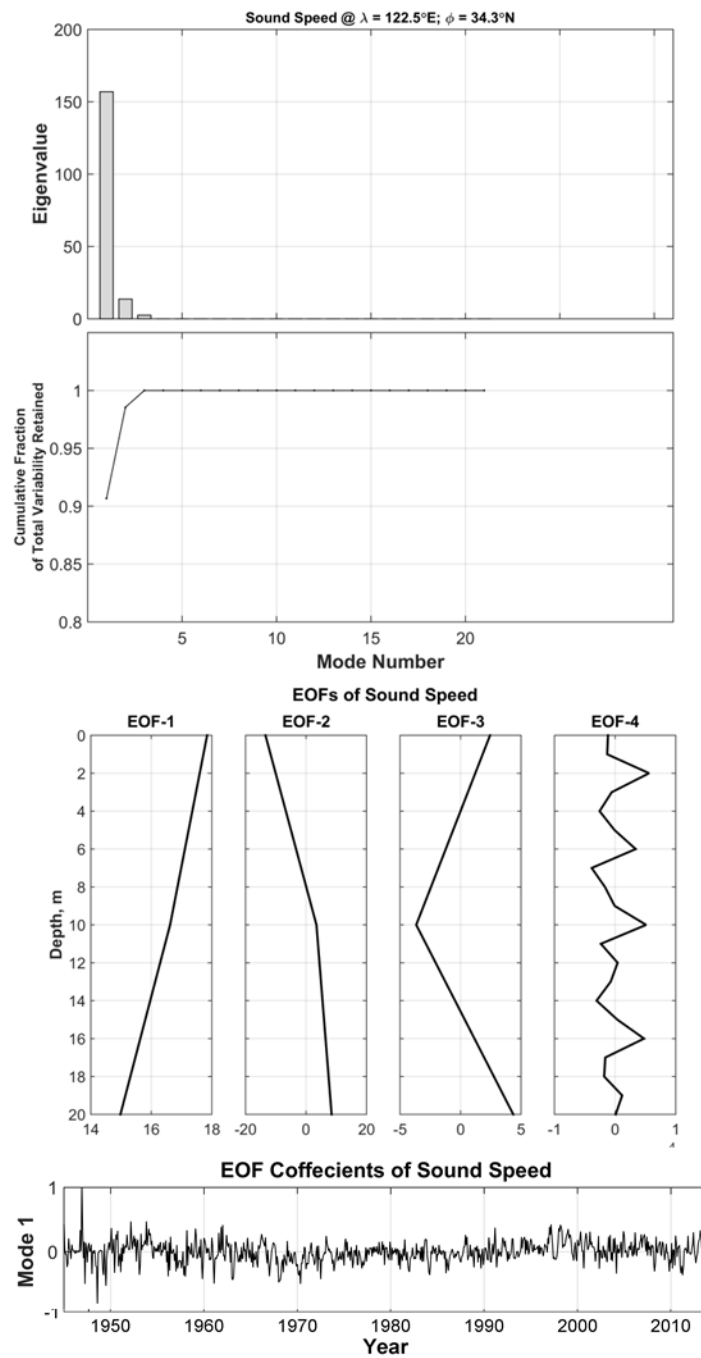
Location A (silty clay)



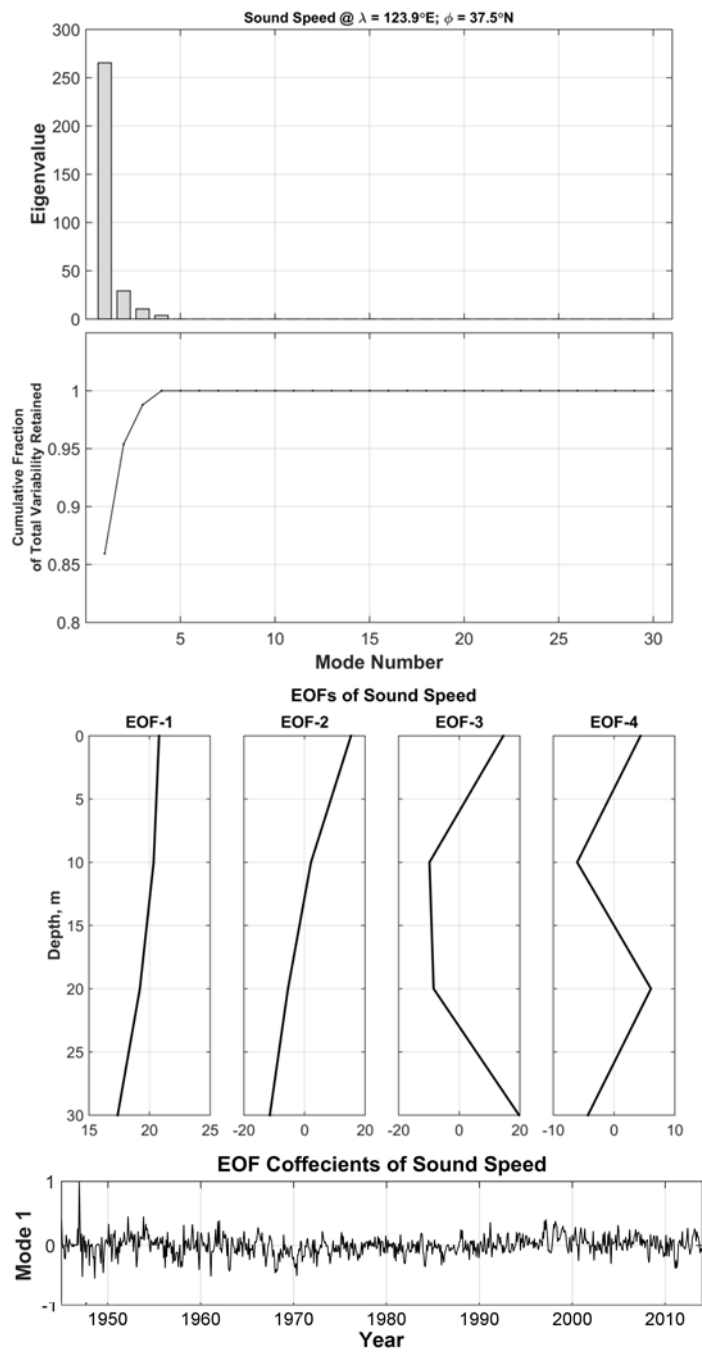
Location B (fine sand)



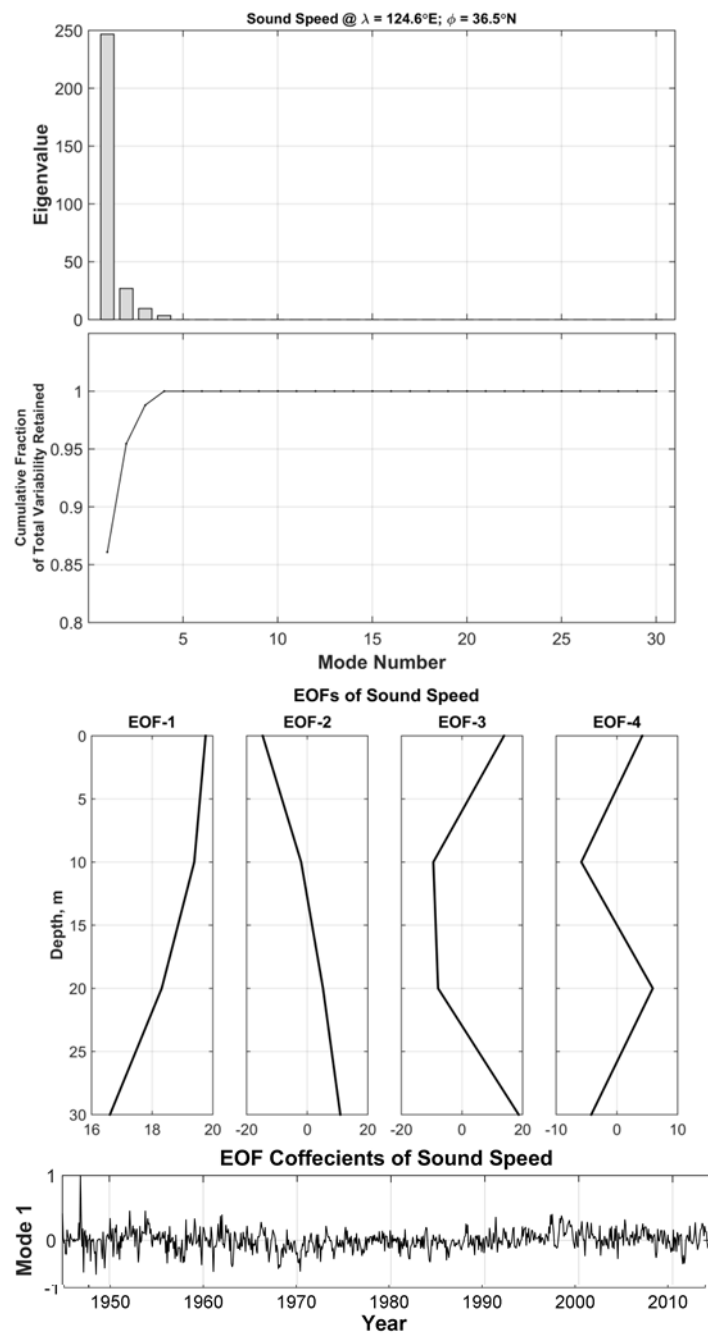
Location C (silty clay)



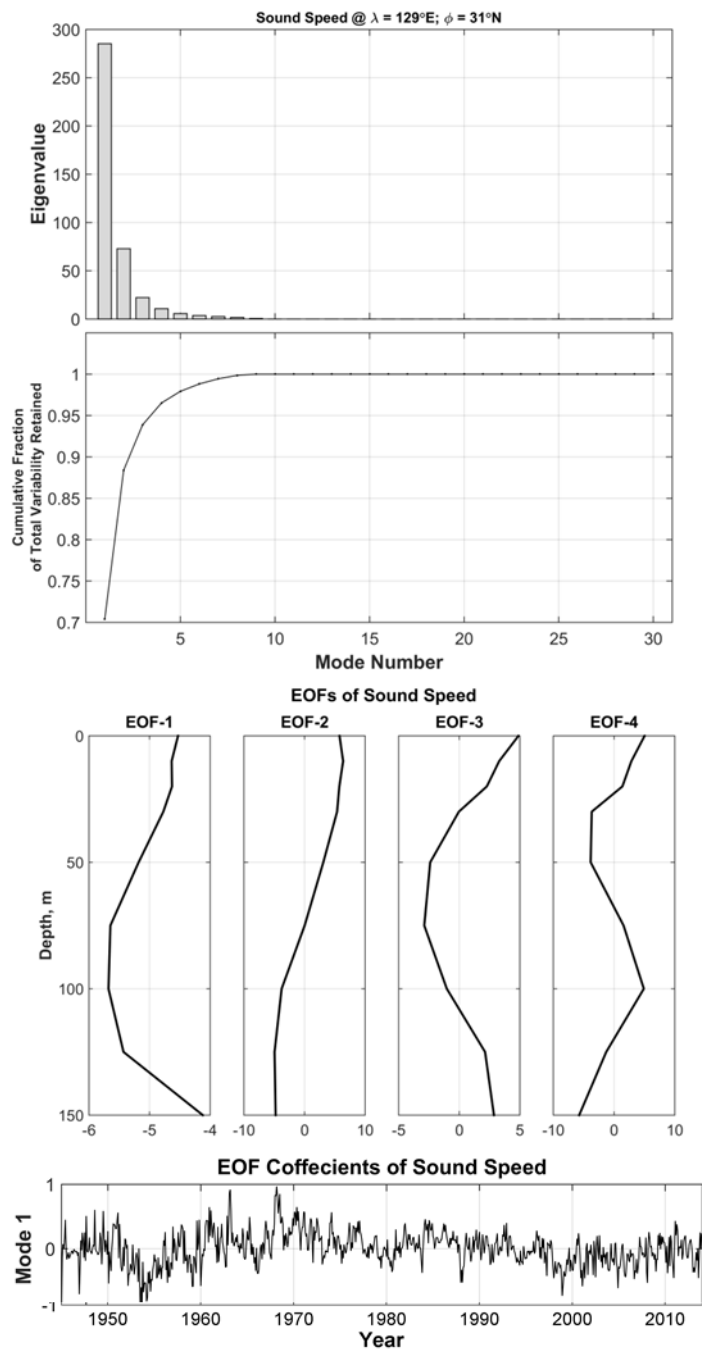
Location D (gravelly mud)



Location E (cobble or gravel)



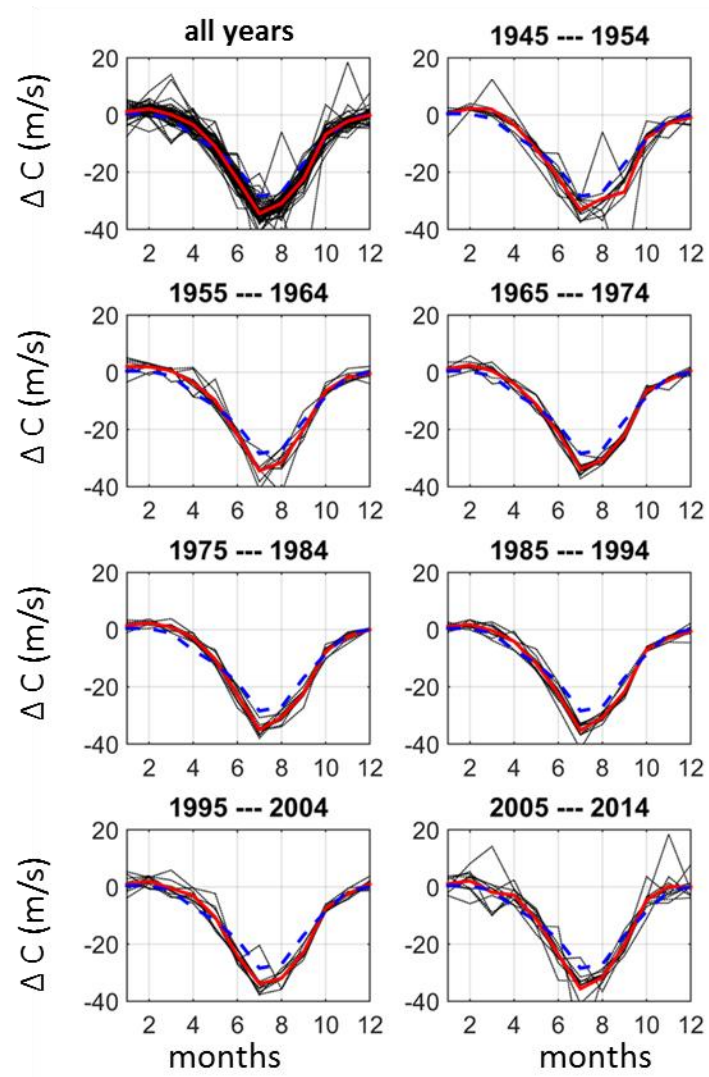
Location F (fine sand)



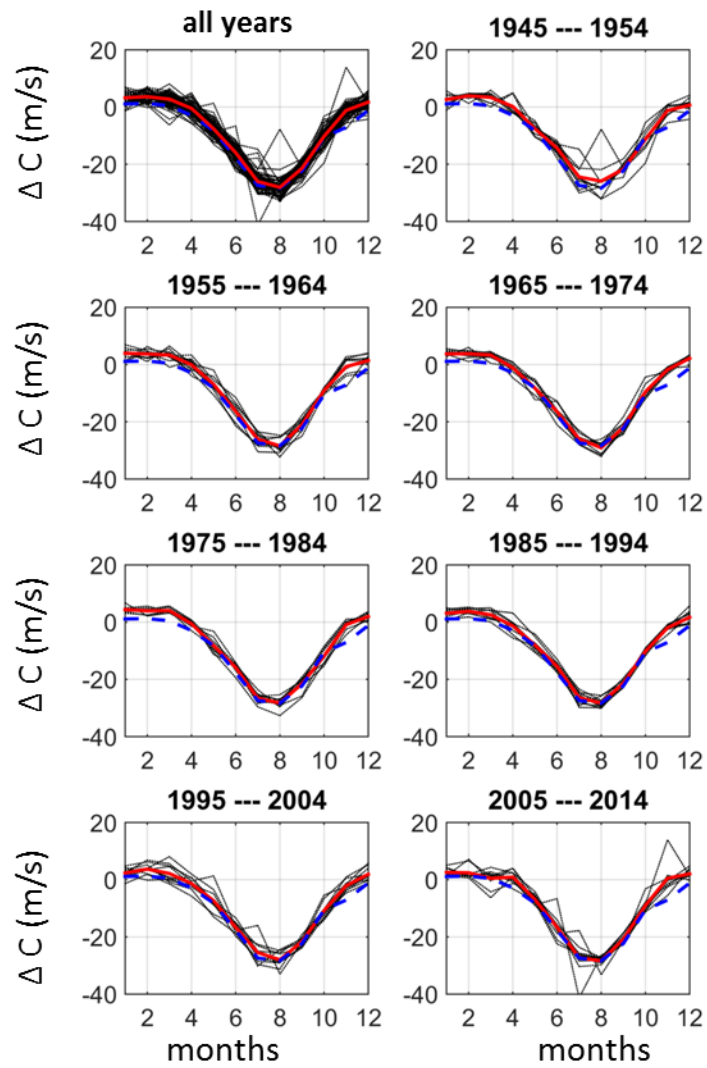
Location O (sandy mud)

THIS PAGE INTENTIONALLY LEFT BLANK

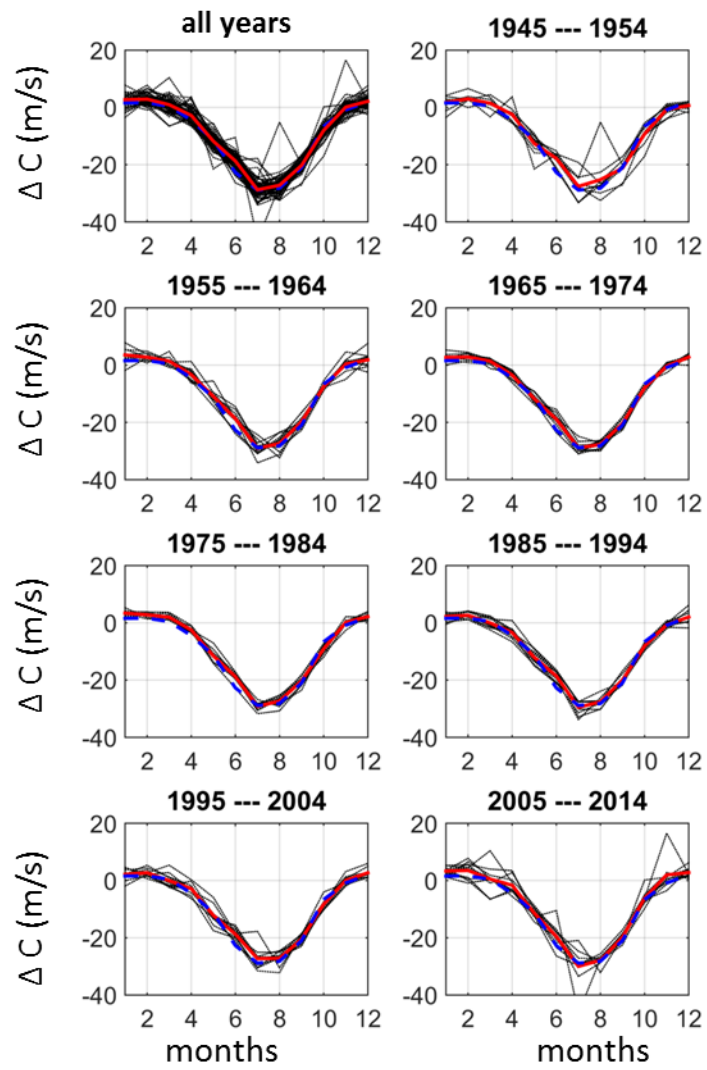
APPENDIX E. SSP VARIABILITY



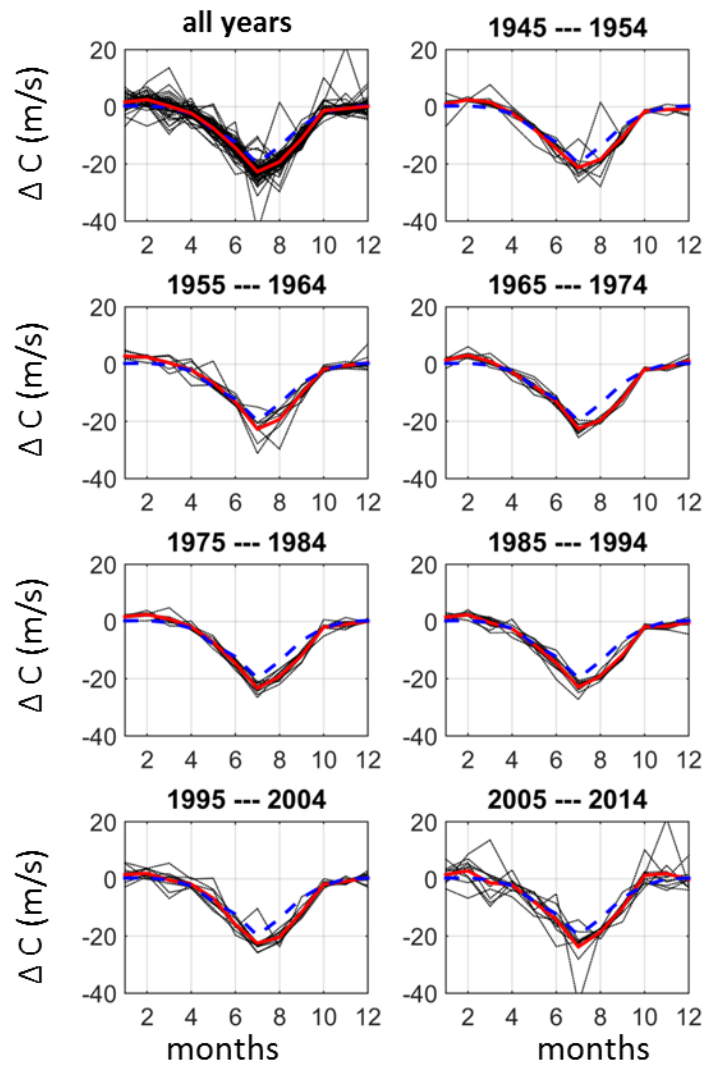
Location A (silty clay)



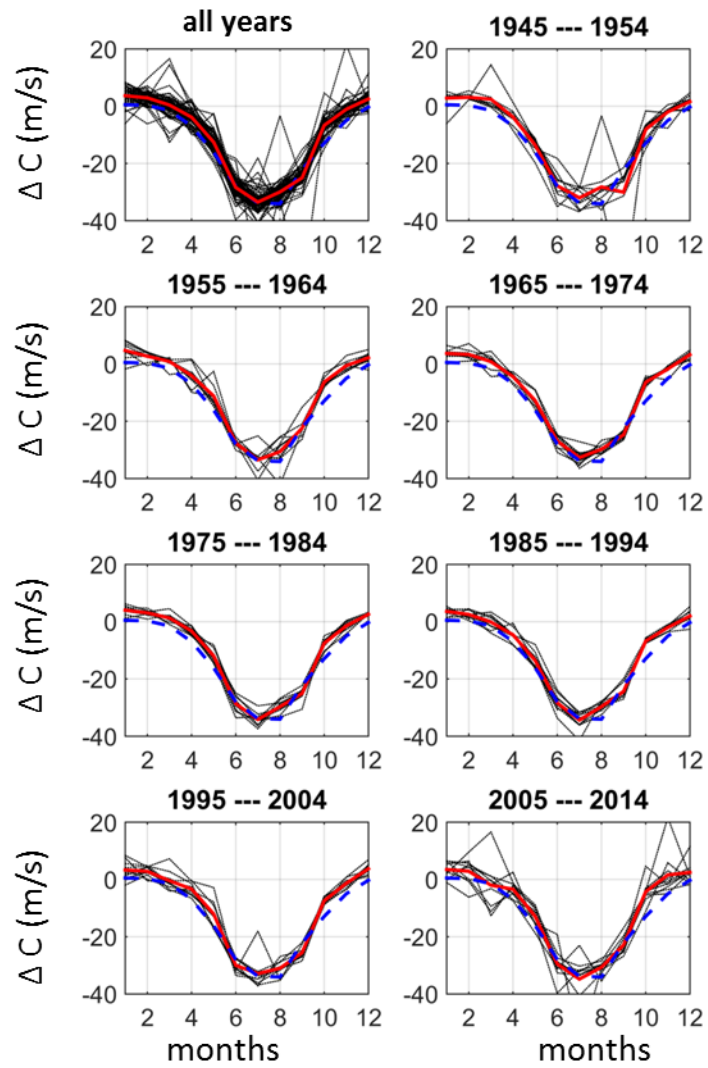
Location B (fine sand)



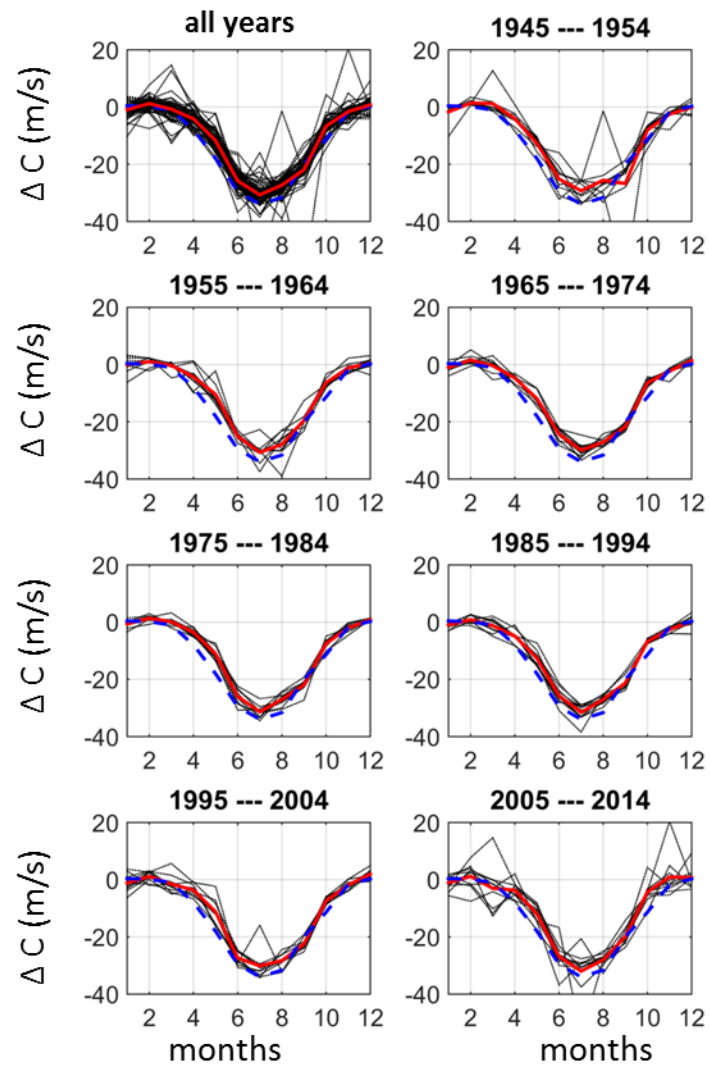
Location C (silty clay)



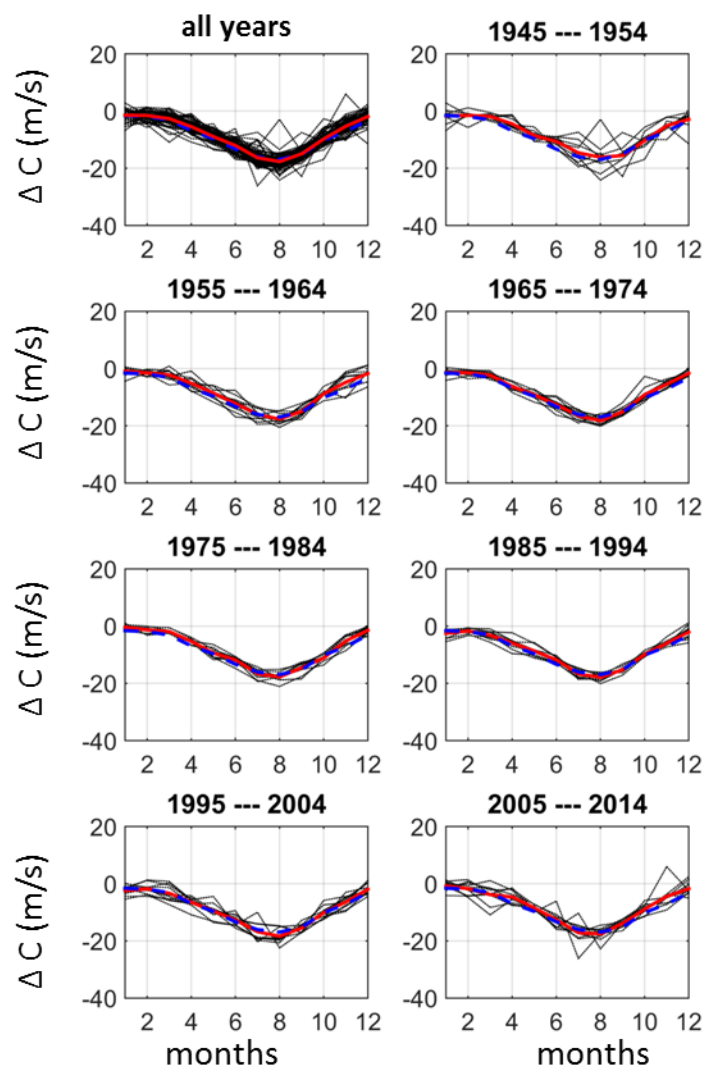
Location D (gravelly mud)



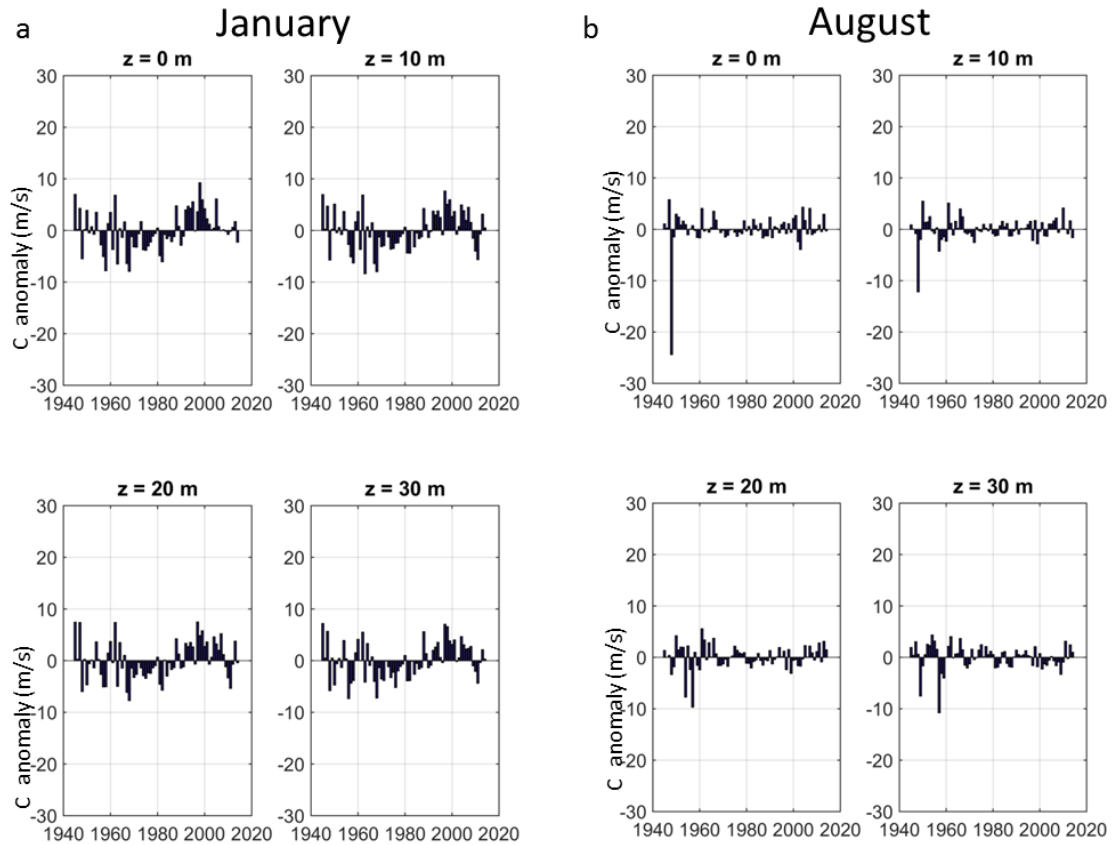
Location E (cobble or gravel)



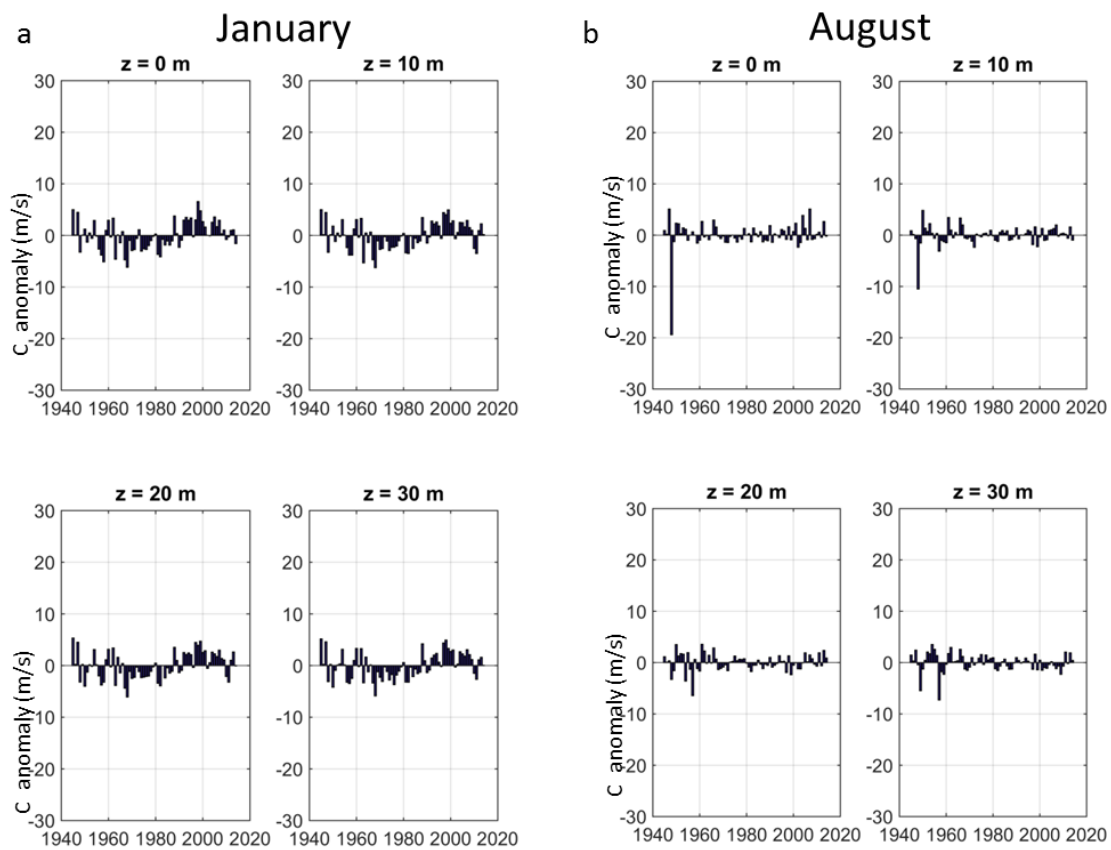
Location F (fine sand)



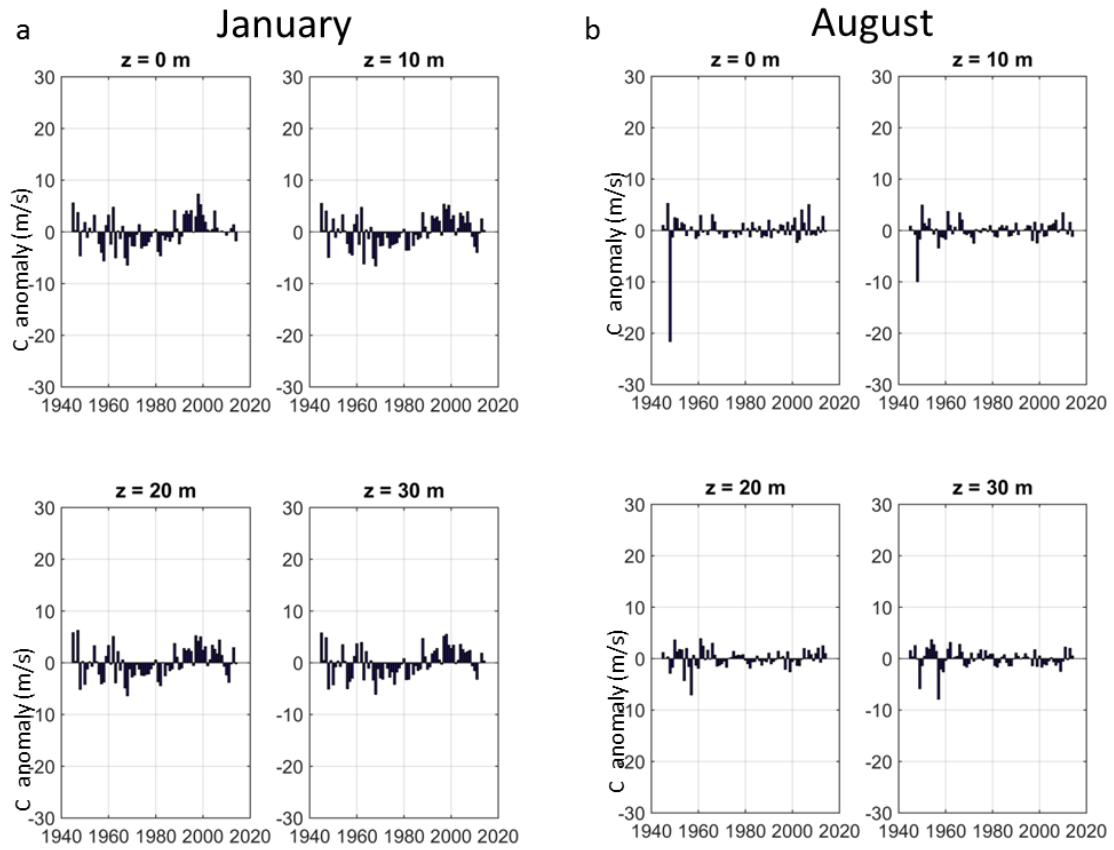
Location O (sandy mud)



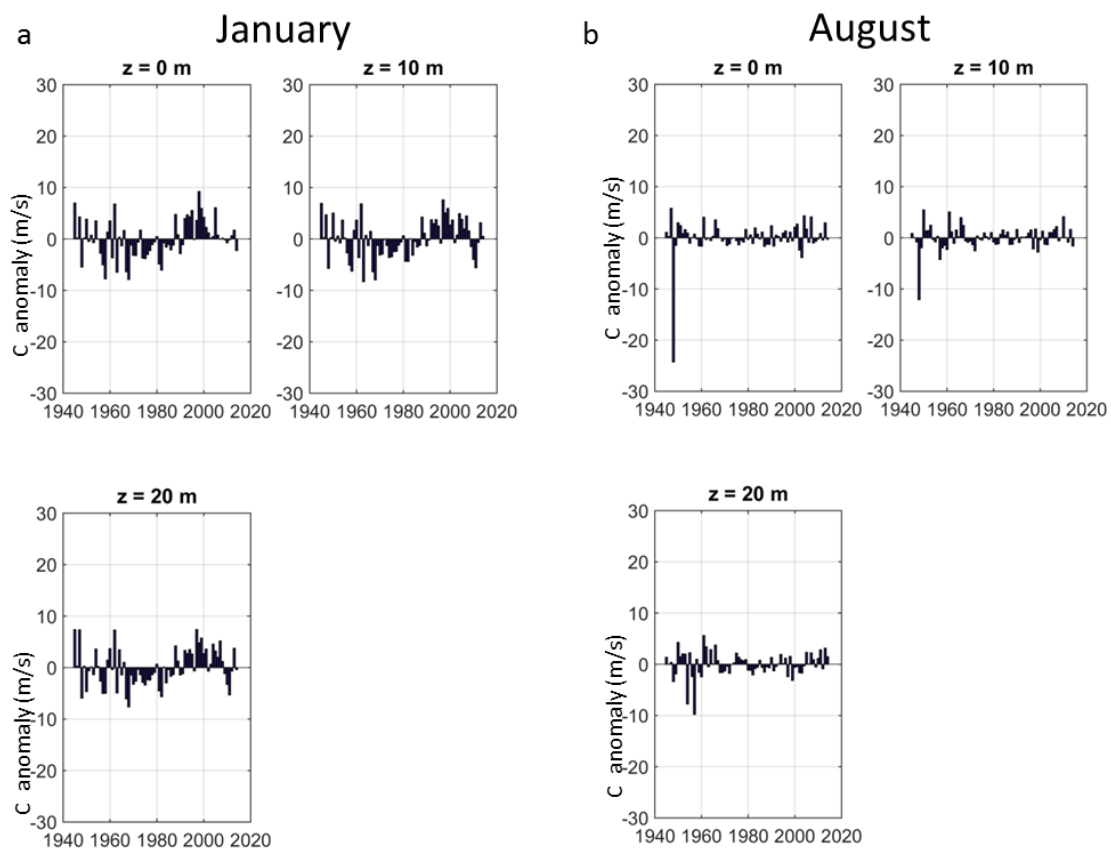
Location A (silty clay)



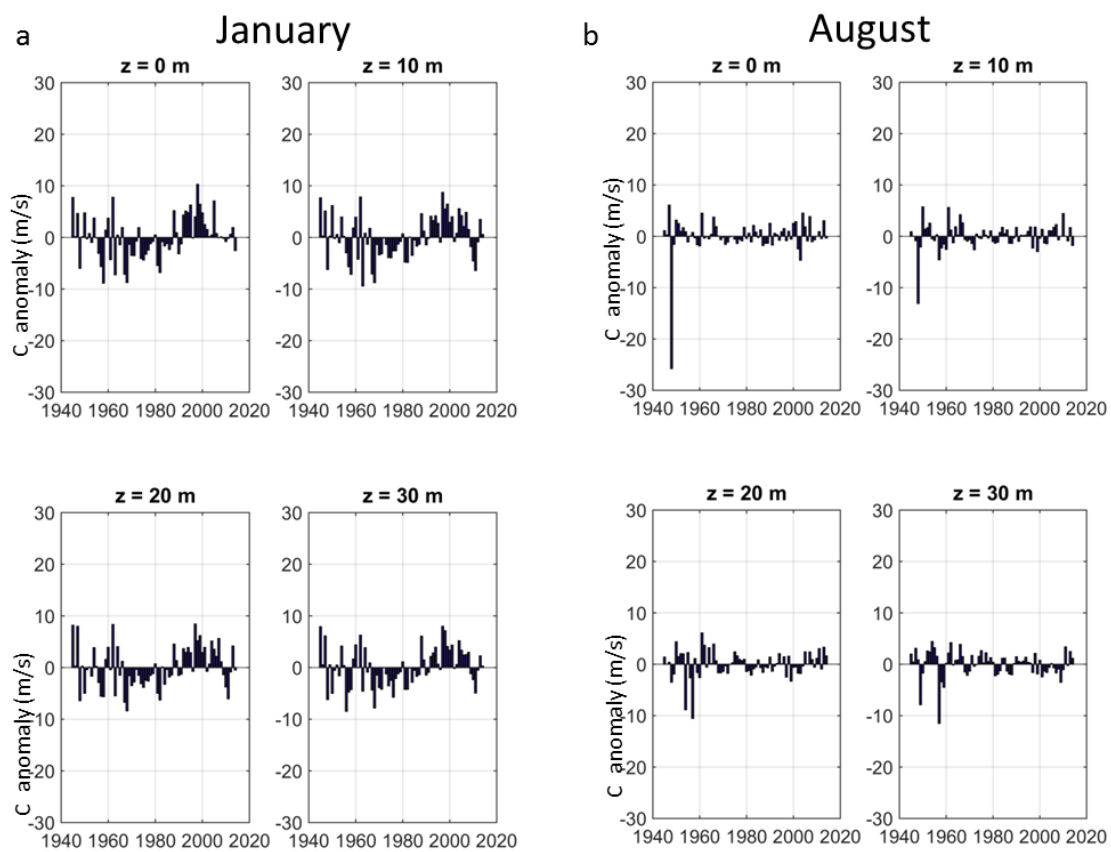
Location B (fine sand)



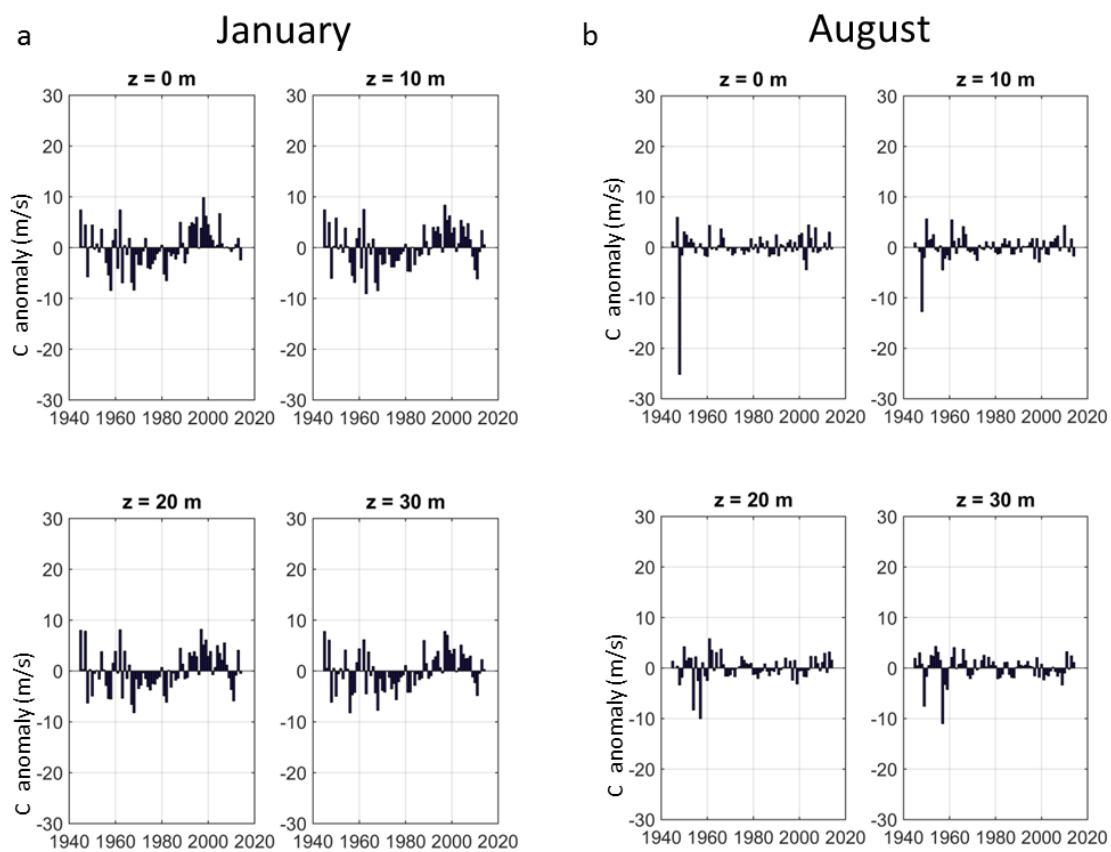
Location C (silty clay)



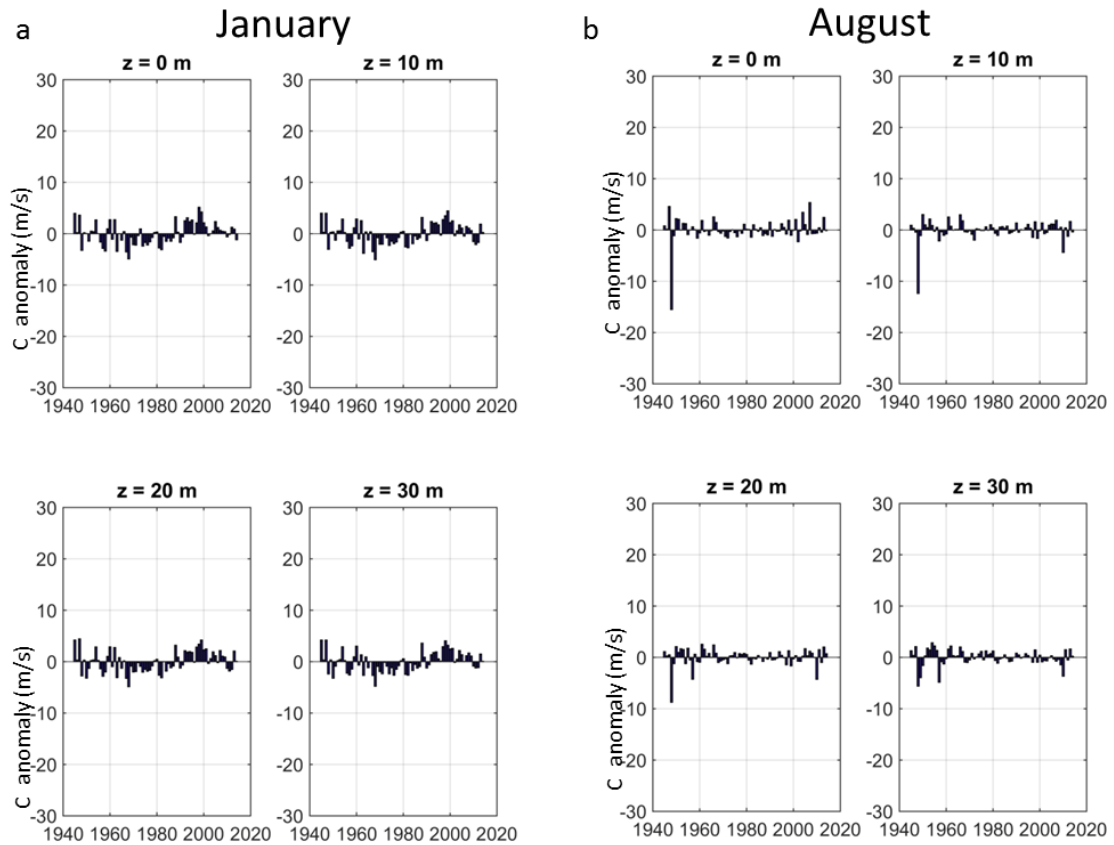
Location D (gravelly mud)



Location E (cobble of gravel)

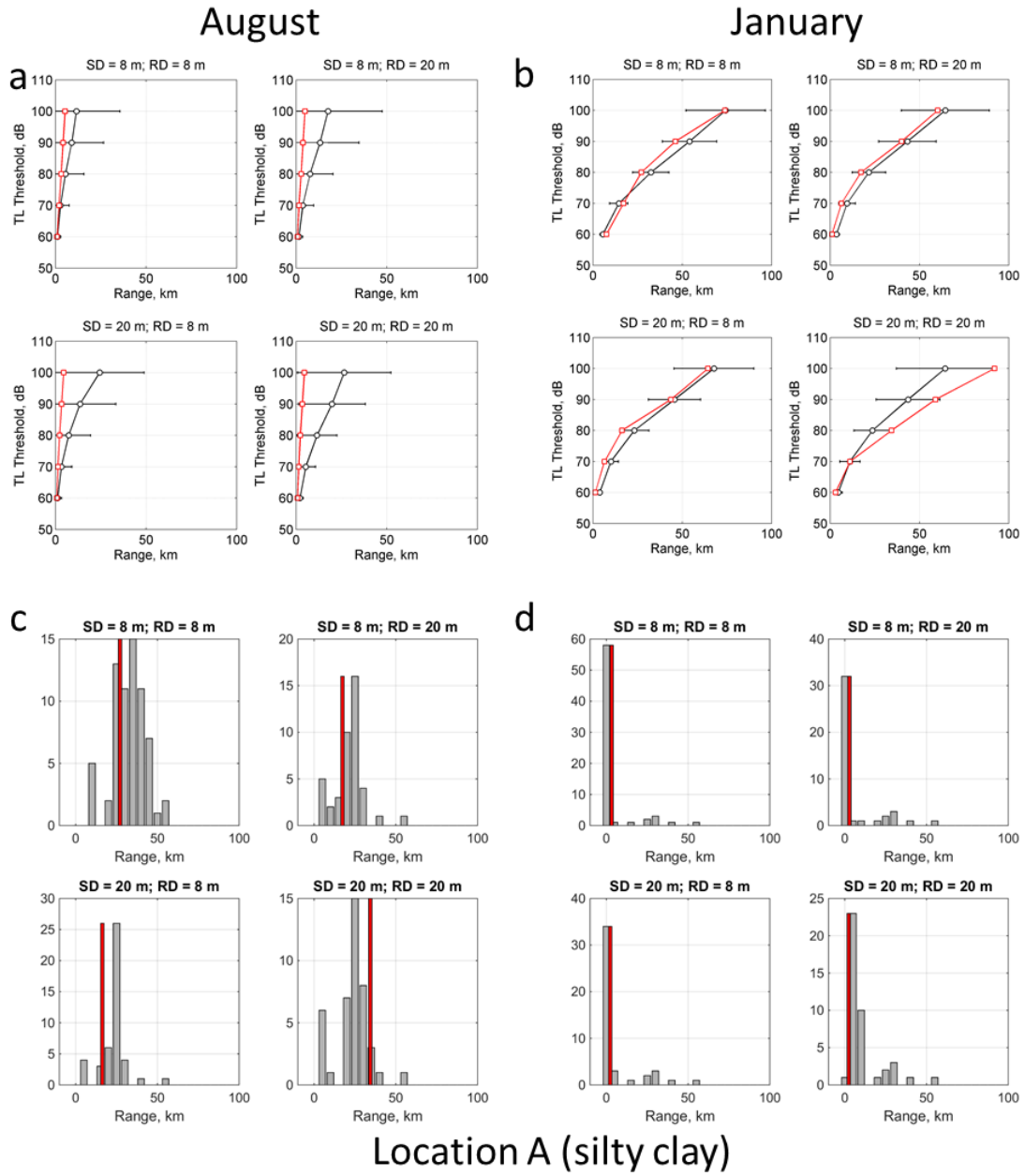


Location F (fine sand)

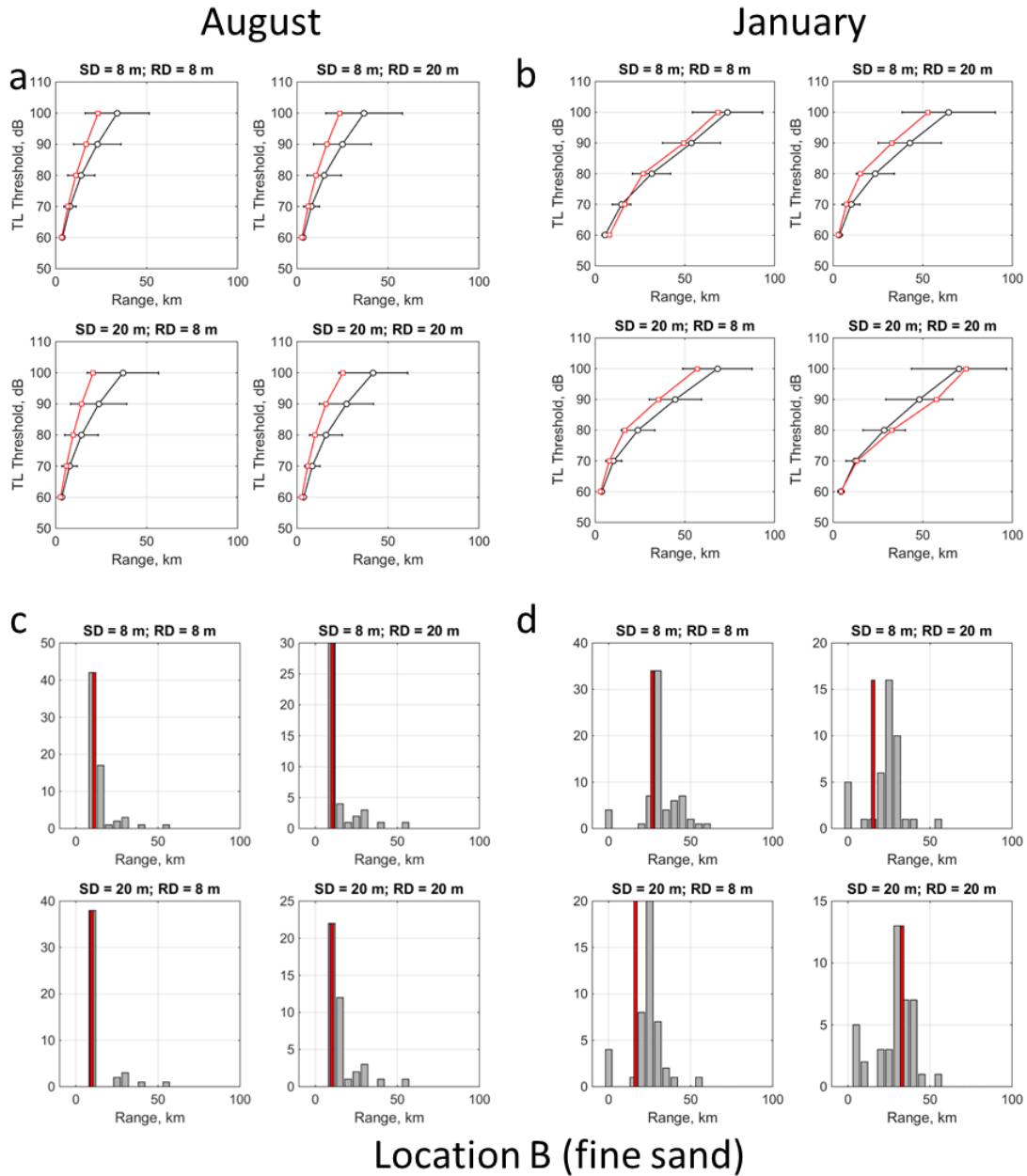


Location O (sandy mud)

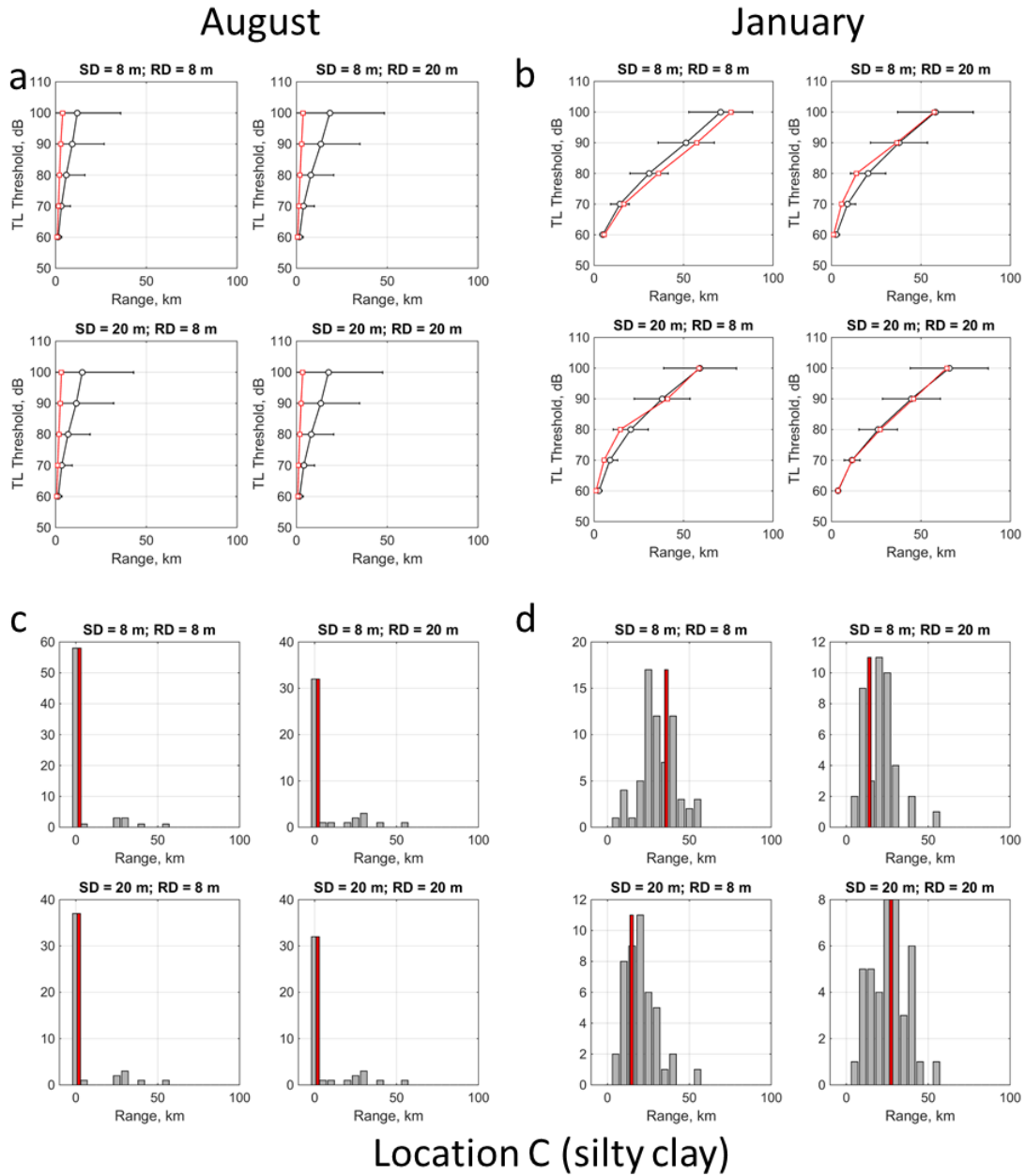
APPENDIX F. TRANSMISSION LOSS



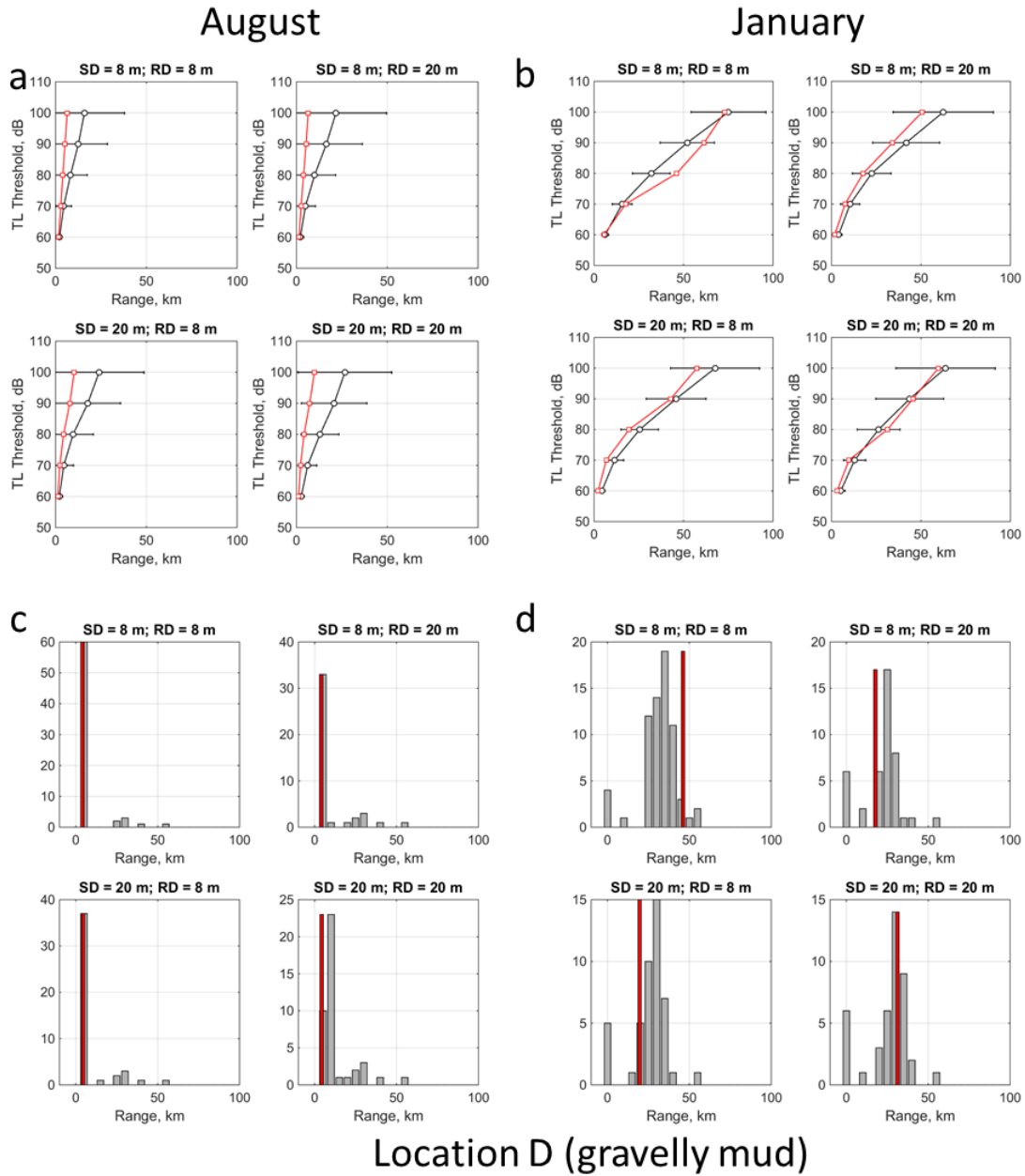
TL loss at varying thresholds of 60dB-100dB, SMG-WOD (black) and GDEM (red)
a) August, b) January. Histogram of 80dB threshold c) August, d) January.



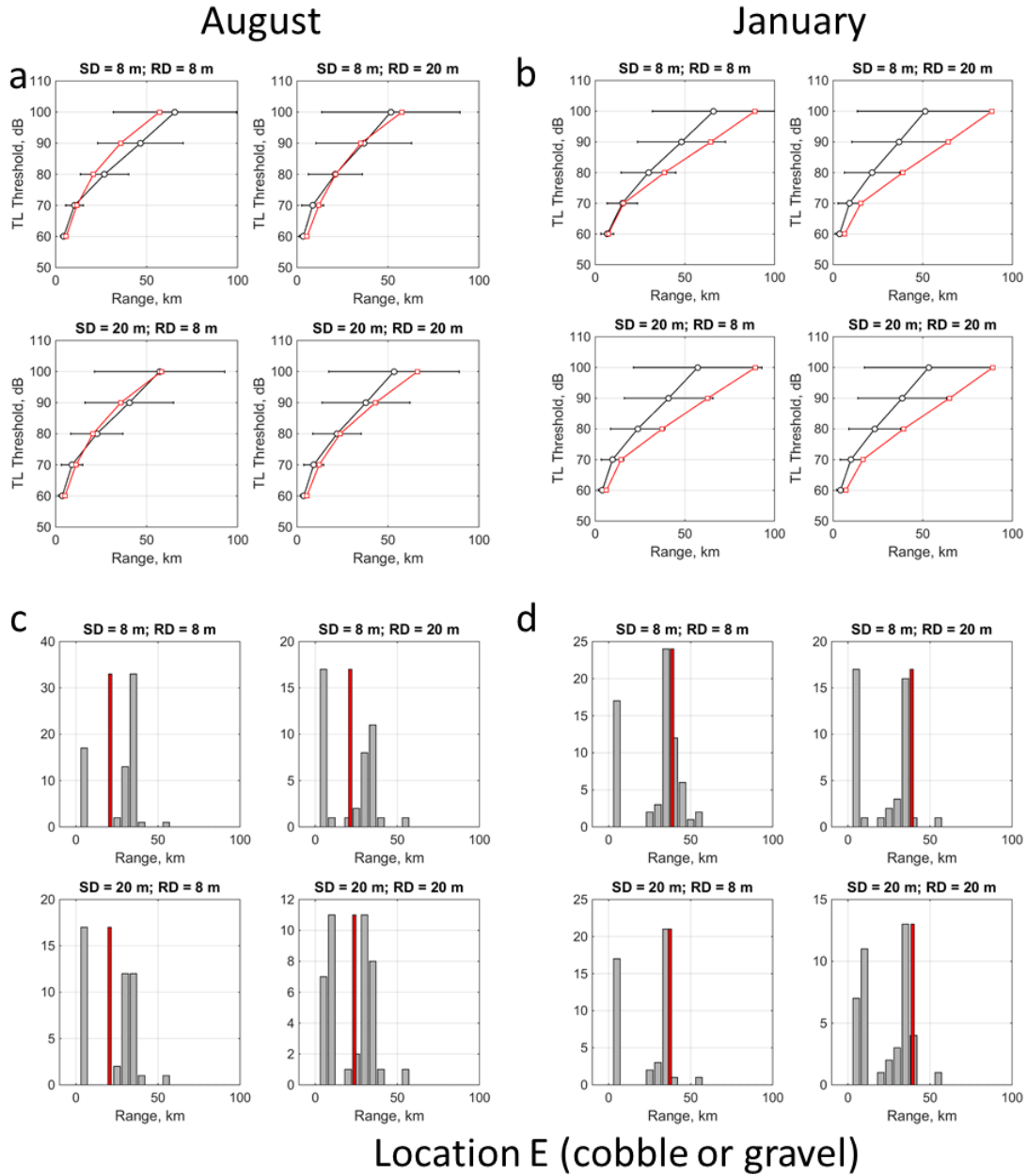
TL loss at varying thresholds of 60dB-100dB, SMG-WOD (black) and GDEM (red)
a) August, b) January. Histogram of 80dB threshold c) August, d) January.



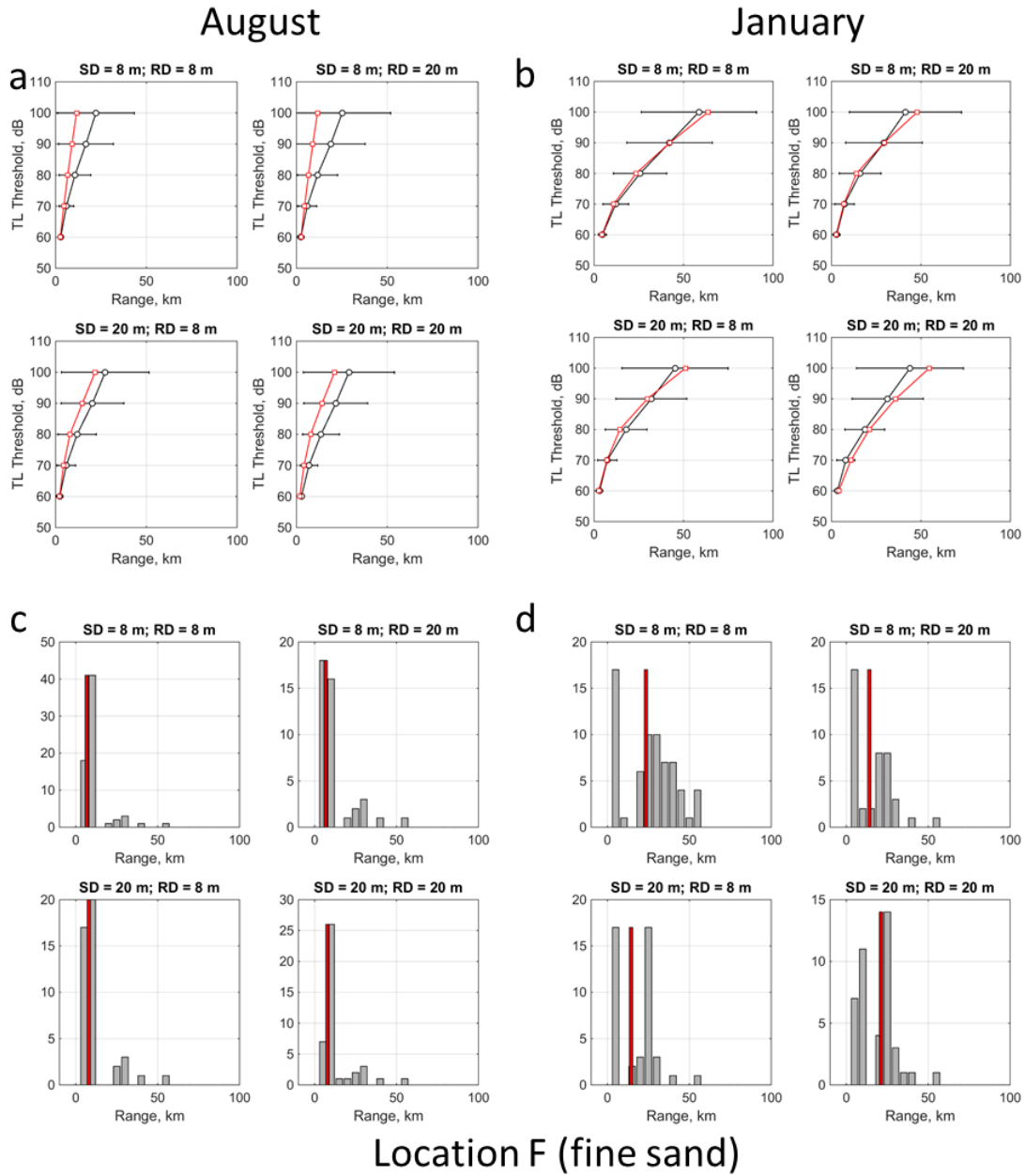
TL loss at varying thresholds of 60dB-100dB, SMG-WOD (black) and GDEM (red) a) August, b) January. Histogram of 80dB threshold c) August, d) January.



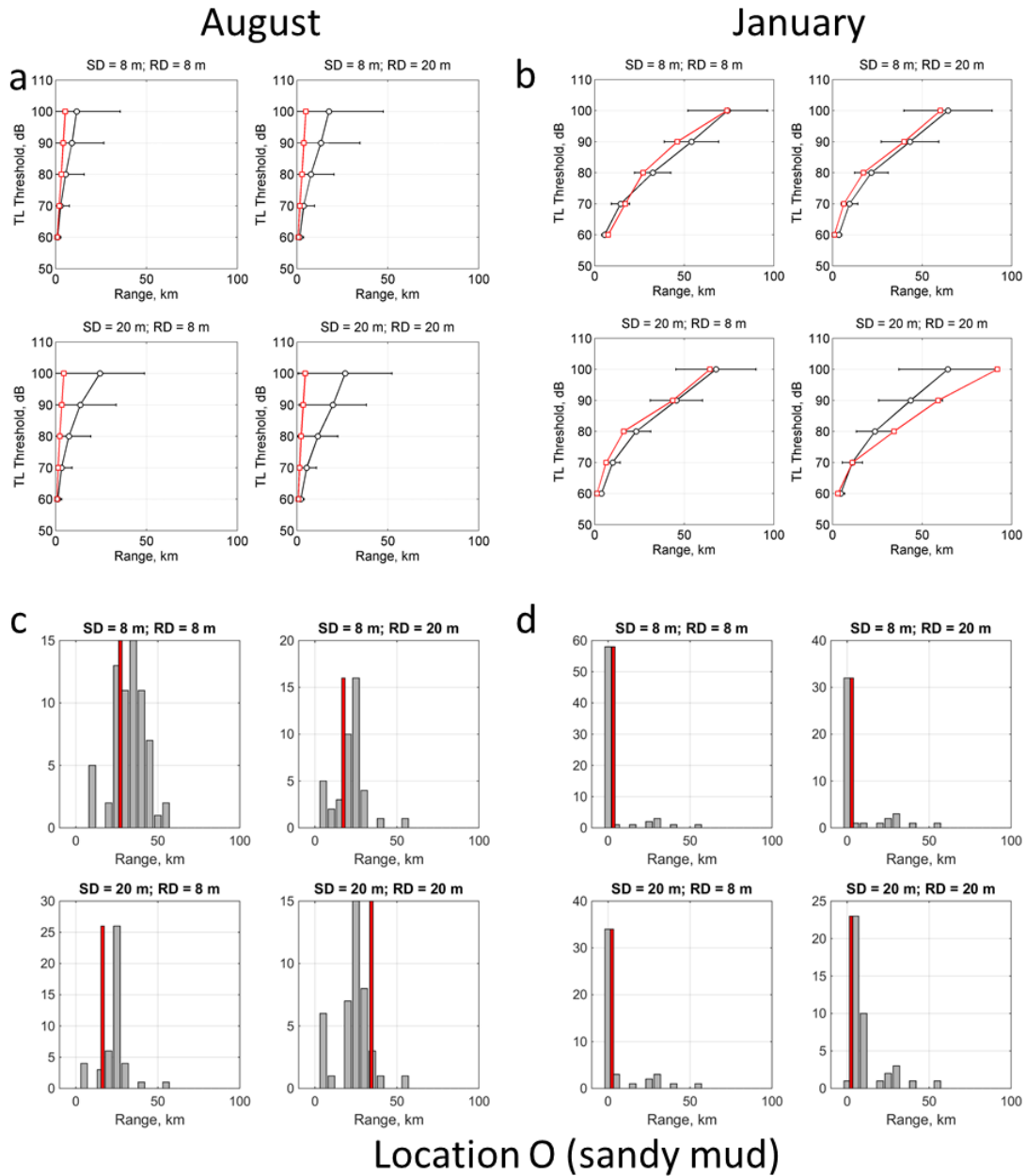
TL loss at varying thresholds of 60dB-100dB, SMG-WOD (black) and GDEM (red) a) August, b) January. Histogram of 80dB threshold c) August, d) January.



TL loss at varying thresholds of 60dB-100dB, SMG-WOD (black) and GDEM (red) a) August, b) January. Histogram of 80dB threshold c) August, d) January.



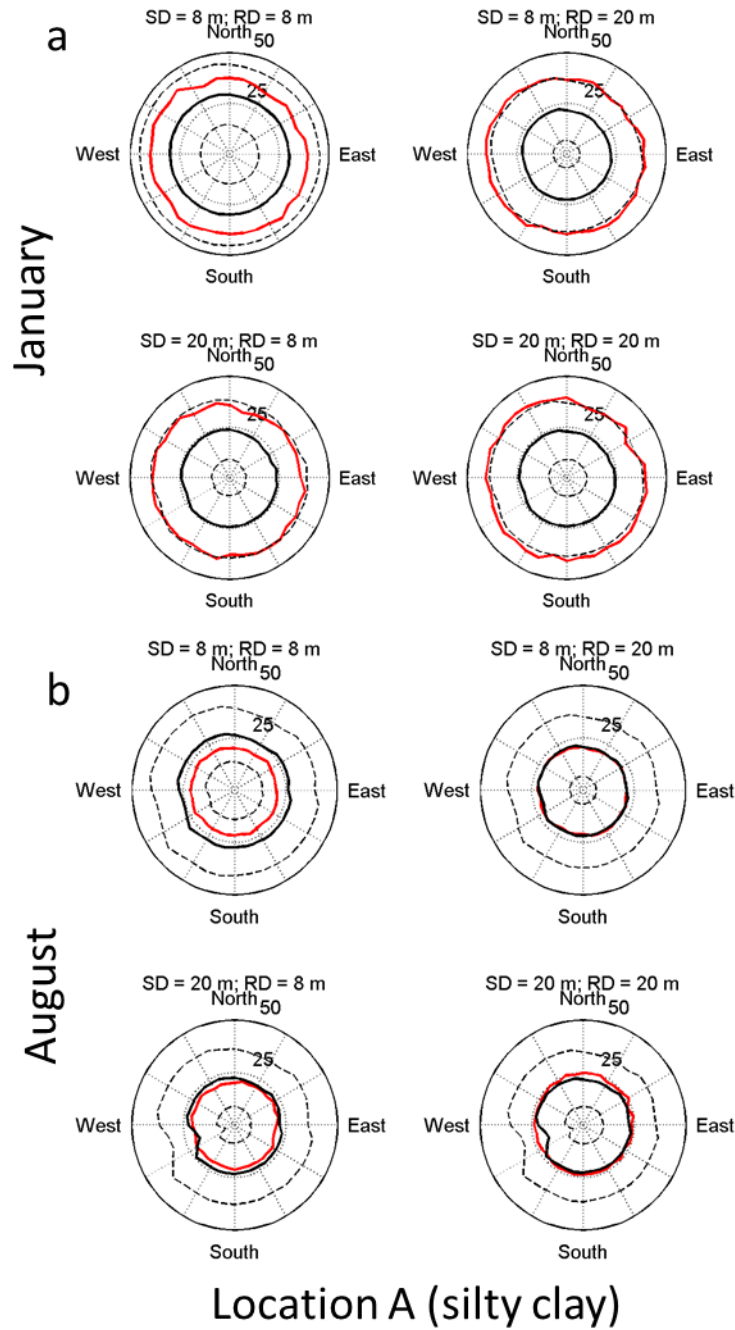
TL loss at varying thresholds of 60dB-100dB, SMG-WOD (black) and GDEM (red) a) August, b) January. Histogram of 80dB threshold c) August, d) January.



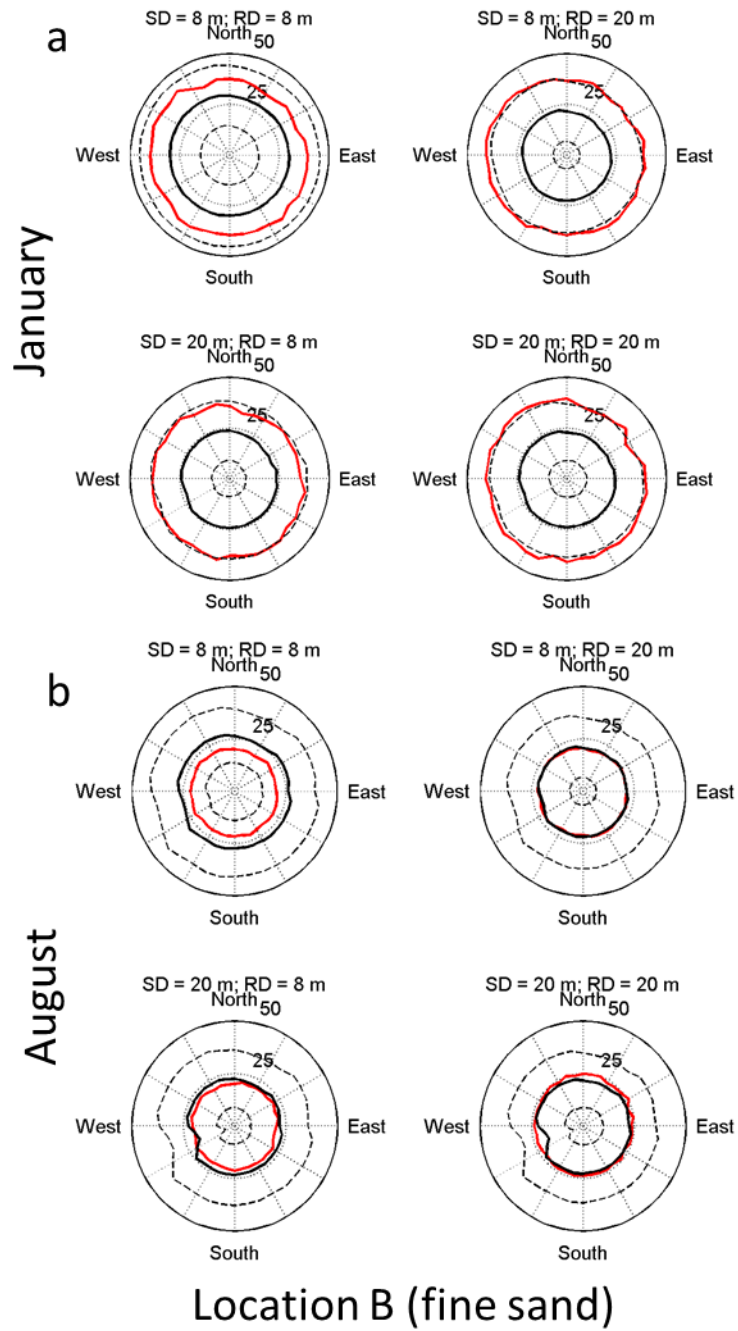
TL loss at varying thresholds of 60dB-100dB, SMG-WOD (black) and GDEM (red) a) August, b) January. Histogram of 80dB threshold c) August, d) January.

THIS PAGE INTENTIONALLY LEFT BLANK

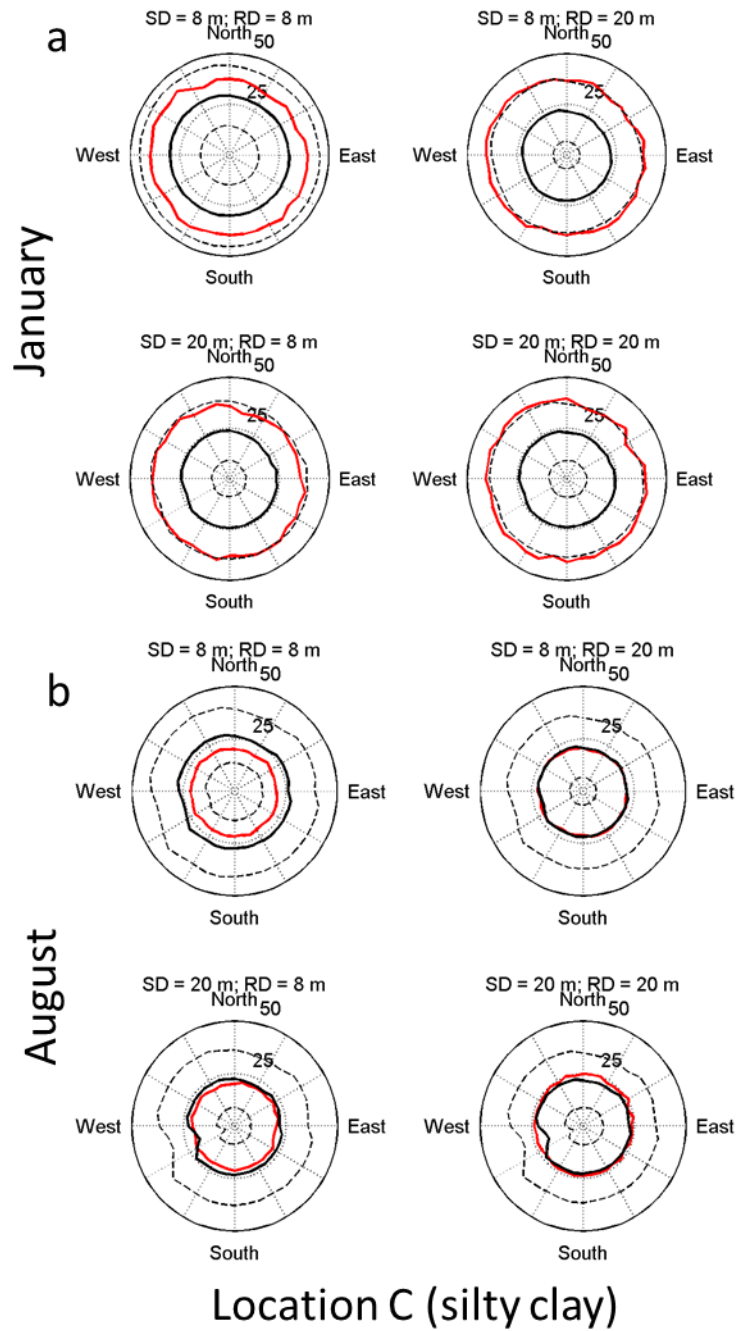
APPENDIX G. PROPAGATION POLAR PLOTS



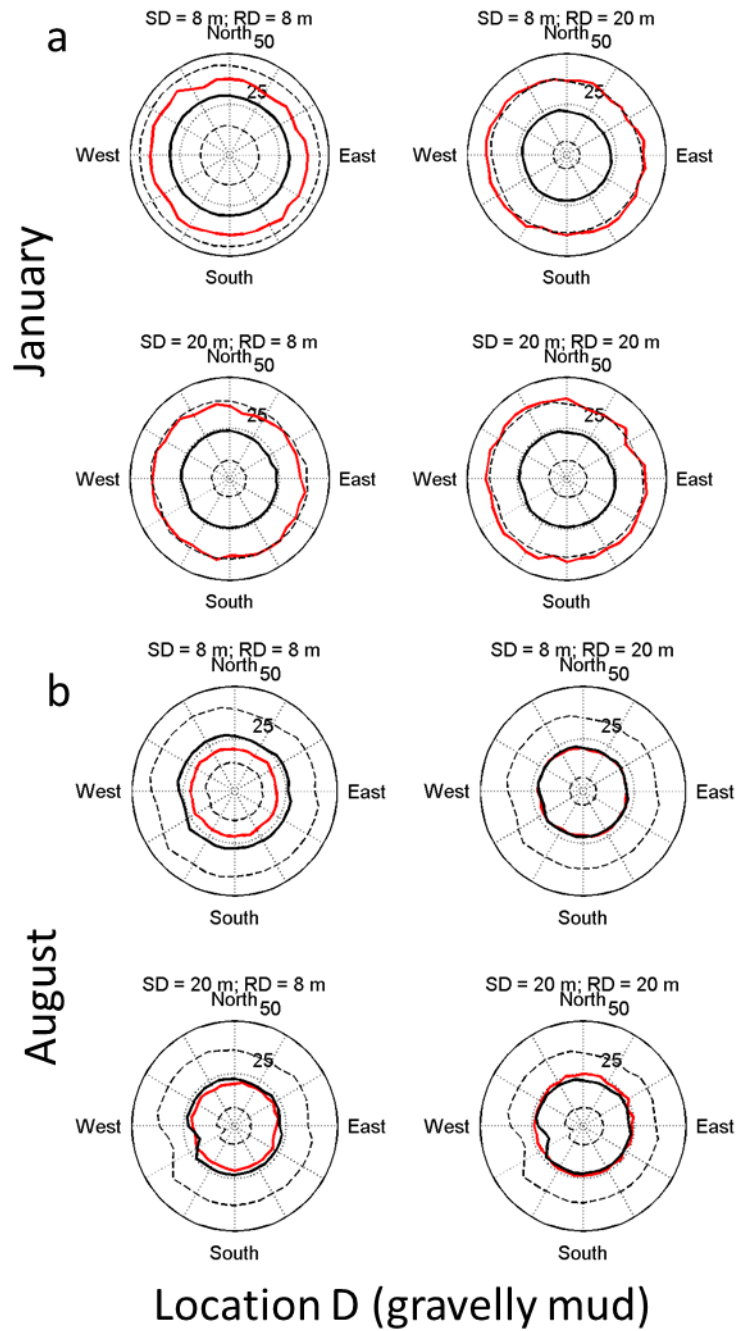
Propagation ranges plotted for SMG-WOD (black) and GDEM (red) the dashed line is one standard deviation for SMG-WOD.



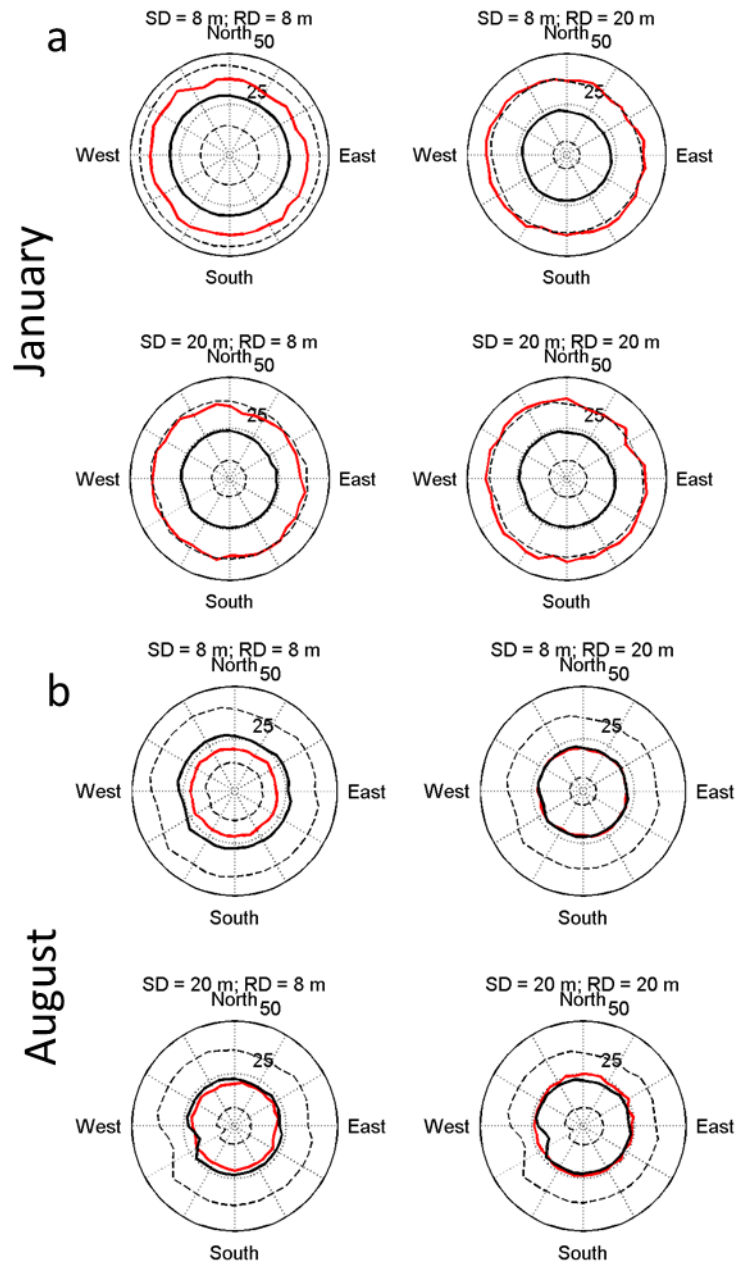
Propagation ranges plotted for SMG-WOD (black) and GDEM (red) the dashed line is one standard deviation for SMG-WOD.



Propagation ranges plotted for SMG-WOD (black) and GDEM (red) the dashed line is one standard deviation for SMG-WOD.

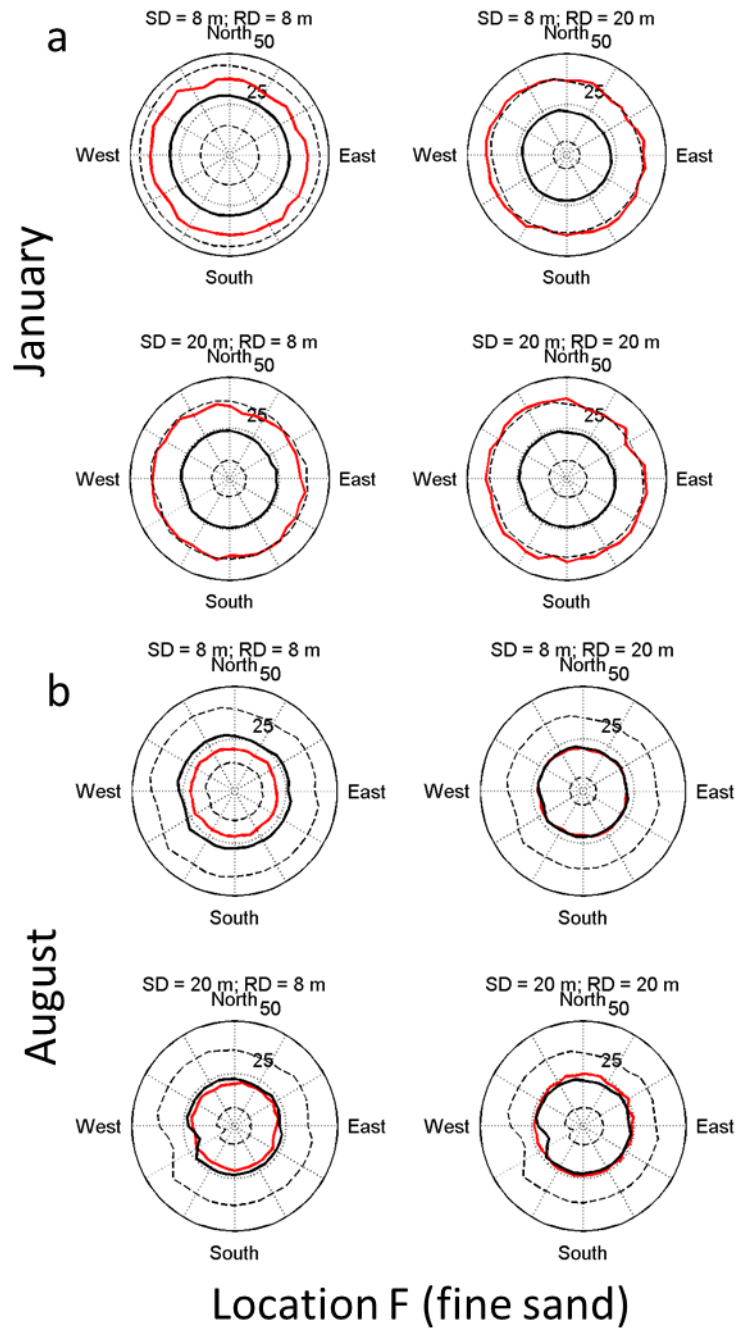


Propagation ranges plotted for SMG-WOD (black) and GDEM (red) the dashed line is one standard deviation for SMG-WOD.

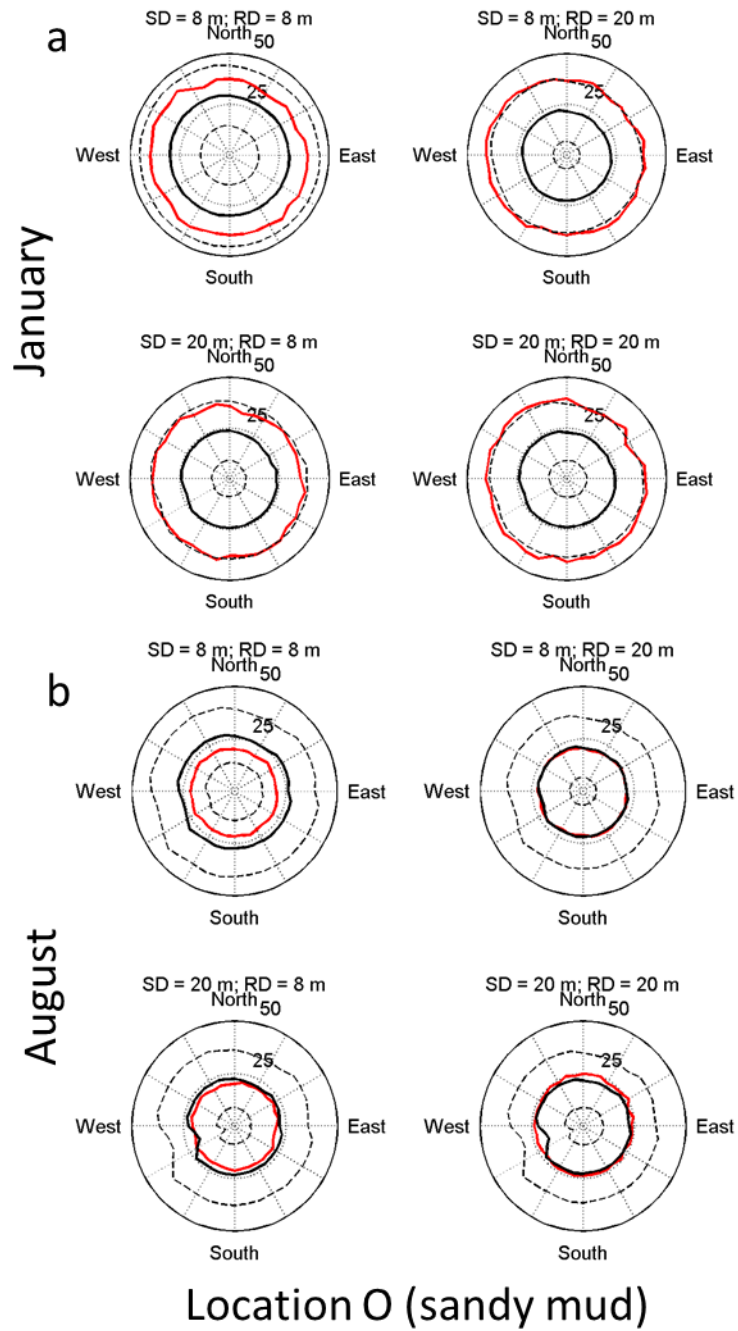


Location E (cobble or gravel)

Propagation ranges plotted for SMG-WOD (black) and GDEM (red) the dashed line is one standard deviation for SMG-WOD.



Propagation ranges plotted for SMG-WOD (black) and GDEM (red) the dashed line is one standard deviation for SMG-WOD.



Propagation ranges plotted for SMG-WOD (black) and GDEM (red) the dashed line is one standard deviation for SMG-WOD.

THIS PAGE INTENTIONALLY LEFT BLANK

APPENDIX H. TRANSMISSION LOSS STANDARD DEVIATION YEARS

SMG-WOD transmission loss 1–3 standard deviations (sigma) by year, listed by
month, source and receiver depth, and location

```

January: SD = 8 m; RD = 8 m; A
>= 3\sigma:
>= 2\sigma: 1950  1984  2000  2001  2002  2003  2004
>= \sigma: 1947  1948  1963  1966  1967  1974  1977  1978  1979  2010
January: SD = 8 m; RD = 20 m; A
>= 3\sigma: 1984
>= 2\sigma: 1987
>= \sigma: 1950  1998  2000  2001  2002  2003  2004  2007
January: SD = 20 m; RD = 8 m; A
>= 3\sigma: 1984
>= 2\sigma: 1987  2000  2001  2003  2004
>= \sigma:
January: SD = 20 m; RD = 20 m; A
>= 3\sigma:
>= 2\sigma: 1984
>= \sigma: 1987  1991  1998  1999  2000  2001  2002  2003  2004  2007
January: SD = 8 m; RD = 8 m; B
>= 3\sigma:
>= 2\sigma: 1984  1995  2000  2001  2003  2004
>= \sigma: 1945  1950  1962  1964  1967  1968  1971  1974  1996  1998
1999
January: SD = 8 m; RD = 20 m; B
>= 3\sigma:
>= 2\sigma: 1984  2000  2001  2002  2003  2004
>= \sigma: 1987  1998  2007
January: SD = 20 m; RD = 8 m; B
>= 3\sigma: 1984
>= 2\sigma: 2000  2001  2003  2004
>= \sigma: 1950  1987  2011
January: SD = 20 m; RD = 20 m; B
>= 3\sigma:
>= 2\sigma: 1984
>= \sigma: 1947  1977  1987  1998  1999  2000  2001  2002  2003  2004
2007
January: SD = 8 m; RD = 8 m; C
>= 3\sigma:
>= 2\sigma: 1950  1984  1995  2009
>= \sigma: 1945  1963  1968  1970  1996  1997  1998  1999  2000  2001
2002  2003  2004  2006  2010
January: SD = 8 m; RD = 20 m; C
>= 3\sigma: 1984
>= 2\sigma: 1987  1998
>= \sigma: 1947  1950  1995  2001  2007
January: SD = 20 m; RD = 8 m; C

```

```

>= 3\sigma: 1984
>= 2\sigma: 1987
>= \sigma: 1947 1950 1975 1988 1997 1998 2000 2001 2002 2003
2007 2011
January: SD = 20 m; RD = 20 m; C
>= 3\sigma:
>= 2\sigma: 1984
>= \sigma: 1947 1950 1951 1975 1978 1987 1991 1995 1998 1999
2000 2001 2002 2003 2004 2005 2007 2011
January: SD = 8 m; RD = 8 m; D
>= 3\sigma:
>= 2\sigma: 1962 1984 2000 2001 2003 2004
>= \sigma: 1950 1968 1992 1994 2009
January: SD = 8 m; RD = 20 m; D
>= 3\sigma:
>= 2\sigma: 1984
>= \sigma: 1950 1987 1999 2000 2001 2002 2003 2004 2007
January: SD = 20 m; RD = 8 m; D
>= 3\sigma:
>= 2\sigma: 1984 2000 2001 2002 2003 2004
>= \sigma: 1950 1987
January: SD = 20 m; RD = 20 m; D
>= 3\sigma:
>= 2\sigma: 1984 2000 2001 2002 2003 2004
>= \sigma: 1987 1999 2007
January: SD = 8 m; RD = 8 m; E
>= 3\sigma:
>= 2\sigma:
>= \sigma: 1953 1975 1978 1979 1984 1988 1989 1990 1991 1992
1993 1994 1995 1996 1997 1998 1999 2000 2001 2002 2003 2004
January: SD = 8 m; RD = 20 m; E
>= 3\sigma:
>= 2\sigma: 1984
>= \sigma: 1987 1988 1989 1990 1991 1992 1993 1994 1995 1996
1997 1998 1999 2000 2001 2002 2003 2004
January: SD = 20 m; RD = 8 m; E
>= 3\sigma:
>= 2\sigma:
>= \sigma: 1984 1987 1988 1989 1990 1991 1992 1993 1994 1995
1996 1997 1998 1999 2000 2001 2002 2003 2004
January: SD = 20 m; RD = 20 m; E
>= 3\sigma:
>= 2\sigma: 1984
>= \sigma: 1987 1988 1989 1990 1992 1993 1994 1995 1996 1998
2000 2001 2002 2003 2004 2005 2007 2008
January: SD = 8 m; RD = 8 m; F
>= 3\sigma:
>= 2\sigma:
>= \sigma: 1948 1950 1965 1967 1969 1972 1977 1978 1984 1987
1988 1989 1990 1991 1992 1993 1994 1995 1996 1997 1998 1999
2000 2001 2002 2003 2004 2009
January: SD = 8 m; RD = 20 m; F
>= 3\sigma: 1984
>= 2\sigma: 1987

```

```

>= \sigma: 1981 1983 1985
January: SD = 20 m; RD = 8 m; F
>= 3\sigma: 1984
>= 2\sigma: 1987
>= \sigma: 1988 1989 1990 1991 1992 1993 1994 1995 1996 1997
1998 1999 2000 2001 2002 2003 2004
January: SD = 20 m; RD = 20 m; F
>= 3\sigma: 1984
>= 2\sigma: 1987
>= \sigma: 1988 1990 1994 1995 1996 2001 2004 2008
January: SD = 8 m; RD = 8 m; O
>= 3\sigma:
>= 2\sigma: 1984
>= \sigma: 1945 1947 1948 1956 1964 1967 1968 1971 1974 1976
1987 1988 1989 1990 1991 1992 1993 1994 1995 1996 1997 1998
1999 2000 2001 2002 2003 2004 2009
January: SD = 8 m; RD = 20 m; O
>= 3\sigma: 1984
>= 2\sigma: 1987
>= \sigma: 1981 1982 1983 1985 1986
January: SD = 20 m; RD = 8 m; O
>= 3\sigma: 1984
>= 2\sigma: 1987
>= \sigma: 1981 1982 1983 1985 1986
January: SD = 20 m; RD = 20 m; O
>= 3\sigma: 1984
>= 2\sigma: 1987
>= \sigma: 1948 1975 2001
August: SD = 8 m; RD = 8 m; A
>= 3\sigma: 1984 1987
>= 2\sigma: 1981 1982 1983 1985 1986
>= \sigma:
August: SD = 8 m; RD = 20 m; A
>= 3\sigma: 1984
>= 2\sigma: 1987
>= \sigma: 1981 1982 1983 1985 1986 2010
August: SD = 20 m; RD = 8 m; A
>= 3\sigma: 1984
>= 2\sigma: 1987
>= \sigma: 1981 1982 1983 1985 1986
August: SD = 20 m; RD = 20 m; A
>= 3\sigma: 1984
>= 2\sigma: 1987
>= \sigma: 1981 1982 1983 1985 1986
August: SD = 8 m; RD = 8 m; B
>= 3\sigma: 1984 1987
>= 2\sigma: 1981
>= \sigma: 1982 1983 1985 1986
August: SD = 8 m; RD = 20 m; B
>= 3\sigma: 1984
>= 2\sigma: 1987
>= \sigma: 1981 1982 1983 1985 1986
August: SD = 20 m; RD = 8 m; B
>= 3\sigma: 1984

```

```

>= 2\sigma: 1987
>= \sigma: 1981 1982 1983 1985 1986
August: SD = 20 m; RD = 20 m; B
>= 3\sigma: 1984
>= 2\sigma: 1987
>= \sigma: 1981 1982 1983 1985 1986
August: SD = 8 m; RD = 8 m; C
>= 3\sigma: 1984 1987
>= 2\sigma: 1981 1983 1985 1986
>= \sigma: 1948 1982
August: SD = 8 m; RD = 20 m; C
>= 3\sigma: 1984
>= 2\sigma: 1987
>= \sigma: 1981 1982 1983 1985 1986 2010
August: SD = 20 m; RD = 8 m; C
>= 3\sigma: 1984
>= 2\sigma: 1987
>= \sigma: 1981 1982 1983 1985 1986
August: SD = 20 m; RD = 20 m; C
>= 3\sigma: 1984
>= 2\sigma: 1987
>= \sigma: 1981 1982 1983 1985 1986 2010
August: SD = 8 m; RD = 8 m; D
>= 3\sigma: 1984 1987
>= 2\sigma: 1981 1983 1985
>= \sigma: 1982 1986
August: SD = 8 m; RD = 20 m; D
>= 3\sigma: 1984
>= 2\sigma: 1987
>= \sigma: 1981 1982 1983 1985 1986
August: SD = 20 m; RD = 8 m; D
>= 3\sigma: 1984
>= 2\sigma: 1987
>= \sigma: 1981 1982 1983 1985 1986
August: SD = 20 m; RD = 20 m; D
>= 3\sigma: 1984
>= 2\sigma: 1987
>= \sigma: 1981 1982 1983 1985 1986
August: SD = 8 m; RD = 8 m; E
>= 3\sigma:
>= 2\sigma: 1984
>= \sigma: 1987 1988 1989 1990 1991 1992 1993 1994 1995 1996
1997 1998 1999 2000 2001 2002 2003 2004
August: SD = 8 m; RD = 20 m; E
>= 3\sigma:
>= 2\sigma: 1984
>= \sigma: 1950 1987 1988 1989 1990 1991 1992 1993 1994 1995
1996 1997 1998 1999 2000 2001 2002 2003 2004
August: SD = 20 m; RD = 8 m; E
>= 3\sigma:
>= 2\sigma: 1984
>= \sigma: 1987 1988 1989 1990 1991 1992 1993 1994 1995 1996
1997 1998 1999 2000 2001 2002 2003 2004
August: SD = 20 m; RD = 20 m; E

```

```

>= 3\sigma:
>= 2\sigma: 1984
>= \sigma: 1948 1987 1988 1989 1990 1992 1993 1994 1995 1996
1998 2001 2002 2003 2004 2007
August: SD = 8 m; RD = 8 m; F
>= 3\sigma: 1984 1987
>= 2\sigma: 1981 1985
>= \sigma: 1982 1983 1986
August: SD = 8 m; RD = 20 m; F
>= 3\sigma: 1984
>= 2\sigma: 1987
>= \sigma: 1981 1982 1983 1985 1986
August: SD = 20 m; RD = 8 m; F
>= 3\sigma: 1984
>= 2\sigma: 1987
>= \sigma: 1981 1982 1983 1985 1986
August: SD = 20 m; RD = 20 m; F
>= 3\sigma: 1984
>= 2\sigma: 1987
>= \sigma: 1981 1982 1983 1985 1986
August: SD = 8 m; RD = 8 m; O
>= 3\sigma: 1984
>= 2\sigma: 1987
>= \sigma: 1949 1978 1981 1983 1985 2008
August: SD = 8 m; RD = 20 m; O
>= 3\sigma: 1984
>= 2\sigma: 1987
>= \sigma: 1981 1982 1983 1985 1986
August: SD = 20 m; RD = 8 m; O
>= 3\sigma: 1984
>= 2\sigma: 1987
>= \sigma: 1981 1982 1983 1985 1986
August: SD = 20 m; RD = 20 m; O
>= 3\sigma: 1984
>= 2\sigma: 1987
>= \sigma: 1981 1982 1983 1985 1986

```

THIS PAGE INTENTIONALLY LEFT BLANK

LIST OF REFERENCES

- Ali, H. B., 1993: Oceanographic variability in shallow-water acoustics and the dual role of the sea bottom. *IEEE J. of Oceanic Eng.*, **18**, 31–41.
- Allen, J.E., 1980: Transmission loss variability in shallow water. *Bottom-interacting Ocean Acoustics.*, **5**, 485–492.
- Allen, R. L. Jr. and U.S. Navy; Naval Oceanographic Office, 2012: Global gridded physical profile data from the U.S. Navy’s Generalized Digital Environmental Model (GDEM) product database (NODC Accession 9600094). Version 1.1. National Oceanographic Data Center, NOAA. Dataset. Accessed 01 April 2016. [Available online at <http://data.nodc.noaa.gov/cgi-bin/iso?id=gov.noaa.nodc:9600094>]
- Anderegg, W.R.L, J.W. Prall, J. Harold, S.H. Schneider, 2010: Expert credibility in climate change. *PNAS.* **107**, 12107-12109.
- Bao, B., and G. Ren, 2014: Climatological characteristics and long-term change of SST over the marginal seas of China. *Continental Shelf Res.*, **77**, 96–106.
- Boyer, T. P., J. I. Antonov, O. K. Baranova, C. Coleman, H. E. Garcia, A. Grodsky, D. R. Johnson, R. A. Locarnini, A.V. Mishonov, T. D. O’Brien, C. R. Paver, J. R. Reagan, D. Seidov, I. V. Smolyar, and M. M. Zweng, 2013: World Ocean Database 2013. Sydney Levitus, Ed.; Alexey Mishonov, Technical Ed., NOAA Atlas NESDIS 72, 209 pp. [Available online at <http://doi.org/10.7289/V5NZ85MT>.]
- Carnes, M.R., 2009: Description and evaluation of GDEM-V 3.0. Naval Research Laboratory. NRL/MR/7330—09-9165, 24 pp.
- Chapman, S.J., 2009: *Essentials of MATLAB programming*. Cengage Learning. 412 pp.
- Chough, S. K., J.W. Kim, S.H. Lee, Y.J. Shinn, J.H. Jin, M.C. Suh, and J.S. Lee, 2002: High-resolution acoustic characteristics of the epicontinental sea deposits, central-eastern Yellow Sea. *Marine Geology*, **188**, 317–331.
- Chu, P.C., 2016: Synoptic monthly gridded and ocean data to assess submarine vulnerability. Naval Research Program. NRWG 16–1 Social/Poster Session NPS. Monterey, California.
- Chu, P.C., Y.C. Chen, A. Kunikaka, 2005: Seasonal variability of the Yellow Sea/East China Sea surface fluxes and thermohaline structure. *Adv in Atm Sci*, **22**, 1–20.

- Chu, P. C., C. Cintron, S.D. Haeger, and R.E. Keenan, 2002: Acoustic mine detection using the Navy's CASS-GRAB. *Fifth International Symposium on Technology and Mine Problem, Society for Counter-Ordnance Technology, Monterey*. 10pp. [Available online at <http://hdl.handle.net/10945/36255>]
- Chu, P. C., and C. W. Fan, 2016a: Synoptic monthly gridded world ocean database (SMG-WOD). *Geoscience Data Journal*, submitted for publication.
- Chu, P. C., and C. W. Fan, 2016b: Synoptic monthly gridded three dimensional (3D) World Ocean Database temperature and salinity from January 1945 to December 2014 (NCEI Accession 0140938). Version 1.1. NOAA National Centers for Environmental Information. Dataset. [Available online at <http://data.nodc.noaa.gov/cgi-bin/iso?id=gov.noaa.nodc:0140938>.]
- Chu, P. C., R. T. Tokmakian, C. W. Fan, and C. L. Sun, 2015: Optimal spectral decomposition (OSD) for ocean data assimilation. *Journal of Atmospheric and Oceanic Technology*, **32**, 828–841.
- Chu, P. C., H. Tseng, C. P. Chang, and J. M. Chen, 2007: South China Sea warm pool detected in spring from the Navy's Master Oceanographic Observational Data Set (MOODS). *Journal of Geophysical Research*, **102**, 15761–15771.
- Chu, P. C., H. Tseng, C. P. Chang, and J. M. Chen, 2011: Global upper ocean heat content and climate variability. *Ocean Dynamics*, **61**, 1189–1204.
- Cintron, C., 2001: Environmental Impact on Mine Hunting in the Yellow Sea using the CASS/GRAB Model. M.S. thesis. Department of Oceanography, Naval Postgraduate School, 262 pp.
- Dong, L., H. Dong and J. Hovem, 2014: Bellhop—a modelling approach to sound propagation in the ocean. Submitted to Proceedings for the 37th Scandinavian Symposium on Physical Acoustics. [Available online at https://www.ntnu.edu/documents/14687435/901262351/SSPA_2014_Dong_Bellhop.pdf/9e4d79dc-1c5a-43d0-9724-9990bd5e2219]
- Emerson, C., J.F. Lynch, P. Abbot, Y.T. Lin, T.F. Duda, G.G. Gawarkiewicz, and C.F. Chen, 2015: Acoustic propagation uncertainty and probabilistic prediction of sonar system performance in the southern East China Sea continental shelf and shelfbreak environments. *IEEE J. Oceanic Eng.*, **40**, 1003–1017.
- Fralick, C.R, 1994: Yellow Sea thermal structure. M.S. thesis. Department of Oceanography, Naval Postgraduate School, 91 pp.
- Garrison, R.E., 1990: Pelagic and hemipelagic sedimentary rocks as a source and reservoir rock. deep-marine sedimentation: depositional models and case histories in hydrocarbon exploration and development. Pacific Section, SEPM. 123–149.

- Hamilton, E. L., 1972: Sound attenuation in marine sediments. Naval Undersea Research and Development Center (NUC). NUC TP 281.
- Hamilton, E.L., 1980: Geoacoustic modeling of the sea floor. *J. Acoust. Soc. Am.*, **65**, 1313–1340.
- Hannachi, A., 2004: A Primer for EOF Analysis of Climate Data: Department of Meteorology, University of Reading, 33 pp. [Available online at <http://www.met.rdg.ac.uk/~han/Monitor/eofprimer.pdf>.]
- Hannachi, A., I.T. Jolliffe, and D.D. Stevenson, 2007: Empirical orthogonal functions and related techniques in atmospheric science: A review. *Int. J. Climatol.*, **27**, 1119–1152.
- Hao, J., Y. Chen, F. Wang, and P. Lin, 2012: seasonal thermocline in the China Seas and northwestern Pacific Ocean. *J. Geophys Res*, **117**, 1–14.
- Hsu, M.-K., A. K. Liu, C. Liu, 2000: A study of internal waves in the China Seas and Yellow Sea using SAR. *Continental Shelf Res.*, **20**, 389–410.
- Ichikawa, H, and R.C. Beardsley, 2002: The current system in the Yellow Sea and East China Seas. *J. of Oceanography*, **58**, 77–92.
- IPCC, 2013: Summary for Policymakers. In: Climate Change 2013: The Physical Science Basis. Contribution of Working Group I to the Fifth Assessment Report of the Intergovernmental Panel on Climate Change [Stocker, T.F., D. Qin, G.-K. Plattner, M. Tignor, S. K. Allen, J. Boschung, A. Nauels, Y. Xia, V. Bex and P.M. Midgley (eds.)]. Cambridge University Press, Cambridge, United Kingdom and New York, NY.
- Kumar, N., F. Feddersen, Y. Uchiyama, J. McWilliams, and W. O'Reilly, 2014: Mid-shelf to surf zone coupled ROMS-SWAN model-data comparison of waves, currents, and temperature: Diagnosis of subtidal forcings and response. 1–12.
- LePage, K. D., 2006: Estimation of acoustic propagation uncertainty through polynomial chaos expansions. *9th International Conference on Information Fusion*, Florence, Italy. doi: 10.1109/icif.2006.301756.
- Lermusiaux, P. F. J., C.-S. Chiu, and A. R. Robinson, 2002: Modeling Uncertainties in the Prediction of the acoustic Wavefield in a Shelfbreak Environment. E.-C. Shang, Q. Li, T.F. Gao (Eds.), *Proc. of the 5th Int. Conf. on Theoretical and Computational Acoustics (ICTCA)*, Beijing, China, World Scientific Publishing Company, Beijing, China (2002), pp. 191–200.
- Li, J., Zeng Q., 2003: A new monsoon index and the geographical distribution of the global monsoons. *Adv Atmos Sci*, **20**, 2, 299–302.

- Liu, Z., H. Wei, I.D. Lozovatsky, H.J.S. Fernando, 2008: Late summer stratification, internal waves, and turbulence in the Yellow Sea. *J. of Mar Sys.* [doi:10.1016/j.jmarsys.2008.11.001]
- Locarnini, R. A., A. V. Mishonov, J. I. Antonov, T. P. Boyer, H. E. Garcia, O. K. Baranova, M. M. Zweng, C. R. Paver, J. R. Reagan, D. R. Johnson, M. Hamilton, D. Seidov, 2013. World Ocean Atlas 2013, Volume 1: Temperature. S. Levitus, Ed.; A. Mishonov, Technical Ed.; NOAA Atlas NESDIS 73, 40 pp. [Available on line at <http://www.nodc.noaa.gov/OC5/indprod.html>].
- Manyin, M.E., S. Daggett, B. Dolven, S.V. Lawrence, M.F. Martin, R. O'Rourke, and B. Vaughn, 2012: Pivot to the Pacific? The Obama administration's "rebalancing" toward Asia. Congressional Research Service.
- McDevitt, M.A., C.K. Lea, A.M. Denmark, K.E. Gause, B.S. Glaser, R.C. Bush, III, and D.M. Hartnett, 2012: The long littoral project: East China and Yellow Seas, A maritime perspective on Indo-Pacific security. Center for Naval Analysis (CNA) Report.
- Medwin, H., and Clay, C.S., 1998: *Fundamentals of Acoustical Oceanography*. Academic Press, 712 pp.
- Morgan, P. 2003: [CSIRO MATLAB Seawater Library](#). CMR (maintained by Lindsay Pender), last updated December 2003.
- National Academy of Sciences (NAS), 2000: *Oceanography and Mine Warfare*. National Academies Press. 112 pp. [Available online at <http://nap.edu/catalog/9773.html>]
- Naval Oceanographic Office, NAVO, 2006: Database description for bottom sediment type Digital Bathymetric Data Base–Variable Resolution (DBDB-V) Version 5.4 (U). Oceanographic and Atmospheric Master Library., OAML-DBD-90, 55 pp.
- Naval Oceanographic Office, NAVO, 2009: Database description for the generalized digital environmental model–variable resolution (GDEM-V) Version 3.0.1 (U). Oceanographic and Atmospheric Master Library., OAML-DBD-72F, 39 pp.
- Office of the Secretary of Defense (OSD), 2012: Annual report to Congress: Military and security developments involving the People's Republic of China 2012, 52 pp. [Available online at http://www.defense.gov/Portals/1/Documents/pubs/2012_CMPR_Final.pdf]
- Oh, S., S. Lee, S. Cho, D. Kang, and Y. Lee, 2013: Temporal variations of acoustic propagation in the strong tidal zone, Yellow Sea in the Northwest Pacific. *Marine Technology Society*.

- Park, K.A., E.Y. Lee, E. Chang, and S. Hong, 2015: Spatial and temporal variability of sea surface temperature and warming trends in the Yellow Sea. *J. Marine Systems*, **143**, 24–38.
- Porter, M. B., 2011: The BELLHOP Manual and User's Guide: PRELIMINARY DRAFT. Heat, Light, and Sound Research, Inc. 57 pp.
- Porter, M.B. and Liu, Y.-C., 1994: Finite-element ray tracing. *Theor. Comput. Acoust.*, **19**, 2, 947–956.
- Rodriguez, D.L., 2016: Inter-annual variability of the California current system and associated biochemical characteristics from prolonged data series. M.S. thesis. Department of Oceanography, Naval Postgraduate School, 129 pp.
- Rogers, P.H., 1981: Onboard prediction of propagation loss in Shallow Water. Naval Research Laboratory. NRL Report 8500, 28pp. [Available online at <http://www.dtic.mil/dtic/tr/fulltext/u2/a104738.pdf>]
- Smith, R. D., and P. R. Gent, 2002: Reference manual for the Parallel Ocean Program (POP): Ocean component of the Community Climate System Model (CCSM 2.0 and 3.0). Los Alamos National Laboratory Tech. Rep. LA-UR-02-2484, 75 pp. [Available online at <http://www.cesm.ucar.edu/models/ccsm3.0/pop/doc/manual.pdf>.]
- Solomon, S., G.-K., Plattner, R. Knutti, P. Friedlingstein, 2009: Irreversible climate change due to carbon dioxide emissions. *PNAS*, **107**, 1704–1709.
- Teague, W. J., Carron, M. J., and Hogan, P. J., 1990: A comparison between the generalized digital environmental model and Levitus climatologies. *J. Geophys. Res.*, **95**, C5, 7167–7183.
- U. S. Department of Justice (DOJ), 2015: Mid and low frequency sonar. Environmental and Natural Resources Division (ENRD). Accessed 14 July 2016. [Available online at <https://www.justic.gov/enrd/mid-and-low-frequency-sonar>]
- Wang, Y., and L. Zhou, 2005: Observed trends in extreme precipitation events in China during 1961–2001 and the associated changes in large-scale circulation. *Geophys. Res. Lett.*, **32**, L09707, 1–4.
- Wilks, D.S., 2011: Principle Component (EOF) Analysis. *Statistical Methods in Atmospheric Sciences*. Elsevier Inc., 519–562.
- World Ocean Atlas Database (WOA), 2016: World Ocean Atlas 2013 version 2 NOAA/NCEI. Accessed 11 April 2016. [Available online at <https://www.nodc.noaa.gov/OC5/woa13/>.]

- World Ocean Database (WOD), 2016: World Ocean Database NOAA/NCEI. Accessed 11 2016. [Available online at https://www.nodc.noaa.gov/OC5/WOD/pr_wod.html.]
- Zang, J., Y. Tang, E. Zou, and H.J. Lie, 2003: Analysis of Yellow Sea circulation. *Chinese Science Bulletin*, **48**, 12–20.
- Zhu, C., W.-S. Lee, H. Kang, and C.-K. Park, 2005: A proper monsoon index for seasonal and interannual variations of the East Asian monsoon. *Geophys. Res. Lett.*, **32**, L02811, 1–5.
- Zingarelli, R.A., and D.B. King, 2003: RAM to navy standard parabolic equation: transition from research to fleet acoustic model. NRL. Accessed on 24 Jul 2016. [Available online at <http://www.nrl.navy.mil/research/nrl-review/2003/simulation-computing-modeling/zingarelli/>]
- Zweng, M. M, J. R. Reagan, J. I. Antonov, R. A. Locarnini, A. V. Mishonov, T. P. Boyer, H. E. Garcia, O.K. Baranova, D.R. Johnson, D. Seidov, M.M. Biddle, 2013. *World Ocean Atlas 2013, Volume 2: Salinity*. S. Levitus, Ed.; A. Mishonov, Technical Ed.; NOAA Atlas NESDIS 74, 39 pp. [Available on line at <http://www.nodc.noaa.gov/OC5/indprod.html>]

INITIAL DISTRIBUTION LIST

1. Defense Technical Information Center
Ft. Belvoir, Virginia
2. Dudley Knox Library
Naval Postgraduate School
Monterey, California